CONTROLLED SPACECRAFT CHARGING FOR COULOMB FORCE CONTROL OF SPACECRAFT FORMATIONS

BY

Satwik H. Deshmukh

A THESIS

Submitted in partial fulfillment of the requirements

for the degree of

MASTER OF SCIENCE IN MECHANICAL ENGINEERING

MICHIGAN TECHNOLOGICAL UNIVERSITY

2002

This thesis, "Controlled Spacecraft Charging for Coulomb Force Control of Spacecraft formations," by Satwik H. Deshmukh, is hereby approved in partial fulfillment of the requirements for the Degree of MASTER OF SCIENCE IN MECHANICAL ENGINEERING.

DEPARTMENT:

MECHANICAL ENGINEERING - ENGINEERING MECHANICS

MICHIGAN TECHNOLOGICAL UNIVERSITY

Signatures:

Thesis Advisor:	Dr. Lyon B. King	Date
Department Chair:	Dr. William W. Predebon	Date

Abstract

In the course of exploring the capabilities of close spacecraft formations in applications such as distributed space-based interferometry, the inter-vehicle separation may be on the order of ten meters. This thesis delves into the effect of spacecraft charging on the dynamics of close formation flying. In certain high Earth orbits or in interplanetary environments the ambient plasma causes significant spacecraft potentials and the characteristic plasma Debye length is also more than 100 meters. In these conditions, natural spacecraft charging may give rise to disruptive inter-vehicle Coulomb forces and torques in close formations, which are comparable to those created by candidate thrusters for formation keeping. Instead of fighting these Coulomb forces, it may be prudent to purposefully charge the spacecraft and incorporate them for formation keeping and attitude control. Existence of feasible static equilibrium formations in Earth orbit using only Coulomb forces was already explored analytically in parallel research work. In this thesis, it is found that the spacecraft potentials required for formations can be created with milliwatts of power and can be changed on a millisecond time scale. The specific impulse of this Coulomb control system can be as high as 10^{13} sec. Thus Coulomb control system will provide almost propellantless means of propulsion, which will be free from plume cross-contamination and collision problem in close formations. It may also improve fine positioning because of its continuous and fine-resolution nature.

Acknowledgement

This thesis is based on the research work done for a project sponsored by NASA Institute of Advanced Concepts (NIAC). I would like to thank NIAC for providing the financial support for this project. I would like to thank my advisor Dr. Lyon B. King for his support and invaluable guidance to complete this research work and my masters degree. It is an honor to work with him. He has been a role model to me. I really appreciate him for helping me by all possible means and being patient with me. I am grateful to Dr. Gordon G. Parker for his guidance and extremely important help in this research. I am very thankful to Dr. Bernhard Bettig and Dr. Yoke Khin Yap for being my thesis committee members and giving useful suggestions. I also thank the ME-EM Department and General Engineering Department for supporting me for my graduate studies. I would also like to thank my colleagues, the Grad-Lab Community, and all other friends at MTU for their academic/non-academic help. Finally I would love to appreciate my parents, sisters, entire Deshmukh family, Mr. Ravindra Damugade, and my friends, without whose well wishes and efforts, I could not have been able to pursue my masters.

Table of Contents

List of Figures

1. Introduction

1.1. Formation Flying Background

Swarms of microsatellites are currently envisioned as an attractive alternative to traditional large spacecraft. Such swarms, acting collectively as virtual satellites, will benefit from the use of cluster orbits where the satellites fly in a close formation.[1] The formation concept, first explored in the 1980's to allow multiple geostationary satellites to share a common orbital slot,[2,3] has recently entered the era of application with many missions slated for flight in the near future. For example, EO-1 will formation fly with LandSat-7 to perform paired earth imagery, ST-3 will use precision formation flight to perform stellar optical interferometry, TechSat 21 will be launched in 2004 to perform sparse-aperture sensing with inter-vehicle spacing as close as 5 m, and the ION-F science mission will perform distributed ionospheric impedance measurements.[4,5] The promised payoff of formation-flying has recently inspired a large amount of research in an attempt to overcome the rich technical problems. A variety of papers can be found in the proceedings of the 1999 AAS/AIAA Space Flight Mechanics Meeting,[6,7,8] the 1998 Joint Air Force/MIT Workshop on Satellite Formation Flying and Micro-Propulsion,[9] a recent textbook on micropropulsion,[10] and numerous other sources.[11,12,13,14,15,16,17]

Relative positional control of multiple spacecraft is an enabling technology for missions seeking to exploit satellite formations. Of the many technologies that must be brought to maturity in order to realize routine formation flying, perhaps the most crucial is the spacecraft propulsion system. In fact, during his keynote address at the 1998 Joint Air Force/MIT Workshop on Satellite Formation Flying and Micro-Propulsion, Dr. David

Miller of the Space Systems Laboratory at MIT delivered a “Top Ten List” of formation-flying technological obstacles. On this list, the two most important technologies were identified as (1) Micropropulsion; and (2) Payload contamination, arising from propellant exhausted from closely spaced satellites.[9]

Constellations of small satellites will require propulsion systems with micro- to milli-Newton thrust levels for deployment, orbit maintenance, disposal, and attitude control.[18,19]. Formation-keeping thrusters must be capable of producing finely controlled, highly repeatable impulse bits. Although no suitable thruster has yet been proven in flight, recent research suggests that the best current technologies are micro-pulsed-plasma thrusters (micro PPT),[5] field-emission electric propulsion thrusters (FEEP),[20] and colloid thrusters.[21]

As identified in item (2) from Dr. Miller’s technology list, current research-level thruster candidates pose significant contamination problems. In close proximity, the propellant emitted by such devices as micro-PPT’s (vaporized Teflon), FEEP (ionized cesium), or colloid thrusters (liquid glycerol droplets doped with NaI) will impinge upon neighboring vehicles and damage payloads. To worsen the problem, orbital mechanics for many clusters of interest mandate continuous thruster firings pointed directly towards other vehicles in the formation. The contamination problem will be amplified as the formation spacing is reduced.

1.2. *Separated Spacecraft Interferometry*

1.2.1. <u>Space-based Imaging Problem</u>

It has long been known that increased astronomical imaging capability could be realized if the optics for the imaging system were placed outside of the earth's atmosphere. Missions such as the current Hubble Space Telescope (HST) and planned Next Generation Space Telescope (NGST) exemplify this principle. The increased clarity offered by space-based astronomy is somewhat offset, however, by practical limits placed on angular resolution of the image. The angular resolution (resolving power) of an optic is related to the physical size of the collector by

Eqn. 1-1
$$\theta = \frac{\lambda}{2d},$$

where θ is the minimum resolvable angular feature, λ is the wavelength to be imaged, and d is the physical size of the collecting aperture. Thus, to obtain fine angular resolution (small θ) requires a large aperture. Herein lies the problem for space-based imaging systems: the physical size of the aperture is limited by launch vehicle fairing dimensions. The largest launch fairing currently available is that of the Ariane V, which is approximately 5 meters in diameter. For space-based imaging in the optical wavelengths (400-700 nm) using a monolithic aperture, missions are limited to angular resolution no better than 4×10^{-8} radians (about 8 milli-arcseconds).

The ability to resolve an astronomical object is directly proportional to the size of the object and inversely proportional to the distance from the observer. At the Spaceborne Interferometry Conference, Ridgeway presented a graphical depiction of the apparent size of "interesting" astronomical objects.[22] Ridgeway's schematic is reproduced in Figure 1-1. In this figure, lines of constant apparent angular size (resolution) are shown. It is significant that most of the science topics begin with angular scales of about 1 milli-arcsecond, approximately a factor of 1000 smaller than the typical limit of optical imaging from the ground.

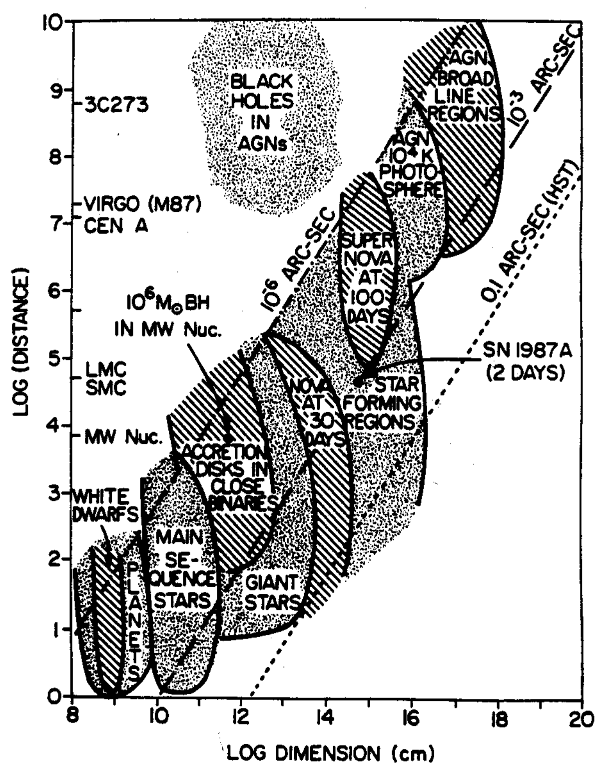

Figure 1-1. Depiction of apparent size of astronomical target objects. The distance to the objects is listed on the vertical axis, with the transverse dimension of the object on the horizontal axis. Diagonal lines denote the angular extent of the target and, thus, the resolution required for imaging. The 0.1 arc-sec line denotes Hubble Space Telescope (HST) capabilities. It is significant that most science topics begin with resolutions better than 1 milli-arcsecond.[22]

1.2.2. Interferometry Fundamentals

There are two options for circumventing the aperture resolution restrictions created by launch vehicles. First, a deployable structure can be designed that can fold to stow into the size-limited fairing. The structure can then be deployed on-orbit to a final size greater than the fairing diameter. Although deployable structures avoid a direct physical size limitation, the stowed structure must still fit within the available launch volume and is thus constrained at some larger, but finite, dimension related to the launch vehicle size. The second method for overcoming vehicle size restrictions is separated spacecraft interferometry.

Separated spacecraft interferometry is a direct extension of an imaging technique that has been employed with ground-based systems for years. In ground-based interferometry, physically separated apertures collect incident radiation from the target at two or more discrete locations and direct this collected radiation to a common combiner station. Using principles of Fourier optics, the radiation can be interfered to produce image data. The power of interferometry arises from the increased angular resolution: the resolving power of the combined optical system is a function of the separation, or baseline, between individual collectors and not on the collector sizes themselves. Quantitatively, the resolving power is still given by Eqn. 1-1, however d is now the distance *between* the collectors, rather than the *size* of a given optic. In principle, the baseline d, and thus the resolving power can be increased without limit. Detailed accounts of interferometry theory can be found in many textbooks[23] and descriptions of space-based interferometry can be found in previous research works.[14,15,16] A basic summary will be presented here.

Qualitatively, the information in an image can be represented in two different formats. The first mode, which is most intuitively familiar, is that of a spatial intensity map. For every location (x, y coordinate) in a spatial plane some value of radiant intensity is given. Mapping the intensity values produces an image in the same fashion that the human eye/retina records optical information. The same information contained in the intensity map can be presented in a second format relating to spatial frequencies.

The spatial frequency representation of an image can most easily be understood in the context of a checker-board tile floor. A spatial intensity map summarizes the floor image by assigning an amplitude to every x, y point on the floor corresponding to, say, the brightness of the floor. One can also recognize obvious patterns in the floor that repeat themselves on a regular spatial period. If the tiles in the floor are square, then the repeating pattern in the x direction has the same period, or spatial frequency, as the pattern in the y direction; if they are rectangular the x and y patterns will have different frequencies. Specification of the spatial frequencies then yields some of the image information. For each spatial frequency in the floor, one must also specify an amplitude to fully describe all of the image information. For the square-wave pattern of the checker-board floor, a large amplitude may correspond to black and white tiles, while a smaller amplitude may represent gray and white tiles.

Fourier mathematics extends the simple qualitative tile floor analogy to images of arbitrary complexity. Any function of intensity in the physical plane (x, y space) can be represented by an infinite series of Fourier terms. Each term of the Fourier series has a spatial frequency (u, v point for x and y spatial frequencies respectively) and an amplitude coefficient. Thus, if one knows the amplitude coefficient for every spatial frequency (u, v point), the Fourier representation of the image information can be transformed to produce the more familiar spatial intensity map of the target.

In interferometry, the u-v points in the Fourier plane are obtained by separated collector points in the x-y physical plane. When light of wavelength λ collected by two spacecraft at locations (x_1, y_1) and (x_2, y_2) is combined (interfered), the resulting interference pattern yields a single value. The single value is the complex amplitude of the Fourier term with spatial frequencies (u, v) denoted by

Eqn. 1-2

$$u = \frac{\pm\left(x_2 - x_1\right)}{?}$$
$$v = \frac{\pm\left(y_2 - y_1\right)}{?}.$$

Thus, each unique spacecraft separation vector, or baseline, yields one term of the Fourier representation of the image. To reconstruct the image one must have information from many (theoretically an infinite number) of unique spacecraft baselines. For multiple spacecraft, the u-v coverage is represented by the correlation function of the physical coverage. For N spacecraft, each of the spacecraft has N-1 different position vectors to other vehicles in the array. Thus the total number of u-v points from an array of N spacecraft is N(N-1) plus a zero baseline point.

Judicious use of spacecraft collector assets mandates intelligent placement of the vehicles in physical space. For instance, redundant baselines (separation vectors) between vehicles in a formation produce redundant Fourier information and represent a “waste” of assets. Ideally, each of the N(N-1) u-v points should be unique. Numerous collector formation possibilities exist based upon optimization of various parameters. Golay performed a study of collector placements based upon optimization of the u-v compactness of the overall formation.[24] The resulting Golay formations are shown in Figure 1-2 for N=3, 6, 9, and 12 spacecraft. Similarly, Cornwell derived formations, which were designed to optimize the uniformity of coverage in the u-v plane.[25]

Representative configurations for N=3-12 spacecraft Cornwell configurations are shown in Figure 1-3.

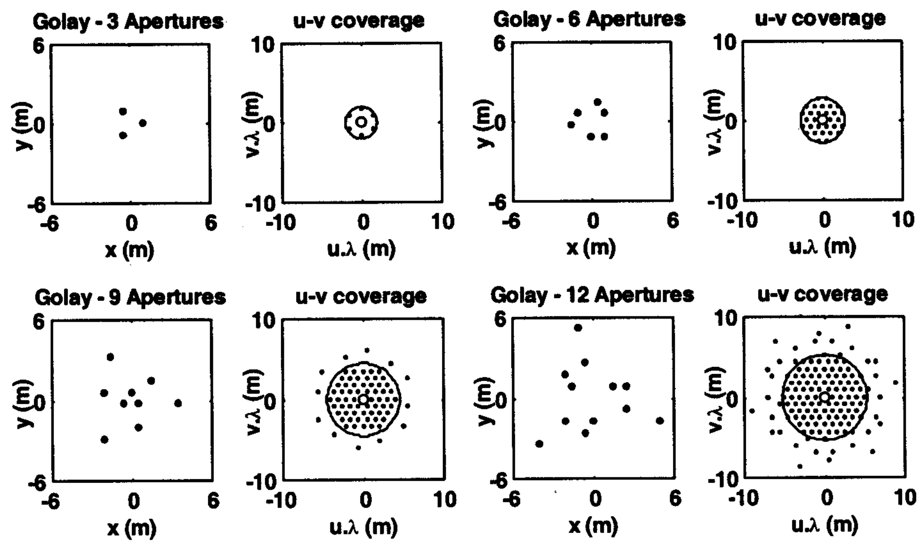

Figure 1-2. Golay interferometric formations based upon optimizing the compactness of the group in u-v space. The aperture locations in x-y space and the corresponding baselines in u-v space are plotted in adjacent diagrams.[15]

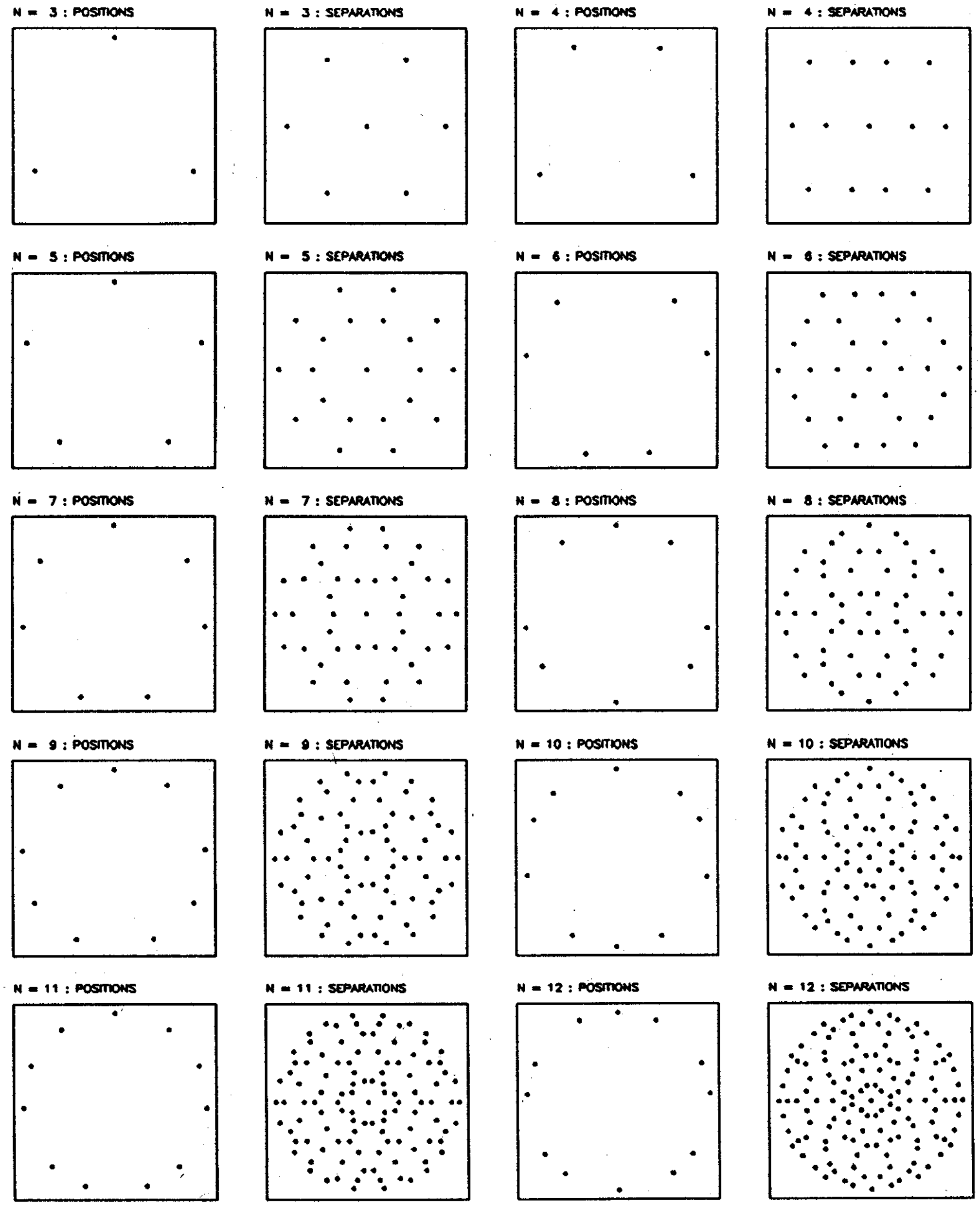

Figure 1-3. Cornwell optimized arrays for uniform u-v coverage for N=3-12. The positions of the apertures (spacecraft) are shown in x-y space, while the unique baselines (separations) show up as points in u-v space. Positions and corresponding separations are plotted in adjacent diagrams.[25]

1.2.3. *Practical Aspects of Space Interferometry*

The method by which the u-v points are mapped out depends upon the nature of the target object. For static targets whose features are relatively constant (such as astronomical objects), the u-v points can be mapped out sequentially with as few as two collector spacecraft. The vehicles simply move to the specified x-y positions, record a data point, and move on to other locations. The image is then processed after a predefined number of u-v points have been recorded. Such is the method employed by missions such as Deep Space 3 and Terrestrial Planet Finder. For rapidly changing targets, such as those on the surface of the Earth, the image features must be recorded in a "snapshot" mode where all of the u-v points are obtained simultaneously. Such configurations are said to produce full, instantaneous u-v coverage. For such snapshots the number of independent collector spacecraft must be equal to the number of u-v points required to produce the image.

Interferometric imaging in the optical regime poses a constraint on an imaging array. For lower frequencies, such as those in the radio spectrum for radar imaging, the incoming wavefront from each collector can be recorded and archived, with the actual interferometry between separate collectors performed later through post-processing. Optical signals, however, have frequencies too high to permit recording of the wavefront for post-processing. Instead, the incoming signals from two collectors must be interfered in real time at the combiner. In order to permit interference between the same wavefront from each collector, the light path length from each collector to the combiner must be equal to within a fraction of the radiation wavelength. It is clear from an examination of Figure 1-2 and Figure 1-3 that Cornwell arrays, with all of the collector apertures lying on the circumference of a circle, are ideally suited to a central combiner for optical path symmetry, while Golay arrays are not amenable to a single combiner vehicle.

For formation-flying spacecraft performing visible imagery, the requirement of equal optical path lengths seems to present an unobtainable formation tolerance between spacecraft of a few nanometers. In practice, however, this constraint is relaxed through the use of on-board delay lines for fine control. In such a delay-line configuration, the individual spacecraft need only keep formation tolerance errors within a few centimeters, while actively controlled movable optics compensate for the coarse position errors down to the interferometry requirement. A schematic is shown in Figure 1-4. By repositioning the optics on-board one or both of the vehicles, the light from one collector can be made to traverse the same distance as that from another collector.

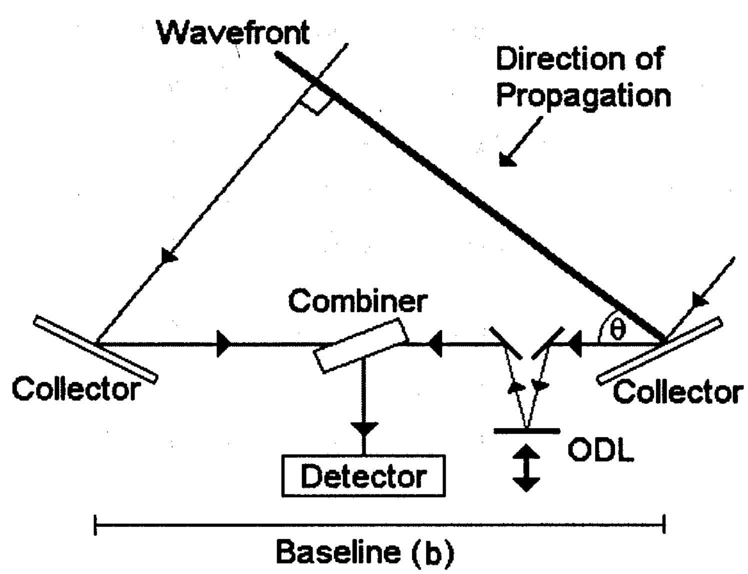

Figure 1-4. Illustration of optical delay line (ODL) for fine adjustment of science light path from collector to combiner in interferometry.[15]

The need for full, instantaneous u-v coverage begs the question of mathematical completeness. To exactly invert the Fourier image information requires an infinite number of amplitude coefficients and, thus, an infinite number of collector locations. This is evidenced in the amount of white space representing missing u-v information in the plots of Figure 1-2 and Figure 1-3. One method for solving the completeness problem lies in post-processing techniques for image reconstruction. Another method relies on intelligent placement of finite-sized collector optics.

To extend the qualitative description of interferometry to finite-sized collectors, one can envision a single collector of diameter *d* as an assembly of sub-collector elements. Image information for u-v points represented by distances between sub-collector elements is then obtained from a single optic as shown in Figure 1-5. In fact, a single optic of diameter d yields an infinite number of u-v points for all baselines less than or equal to d. All baselines (u-v points) greater than *d* must then come from sub-elements on separated spacecraft. In terms of full, instantaneous u-v coverage, this implies that spacecraft must be separated by a distance comparable to their individual size, d, to avoid omission of u-v points. Thus, snapshot-style imaging requires very close formation flying.

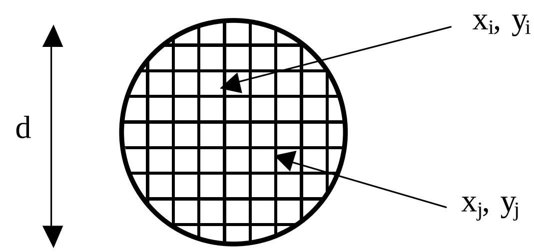

Figure 1-5. Conceptual image of single collector optic as array of sub-collectors. The elements i and j will yield interferometric information for the u-v point representing the baseline between the elements.

1.3. Spacecraft Charging Literature Survey

The basic concept of spacecraft charging phenomenon and its subtypes will be explained in brief. A brief overview of previous work performed in the spacecraft charging field from the early 1920s to recent advances in internal spacecraft charging studies will be provided. Relationship of the present thesis with the previous work in this field will be established. Objectives of the present study will be enlisted.

1.3.1. Spacecraft Charging Concept[26,27]

A spacecraft in space attains some potential with respect to the surrounding plasma due to accumulation of charged plasma particles and due to other mechanisms like photoemission and secondary electron emission. This phenomenon is referred to as spacecraft charging. It can be divided into two types, namely surface charging and internal charging. Surface charging refers to charging on the exterior surfaces of a spacecraft, while internal charging is concerned with accumulation of charged particles on or in ungrounded metals and dielectrics in the interior of the spacecraft.

Surface charging can be subdivided into absolute and differential charging. If the entire spacecraft surface attains some continuous potential, it is regarded as absolute charging. Differential charging refers to potential difference between different surfaces due to spacecraft geometry and surface material etc. So far differential charging has been the main impetus for spacecraft charging study as differential charging above about 400V makes the spacecraft prone to electrostatic discharge, which can result in numerous serious problems such as damage to the solar array.

Incident ion and electron current is the most influential factor for spacecraft charging. Some spacecraft surface materials emit photoelectrons when exposed to ultraviolet component of the solar flux representing an added source of current to the vehicle. Electron incident on the spacecraft surface is either reflected back or it is absorbed in the surface material. Some of the electrons can collide with the atoms in the material and get backscattered out of the surface. The rest of the electrons loose energy to the material, which can excite other electrons in the material and make them escape out of the material. These escaping electrons are called backscattered or secondary electrons. Backscattered electrons are emitted back with energy slightly lower than that of incident electrons, while secondary electrons are those electrons, which are emitted back with characteristic spectrum of energy (a few eV). Ions incident to the spacecraft surface can also give rise to backscattered electrons.

Ions coming to the spacecraft (or equivalently electrons leaving the spacecraft) are defined as positive current. The current balance equation for a spacecraft considering all these currents can be written as follows.

Eqn. 1-3

$$I_{total}(V_{SC}) = -I_e(V_{SC}) + I_i(V_{SC}) + I_{se}(V_{SC}) + I_{si}(V_{SC}) + I_{bse}(V_{SC}) + I_{ph}(V_{SC})$$

where, all currents are a function of V_{SC}, and V_{SC} is spacecraft surface potential with respect to surrounding plasma, I_{total} is the total current to the spacecraft surface. I_e and I_i are incident electron and ion currents. I_{se} and I_{si} are secondary electron currents due to electrons and ions respectively. I_{bse} is backscattered electron current and I_{ph} is the photoelectron current. In a state of equilibrium all currents balance, and I_{total} is zero.

1.3.2. Brief Review of Spacecraft Charging Field

The field of spacecraft charging is as old as spacecraft itself. Early traces of this field can be found as far back as 1920s in Langmuir and Mott-Smith's[28,29] work on the potential of an electrostatic probe in a plasma environment. Chopra[30], Whipple[31], Garrett[32], and Whittlesey [26] have provided excellent reviews of the progress in the spacecraft charging field in different phases. The first phase from 1937-1957, began with the investigation of the charging of a body in space. Jung [33] obtained equations for fluxes of ions and electrons to an interstellar grain (or dust particle). Later on Spitzer[34], Cernuschi[35], and Savendoff [36] elaborated on charge accumulation and emission processes for an interstellar grain. Johnson and Meadows[37] mentioned the spacecraft charging phenomenon for the first time in which they investigated the ambient ion composition at 219 km using a rocket-born spectrometer. Lehnert[38] calculated the charge on a macroscopic body considering the ion ram effect. Jastrow and Pearse[39] calculated the potential, screening distance and ion drag for a spacecraft marking the end of early 20 years of spacecraft charging field.

The second phase started with launch of sputnik in 1957. Gringauz and Zelikman[40] investigated the distribution of charged particles around a spacecraft and derived equilibrium potential of spacecraft considering spacecraft velocity and photoemission current. Beard and Johnson[41] discussed the possibility of achieving high electric potentials by electron / ion emission. Chopra[30] reviewed the progress in this field by the year 1961, and derived expressions for a body at rest as well as in motion and mentioned that photoelectron current will be considerable at higher altitudes. Numerous attempts were made to obtain better measurements of spacecraft potential at different attitudes, self-consistent models and inclusion of factors such as secondary emission. Whipple's thesis[42] presents a complete and clear picture of spacecraft charging taking into account photoemission, secondary emission, backscatter, and magnetic field effect, which can be regarded as the end of the second phase.

In the third phase, efforts were made to understand the space environment thoroughly and develop rigorous mathematical models. Deforest [43] observed that ATS-6 spacecraft in GEO could achieve potential as high as -10kV. It was found that potential decreases in an eclipse environment and increases in a non-eclipse environment. Spacecraft charging analysis was taken seriously by the space community when one satellite lost 90% of its functionality[44] and others suffered from serious anomalies[45,46] attributed to detrimental charging effects. The most ambitious and successful mission in this area was the SCATHA mission in1979, which was totally devoted to spacecraft charging. The primary objective was to collect environmental and engineering data to determine the relationship of electric discharge with natural charging in different plasma environments and forced ion/electron emission. The findings of this mission have been published by Adamo and Matarreze[47]; Koons et al[48,49,50], Gussenhoven and Mullen[51, 52], and Craven[53]. Garrett and DeForest[54] developed analytical model of plasma environment to predict the spacecraft potentials. Design guidelines were developed[55] to avoid differential as well as absolute charging at GEO and LEO, such as providing common electrical ground to all surfaces, keeping all the exterior surfaces at least partially conductive etc.

The NASA Space Environments & Effects Program developed the NASA Charging Analyzer Code NASCAP[56], which simulates spacecraft charging with respect to time in GEO and LEO. Spacecraft surface potentials, potential distribution in space, low energy sheath properties, and trajectories of the charged particles can be predicted with respect to time using this code by varying parameters like plasma environment, spacecraft geometry, materials, and spacecraft potential.[57] Areas prone to differential charging can be detected and modified in material and design to avoid arcing. The web-based multimedia Interactive Spacecraft Charging Handbook is the simplest form of this code, which can be used for preliminary design. Another code NASCAP2K is under development, which will combine the functionalities of NASCAP GEO, LEO, POLAR and will have expanded material properties database. The Environmental Workbench allows us to study the transient response of a spacecraft with particular geometry by applying over 100 different environments and other orbital parameters.

After laying down proper guidelines to avoid differential surface charging, the space community became more interested in internal charging and spacecraft charging at low altitudes due to the launch of the International Space Station and increasing use of high voltages and space tethers[58, 59] in the last 20 years. NASA and DoD launched Combined Release and Radiation Effects Satellite, CRRES in1990 to study the effects of the natural radiation environment on microelectronic components and high efficiency solar cells.

The Shuttle Charging Hazards and Wake Studies i.e. CHAWS[60,61] experiment found the plasma current in the wake of the spacecraft in LEO. Two codes, Potentials of Large Objects in the Auroral Region (POLAR)[62,63] and Dynamic Plasma Analysis (DynaPAC)[64] were developed for this analysis. Controlling absolute charging of the International Space Station using plasma contactors (by ion or electron emission) is an interesting example of spacecraft potential control in LEO.

It is obvious from this literature review that the prime concern of spacecraft study has been mitigating differential charging and internal charging to avoid arcing. In other words spacecraft charging effects have been proved to be a serious problem to the space community for more than half a century. This thesis proposes a technology, which takes advantage of spacecraft charging in an innovative way.

1.3.3. Relationship With Previous Work

Three key points can be noticed from the previous work done on spacecraft charging which are,

1) Spacecraft can assume potential as high as tens of kilovolts due to natural charging.
2) Spacecraft potential can be manipulated from positive to negative or vice versa by electron/ion emission.
3) The densities and temperatures of ions and electrons in plasma environment in GEO are found by applying the analytical model by Garrett and DeForest to the SCATHA results[27]. From these plasma parameters, the Debye length (explained in detail in Section 2.1.4) in low-density plasma like the one in GEO can be calculated, which is of the order of tens of meters.

The important relationship of the current work with the previous work done is that although the latter provides detailed charge analysis, studies were all done for a single vehicle, never addressing multi-vehicle interactions. According to Coulomb's law, there will be a Coulomb force between charged microspacecraft in a formation in GEO, if they are separated by any distance, which is less than the Debye length (which is up to 350m). The potential of the spacecraft can be made either positive or negative by active electron/ion emission resulting in attractive or repulsive Coulomb forces among themselves. These Coulomb forces can be employed for attitude control and formation keeping of microspacecraft swarms in GEO.

1.3.4. Objectives of the present study:

To realize the idea of utilizing Coulomb forces among spacecraft for formation flying following objectives were identified:

Objective # 1: Determination of the Coulomb force and torque on a spacecraft flying in a formation.

Output of the Spacecraft Charging Handbook (SEE program) in terms of potentials of surface elements were used to calculate Coulomb force and torque between two identical spacecraft flying in a leader – follower formation at GEO. Spacecraft separation and plasma environment were varied. The geometry for both the spacecraft was kept constant. Electric propulsion system parameters to compensate for the Coulomb force and torque were determined.

Objective # 2: Determination of the power requirement and the transient response of a spacecraft.

Power required in maintaining the spacecraft potential at a desired level and changing the spacecraft potential to a desired level were determined. Transient response of a spacecraft with simplified geometry was determined numerically as a function of power of ion/electron emission gun, keeping the plasma environment constant.

Objective # 3: Mission trade study of the Coulomb Control Technology.

Performance of the Coulomb Control Technology was compared with traditional Electric Propulsion technologies. The study was focused on canonical spacecraft formations for which Chong et al found static equilibrium solutions only using Coulomb forces, in the parallel research work. The electric propulsion technologies such as Micro-PPT, Colloid Thruster, and Field Emission Electric Propulsion Thruster were considered. Performance parameters such as total input power, total propulsion system mass, and specific impulse were compared.

2. Spacecraft Plasma Interactions

This chapter addresses the plasma conditions in low Earth orbit (LEO), Geosynchronous Earth orbit (GEO), and Interplanetary space. A spacecraft immersed in space plasma develops an absolute charge relative to this plasma. There also can be differential charging between various parts of the spacecraft. Both of these are compared here. The spacecraft and ambient plasma are represented by an equivalent electrical circuit to study the transient response of the system.

2.1. Plasma Environment

Near the Earth in LEO the cold, dense plasma is near equilibrium. Farther away from Earth its density drops significantly and mean energy increases out to GEO. Eventually it transmits into solar wind plasma outside the magnetosphere. Hastings has described these plasma environments in detail.[27] For convenience sake, we will summarize the plasma environment from LEO to interplanetary orbit in this section.

2.1.1. <u>Low Earth Orbit</u>

The Ionosphere is a transition region from a relatively un-ionized atmosphere to a fully ionized region called plasmasphere. It is divided into layers like F-Layer between 150 and 1000 km, E-Layer between 100 and 150 km, and D-layer between 60 and 100 km. Ionosphere has electron densities of 10^{10} to 10^{11} m^{-3} at an altitude of 1000 km and then drops to about 10^{9} m^{-3} at its outer boundary called plasmapause. Plasmapause is characterized by a rapid drop in electron density to 10^{5} to 10^{6} m^{-3}. Plasma density profiles in LEO are shown in Figure 2-1 and Figure 2-2.

The ion densities reach 10^{12} m^{-3} at the peak in the F-region at about 300 km on the sunlit side. At night, the peak ion density falls below 10^{11} m^{-3} and the composition changes from O^+ to H^+. Ion temperatures follow roughly that of the neutral atmosphere, increasing exponentially from a few hundred Kelvin at 50-60 km to 2000 - 3000 K above 500 km (i.e. a few tenths of an eV). The electron temperature tends to be a factor of two greater than that of the neutral, with the ion temperature falling in between.

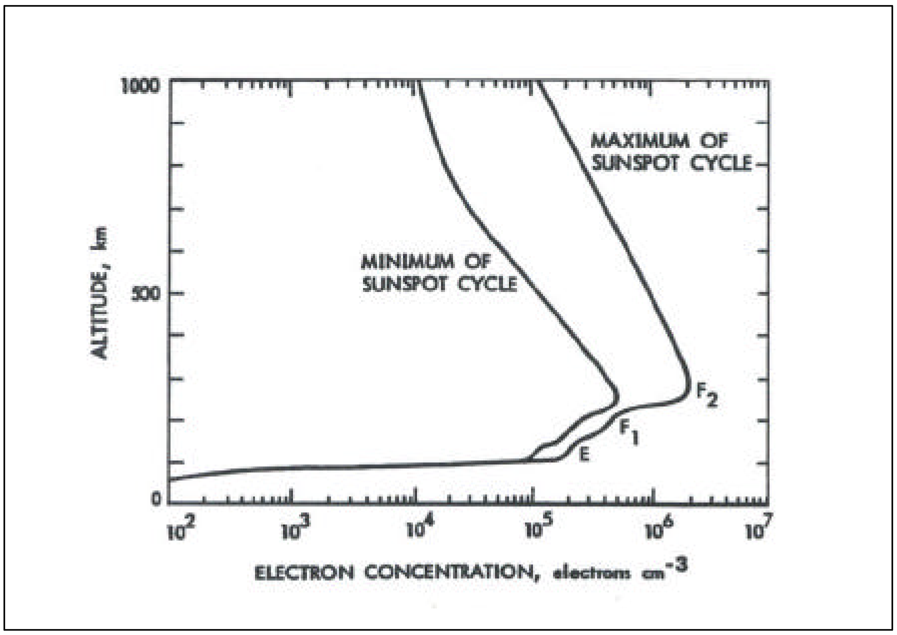

Figure 2-1. Plot of altitude (km) Vs electron density (cm^{-3}) for the Ionosphere (LEO)[27]

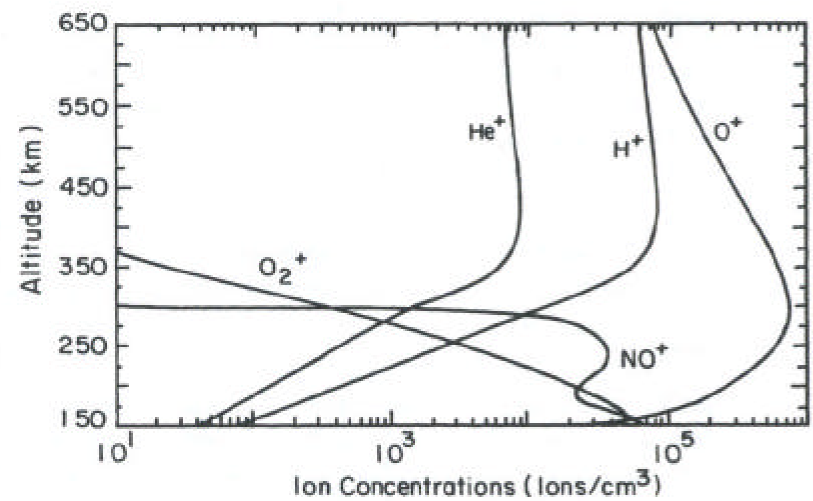

Figure 2-2. Plot of altitude (km) Vs ion composition (cm^{-3}) for the Ionosphere (LEO)[27]

2.1.2. GEO Plasma Environment

A spacecraft at GEO is at the edge of plasmapause. GEO plasma is tenuous, and cool as compared to LEO plasma although sudden injections of high energy plasma (with mean energy of a few tens of keV during substorms are observed. This collisionless plasma does not follow a single Maxwellian distribution. Instead, plasma parameters must be measured experimentally. The particle detectors on the ATS[54,65,66] and SCATHA[67] spacecraft have measured plasma variations between 5-10 eV and 50-80 eV approximately, for 50 complete days at 1 to 10 minute resolution from 1969 through 1980, bracketing one solar cycle.

Garrett and Deforest[54] fitted an analytical two-temperature model to data collected over 10 different days from ATS-5 spacecraft between 1969 and 1972. These data were selected in such a way to show a wide range of geomagnetic activity including plasma injection events (i.e. sudden appearance of dense, relatively high energy plasma at GEO occurring at local midnight). The model gives reasonable and consistent representation of the variations following a substorm injection event at GEO. The parameters for this model during average GEO conditions are shown in Table 2-1 with Worst-case GEO conditions given in Table 2-2.

Parameter	**Electrons**	**Ions**
Number density m^{-3}	$1.09 \pm 0.89 \times 10^6$	$0.58 \pm 0.35 \times 10^6$
Number density n_1 (1st Maxwellian fit) m^{-3}	$0.78 \pm 0.7 \times 10^6$	$0.19 \pm 0.16 \times 10^6$
Temperature kT_1/e (1st Maxwellian fit) eV	$0.55 \pm 0.32 \times 10^3$	$0.8 \pm 1.0 \times 10^3$
Number density n_2 (2nd Maxwellian fit) m^{-3}	$0.31 \pm 0.37 \times 10^6$	$0.39 \pm 0.26 \times 10^6$
Temperature kT_2/e (2nd Maxwellian fit) eV	$8.68 \pm 4.0 \times 10^3$	$15.8 \pm 5.0 \times 10^3$

Table 2-1. Average GEO environment[67]

Parameter	**Electrons**	**Ions**
Number density m^{-3}	3.0×10^6	3.0×10^6
Number density n_1 (1st Maxwellian fit) m^{-3}	1.0×10^6	1.1×10^6
Temperature kT_1/e (1st Maxwellian fit) eV	600	400
Number density n_2 (2nd Maxwellian fit) m^{-3}	1.4×10^6	1.7×10^6
Temperature kT_2/e (2nd Maxwellian fit) eV	2.51×10^4	2.47×10^4

Table 2-2. Worst-case GEO environment[67]

2.1.3. *Interplanetary Plasma Environment*

The sun is the dominant source for the space plasma environment in the solar system. The sun's main influence on the space environment is through its electromagnetic flux and emitted charged particles. The solar particle flux is basically composed of two components: The very sporadic, high energy (E > 1 MeV) plasma bursts associated with solar events (flares, coronal mass ejections, proton events, and so forth) and the variable, low-energy (E ≈ tens of eV) background plasma referred to as the solar wind. The solar wind, because of its density (tens of particles per cm^3) and velocity (≈ 200-2000 km/s), energetically dominates the interplanetary environment and can directly reach the GEO environment on occasion.

2.1.4. *Debye Length in Space Plasmas*

It is easily shown[68] that an isolated charged body, when placed in plasma, attracts charges of the opposite sign such that the effect of its charge is limited in extent. Within the distance known as Debye length of a charge, the electrostatic potential field is essentially the same as that of the charge in vacuum. Far from the central charge, however, the long-range electrostatic force field is effectively shielded due to the enveloping plasma space charge.

On a large enough scale, plasma that is near equilibrium must be approximately charge neutral. If this were not the case, the strong Coulomb interactions would drive the particles apart and not allow an equilibrium state to exist. The length scale over which the charge neutrality is established in plasma is called Debye length.

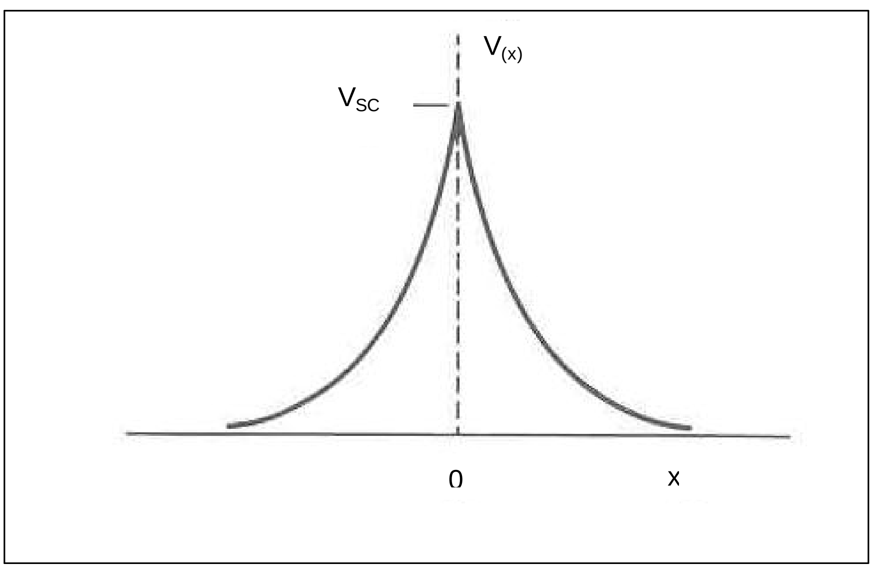

Figure 2-3. Potential distribution near a grid in plasma[69]

Consider a perfectly transparent grid as shown in Figure 2-3, in a plasma held at spacecraft potential V_{SC} in the plane x = 0. Let V_x be the potential due to charge on a spacecraft at some distance x from the spacecraft. For simplicity, we assume that the ion-electron mass ratio M/m is large enough that the inertia of ions prevents them from moving significantly on the time scale of the experiment. Poisson's equation in one dimension is

Eqn. 2-1 $$e_0 \frac{d^2V}{dx^2} = -e(n_i - n_e)$$

where e is the charge on electron, and n_i (n_e) is the density of ions (electrons) at distance x. If the density far away is n_∞, we have

Eqn. 2-2 $$n_i = n_\infty$$

The electron density will be[69]

Eqn. 2-3 $$n_e = n_\infty \exp(eV/kT_e)$$

Where k is Boltzman constant and T_e is electron temperature. Substituting for n_i and n_e in Eqn. 2-1, we get

Eqn. 2-4 $$e_0 \frac{d^2V}{dx^2} = en_\infty \left\{ \left[\exp\left(\frac{eV}{KT_e} \right) \right] - 1 \right\}$$

In the region where $|eV/kT_e| << 1$, we can expand the exponential in a Taylor Series as follows,

Eqn. 2-5 $$e_0 \frac{d^2V}{dx^2} = en_\infty \left\{ \frac{eV}{KT_e} + \frac{1}{2} \left(\frac{eV}{KT_e} \right)^2 + ... \right\}$$

Keeping only the linear terms in Eqn. 2-5, we get, Eqn. 2-6 $$e_0 \frac{d^2V}{dx^2} = \frac{n_\infty e^2 V}{KT_e}$$

The Debye length, $?_d$ is then defined as,

Eqn. 2-7 $$?_d \equiv \left(\frac{e_0 KT_e}{ne^2} \right)^{1/2}$$

where n stands for n_∞. Now we can write the solution of Eqn. 2-6 as

Eqn. 2-8 $$V = V_{SC} \exp(-|x|/?_d)$$

Debye length is the measure of the shielding distance or thickness of the sheath. Table 2-3 lists Debye lengths calculated by this formula using parameters from Table 2-1, Table 2-2, Section 2.1.1 and Section 2.1.3.

Plasma Environment	**Lowest Debye Length** m	**Highest Debye length** m
LEO plasma environment	0.02	0.4
GEO plasma environment	142	1,496
Interplanetary plasma	7.4	24

Table 2-3. Range of Debye length in various plasma environments

2.2. *Spacecraft Charging*

A spacecraft in the ambient plasma behaves like an isolated probe (Langmuir Probe)[27], repelling or collecting free charges depending upon the vehicle potential as shown in figure Figure 2-4.

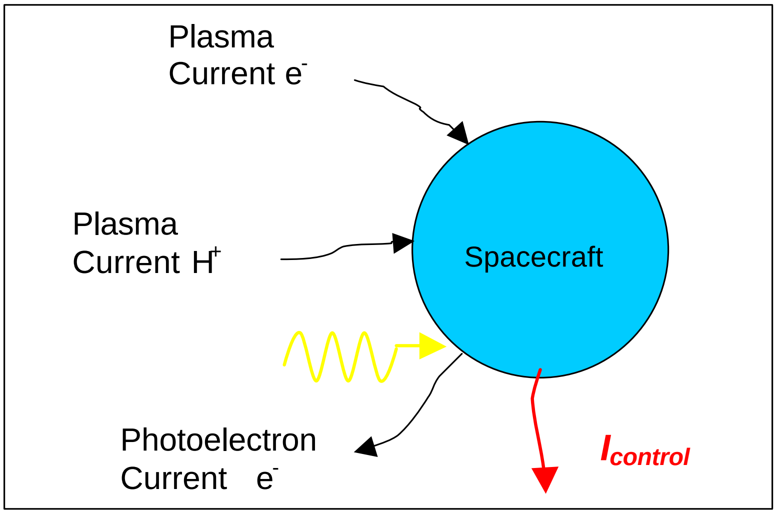

Figure 2-4. Currents flowing to and from the spacecraft

When an electrically neutral spacecraft is exposed to the ambient plasma environment as that in GEO, consisting of ions and electrons of approximately the same density, and temperature; the electrons and ions start sticking to the spacecraft surface because of their thermal kinetic energy. As the electrons are lighter than the ions, the electron current is higher than the ion current. As the time scale of this phenomenon is very short, within microseconds the spacecraft grows negative with respect to the surrounding plasma. It continues to grow negative, and in turn repels more and more electrons, until at certain negative potential the electron current balances the ion current. In other words, it grows negative until the same number of electrons and ions reach the spacecraft surface per unit time and per unit surface area so that the net current between the spacecraft and the ambient plasma is zero and the spacecraft attains an equilibrium. This equilibrium potential of the spacecraft is called the floating potential and is denoted by V_f.

The current voltage characteristics of a spacecraft in the absence of an external magnetic field is shown in Figure 2-5. In region 1, where spacecraft voltage, Vsc is biased to a large negative value, almost all the electrons are repelled and the current to the vehicle is dominated by plasma ions. As the potential of the vehicle is increased, the ion current is reduced and a greater number of electrons are able to reach the spacecraft as a result of their kinetic energy. At floating potential, or V_f, the electron current will balance with the ion current, resulting in a zero net current to the vehicle. V_f is given by (for $V_{SC}<0$)

Eqn. 2-9
$$V_f = -\frac{kT_e}{e}\ln\left[\sqrt{\frac{T_i m_i}{T_e m_e}}\left(1-\frac{eV_{sc}}{kT_i}\right)\right].$$

where m_i (m_e) is the mass of ion (electron) and T_i (T_e) is the ion (electron) temperature. For a plasma consisting of protons and electrons at approximately the same temperatures,

Eqn. 2-10
$$V_f \approx -2.5\frac{kT_e}{e}.$$

The spacecraft floating potential is thus on the order of, and scales proportionally with, the electron temperature. As the vehicle potential increases above the floating potential, the number of plasma electrons reaching the surface keeps increasing, while the ion current is reduced further. The point at which most of the ions are prohibited from reaching the vehicle is known as the plasma potential, V_{plasma}, and is characterized by the "knee" in the I-V characteristic. For spacecraft potentials greater than the plasma potential, the current is composed entirely of plasma electrons.

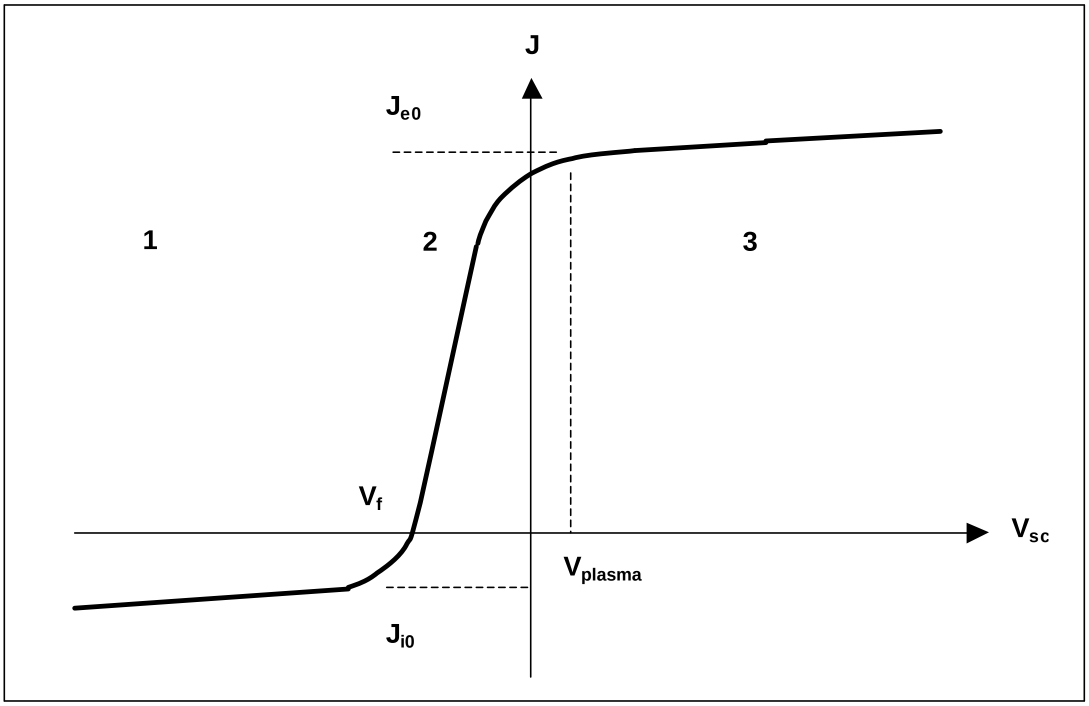

Figure 2-5. I Vs V graph for spacecraft. Vertical axis represents net current collected by the vehicle at a given spacecraft potential represented by horizontal axis.

Considering a simple spherical geometry for the spacecraft, the entire I-V characteristic of the vehicle within a space plasma can be given as an expression for the plasma current density, J_p, as a function of spacecraft potential, V_{sc} in two parts:

Eqn. 2-11 For $V_{sc} < 0$

$$J_p = J_{e0}\exp\left(\frac{-e|V_{sc}|}{kT_e}\right) - J_{i0}\left(1+\frac{e|V_{sc}|}{kT_i}\right)$$

Eqn. 2-12 For $V_{sc} > 0$

$$J_p = J_{e0}\left(1+\frac{eV_{sc}}{kT_e}\right) - J_{i0}\exp\left(\frac{-eV_{sc}}{kT_i}\right)$$

where J_{e0} and J_{e0} are termed the electron and ion saturation currents, respectively, and are given by

Eqn. 2-13 $$J_{e0} = en_e \left[\frac{kT_e}{2p\, m_e} \right]^{1/2}$$

Eqn. 2-14 $$J_{i0} = -en_i \left[\frac{kT_i}{2\, p\, m_i} \right]^{1/2}$$

Where e is electron charge in C, $n_{i(e)}$ is ion (electron) density in m^{-3}, k is Boltzmann constant in J/K, $T_{i(e)}$ is ion/electron temperature and $m_{i(e)}$ is mass of ion (electron) measured in kg. The behavior of the ion/electron saturation currents for plasma conditions of interest to this report are demonstrated in Figure 2-6 and Figure 2-7.

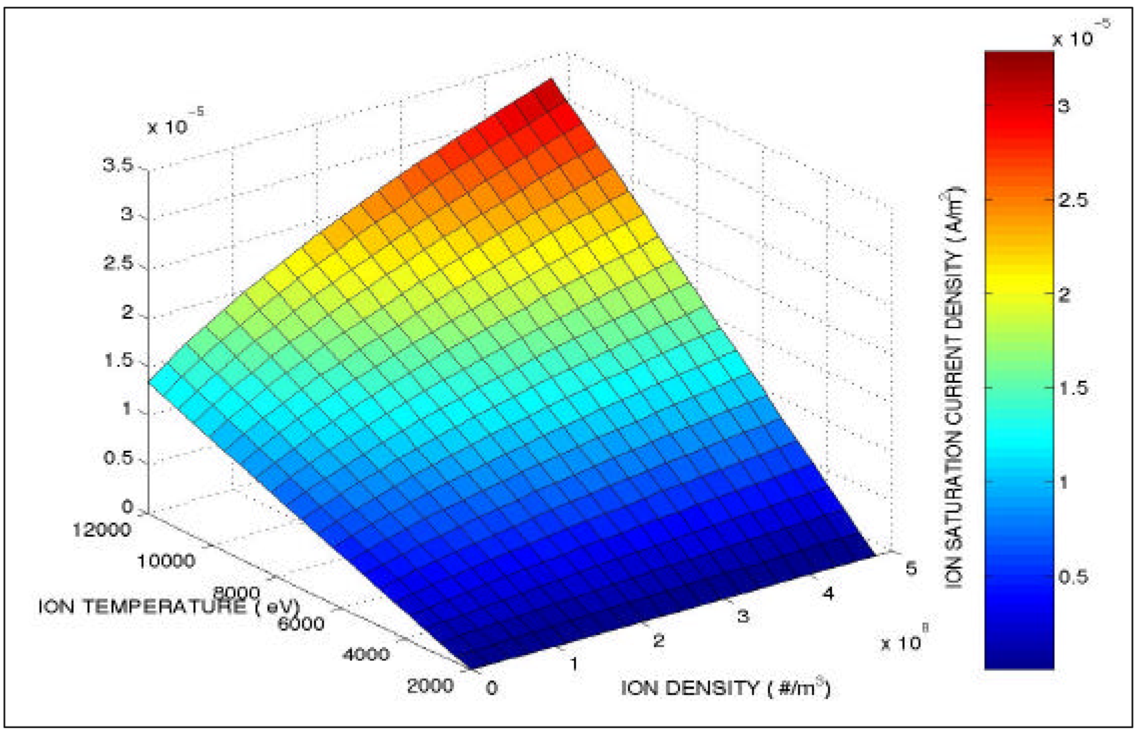

Figure 2-6. Plot of ion saturation current density as a function of ion temperature and ion density

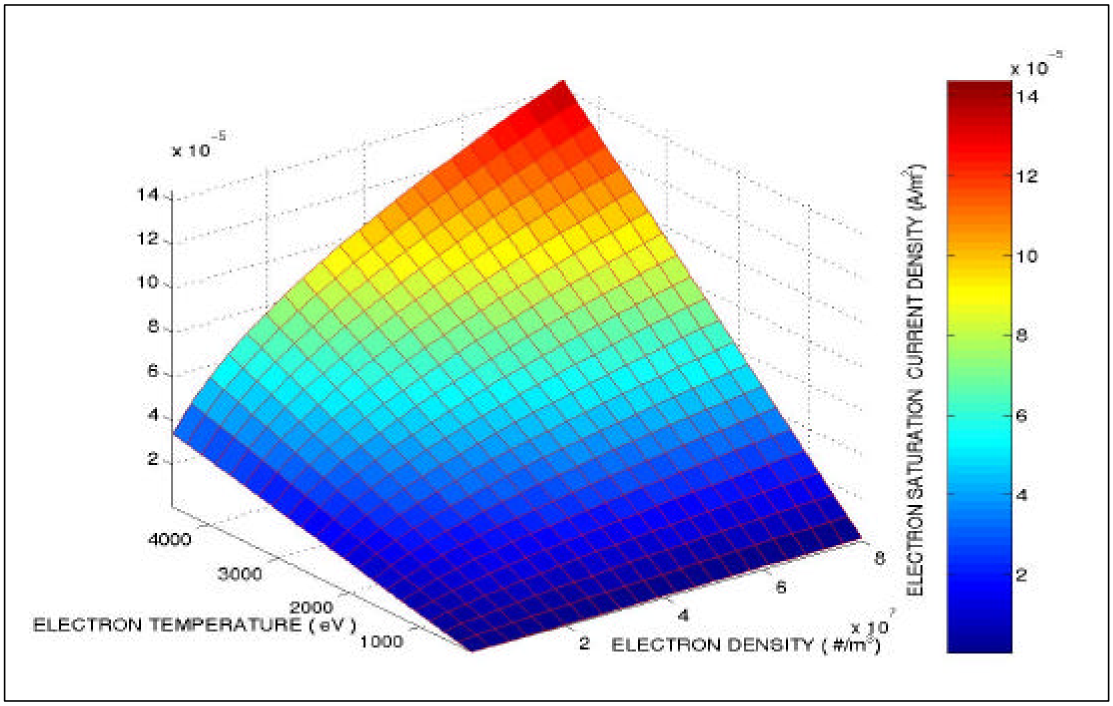

Figure 2-7. Plot of electron saturation current density as a function of electron temperature and electron density

In addition to the plasma current to the vehicle, light absorption results in emission of photoelectrons during the day. The flux of electron emission is proportional to the flux of absorbed photons. For the sake of simplicity, we assume that the emitted photoelectrons follow a Maxwellian velocity distribution characterized by an average temperature of T_{pe}. The photoelectron current density is

Eqn. 2-15 For $V_{sc} < 0$

$$J_{pe} = J_{pe0} = \text{const}$$

Eqn. 2-16 For $V_{sc} > 0$

$$J_{pe} = J_{pe0} \exp\left(\frac{-eV_{sc}}{kT_{pe}}\right)\left(1 + \frac{eV_{sc}}{kT_{pe}}\right)$$

where T_{pe} is temperature of photoelectrons.

So total current density to the vehicle can be given by the sum of the electron plasma current, ion plasma current, and photoelectron current as follows:

Eqn. 2-17 If $V_{sc} \leq 0$,

$$J_p = J_{e0}\exp\left(\frac{-e|V_{sc}|}{kT_e}\right) - J_{i0}\left(1+\frac{e|V_{sc}|}{kT_i}\right) - J_{pe0}$$

Eqn. 2-18 If $V_{sc} > 0$,

$$J_p = J_{e0}\left(1+\frac{eV_{sc}}{kT_e}\right) - J_{i0}\exp\left(\frac{-eV_{sc}}{kT_i}\right) - J_{pe0}\exp\left(\frac{-eV_{sc}}{kT_{pe}}\right)\left(1+\frac{eV_{sc}}{kT_{pe}}\right)$$

2.3. Modeling Spacecraft Charging

Spacecraft charging, especially differential charging has been of prime concern to spacecraft designers because of its detrimental effects such as electrostatic discharge in spacecraft and spacecraft subsystems. The Space Environments & Effects (SEE) program[70] is one of the tools available to model the plasma environment and spacecraft charging. In the SEE model the plasma parameters, spacecraft size, materials of different parts of spacecraft surface, and charging time can all be specified by the user. The program then predicts potentials of a finite number of elements of the spacecraft surface.

The transient response of a spacecraft in a plasma is calculated by modeling the spacecraft – ambient plasma system as an equivalent electric circuit. The SEE uses a simple three axis stabilized satellite model with a single solar array wing as shown in Figure 2-8a and a simplified circuit model for this satellite shown in Figure 2-8b. In this model, we assume that the satellite is entirely covered with a perfect conductor, e.g. conducting thermal blankets (blue), and that the only insulators are the solar cell cover glasses (green). The circuit has only three nodes: 1) 0 or Ground - magnetosphere potential, 2) V_A - Spacecraft chassis potential, and 3) V_B - Cover glass potential.

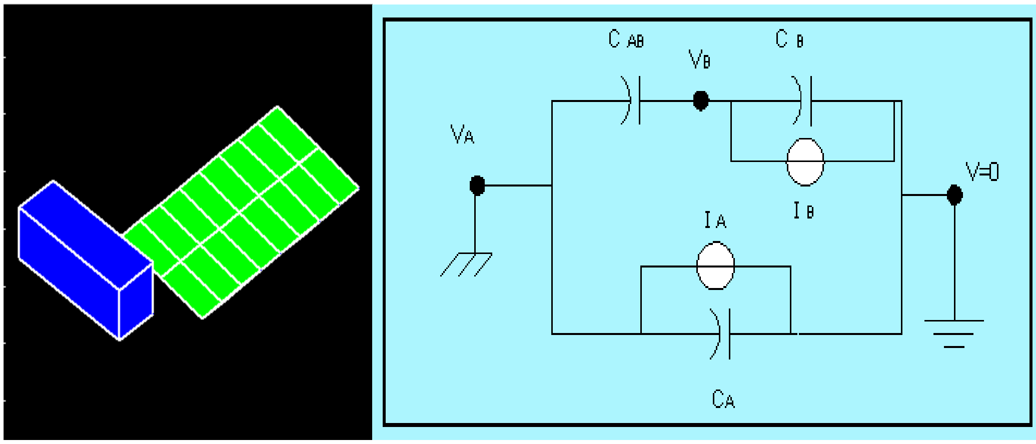

Figure 2-8. a) Simple geometric model and b) Equivalent circuit for spacecraft and ambient plasma used by the SEE Spacecraft Charging Handbook.

I_A and I_B are the currents from ambient plasma to the chassis of the spacecraft and solar array respectively. C_A is capacitance between spacecraft chassis surface and plasma. C_B is the capacitance between solar array and plasma. C_{AB} is capacitance between chassis and solar array. Typical values for these capacitances are $C_A \approx C_B \approx 4\pi\varepsilon_0 R \approx R \times 10^{-10}$ F. Where R (meters) is the effective spacecraft radius. C_{AB} is usually much larger as compared to C_A, and C_B.

We know that

Eqn. 2-19
$$\frac{dV}{dt} = \frac{I}{C}$$

where V is the potential, I is the current and C is the capacitance. The SEE program uses the same relation to calculate the changes in V_A, V_B and $(V_B\text{-}V_A)$ with respect to time as follows, Eqn. 2-20

$$\frac{dV_A}{dt} \approx \frac{dV_B}{dt} \approx \frac{I_A}{C_A} \approx -R \times 10^4 \text{ V/s}$$
$$\frac{d(V_B - V_A)}{dt} \approx \frac{I_B - I_C}{C_{AB}} \approx 10 \text{ V/s}$$

As discussed in Section 2.2, an isolated spacecraft in plasma will assume an equilibrium (or floating or absolute) potential given by Eqn. 2-10, such that the net current to the vehicle is zero. This absolute potential can reach up to tens of thousands of volts depending upon plasma parameters but it is not, by itself, hazardous to spacecraft operations. In the simplest application of the SEE program we can calculate the absolute potential of a spherical spacecraft made up of a single material. If we use a single material like Kapton or Teflon to build the entire spherical spacecraft of 1 m diameter, and if we select the ATS-6 Environment, the spacecraft shows absolute charging of tens of thousands of volts as shown in Figure 2-9.

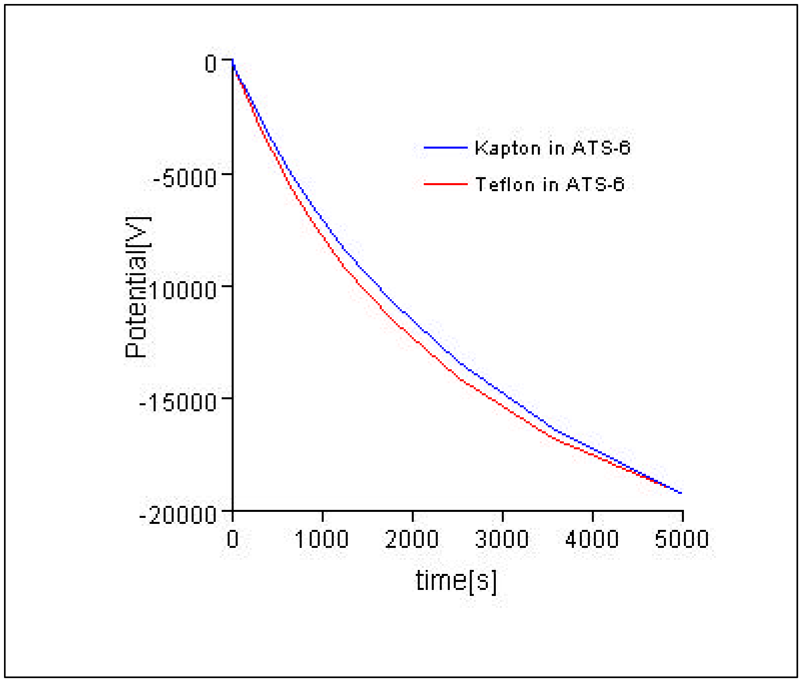

Figure 2-9. Potential Vs Time plot for spacecraft using Kapton and Teflon as materials and ATS-6 plasma environment.[70] (Spacecraft diameter: 1 m)

Differential charging occurs when different portions of the same spacecraft assume different potentials (voltages). It can occur because of more than one cause. Each exposed spacecraft surface will interact with the ambient plasma differently depending on the material composing the surface, whether that surface is in sunlight or shadow, and the flux of particles to that surface. When the breakdown threshold is exceeded between the surfaces or within the dielectrics, an electrostatic discharge (ESD) can occur. The ESD can couple into spacecraft electronics and cause upsets ranging from logic switching to complete system failure.

In the SEE program we can also select the complicated geometry for the typical communications satellite and different materials for its different parts as shown in Figure

2-10. In Figure 2-11, the potentials for different elements of spacecraft surface are shown in different colors.

Part	**Color**	**Material**
Chassis	Green	Kapton
Solar Arrays	Red	Solar Cells
Antenna	Blue	Teflon
Omni Antenna	Blue	Teflon

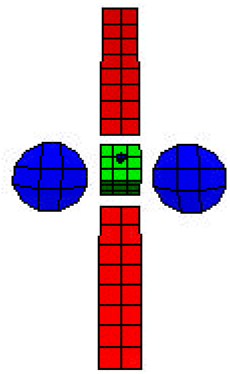

Figure 2-10. Materials selected for different parts of the spacecraft[70]

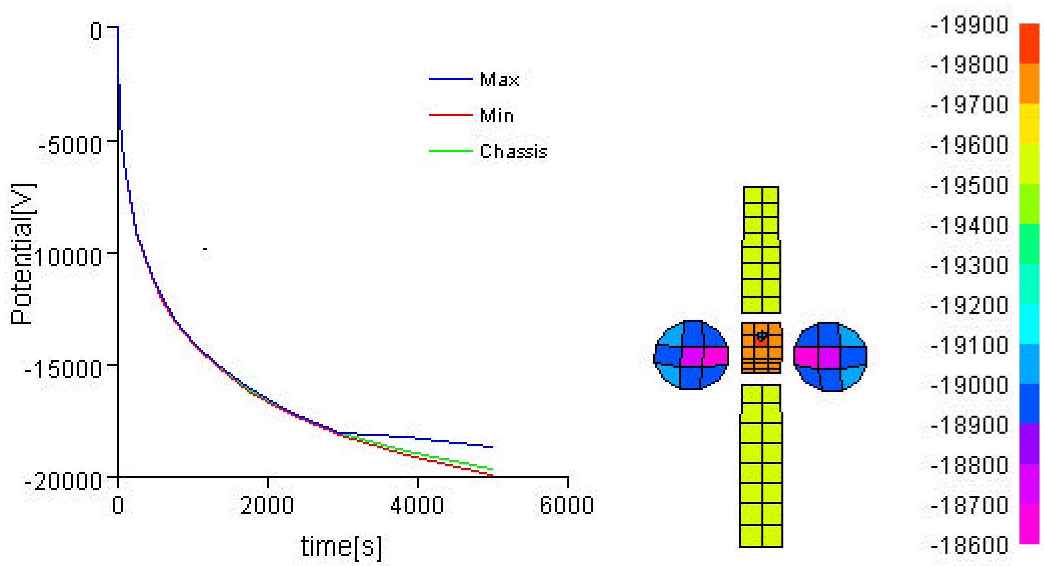

Figure 2-11. Max., min and chassis potential Vs time plot for the spacecraft[70]

3. Uncontrolled Spacecraft Interactions

This chapter addresses calculation of charge density on the spacecraft surface due to the ambient plasma interactions only, using surface potential values calculated from the NASA Interactive Spacecraft Charging Handbook. Electric dipole moment of the charged spacecraft will be determined. The electric force and electric torque acting on a spacecraft flying in a formation due to the other spacecraft in the formation will be computed. Assuming that an electric thruster will be used to negate the parasitic coulomb force and torque, propulsion requirements will be estimated.

3.1. Spacecraft Charging Predictions

As mentioned in section 2.3, we can simulate spacecraft charging using the SEE handbook. If we specify the plasma environment, the 3D geosynchronous surface charging tool of this program uses the Boundary Element Method (BEM) to compute self-consistent potentials and electric fields along the vehicle.

3.1.1. Spacecraft Geometry, Materials & Plasma Environment

The default spacecraft materials of the SEE code were used for these tests, which are shown in Figure 3-1.

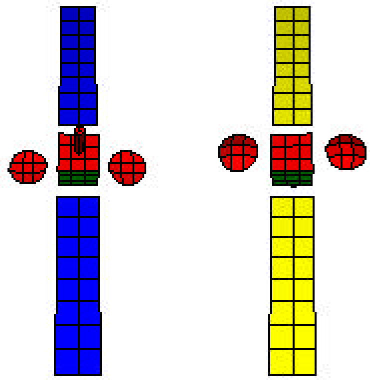

Part	Color	Size	Material
Chassis	Red Green	$1m \times 1m \times 1m$	Kapton OSR*
Solar Arrays	Blue Yellow	$1m \times 4m$	Solar Cells Black Kapton
Antenna	Red	$\phi 1m$	Kapton
Omni Antenna	Red	ϕ 0.2m, 1m long	Kapton

* : Optical solar Reflectors

Figure 3-1. Spacecraft model seen from the sun direction (left) and from the opposite direction (right)

The SEE code has three inbuilt plasma environments in GEO namely Worst-case environment, ATS-6 environment, and 4Sept97 environment. The specifications of these environments are given in Table 3-1.

Parameters	Plasma Environment		
	Worst-case	ATS-6	4Sept97
Electron Density in m^{-3}	1.12×10^6	1.22×10^6	3.00×10^5
Electron Temperature in eV	1.20×10^4	1.60×10^4	0.40×10^4
Ion Density in m^{-3}	2.36×10^5	2.36×10^5	0.30×10^6
Ion Temperature in eV	2.95×10^4	2.95×10^4	0.40×10^4

Table 3-1. Specifications of the inbuilt plasma environments in SEE code.

3.1.2. <u>Spacecraft Surface Potential Distributions</u>

The BEM solves for surface potentials using the vacuum Green's function.

Eqn. 3-1

$$4\,p\,e_0 V_i = \sum_j d^2\,|\bar{r}_j|\,\frac{s_j}{|\bar{r}_{ij}|} = \sum_j \frac{q_j}{|\bar{r}_{ij}|}$$

where i or j is the index number of surface element of the spacecraft, which are created automatically by the SEE program. V_i is potential of i^{th} surface element of the spacecraft, r_j is the position vector of j^{th} surface element of the spacecraft, $|\bar{r}_{ij}|$ is the vector directed from center of i^{th} element to the center of j^{th} element of spacecraft, σ_j is the surface charge density of the j^{th} surface element of the spacecraft, and q_j is the equivalent point charge located at the center of j^{th} surface element.

The spacecraft charging analysis was carried out in the eclipse and non-eclipse conditions for different plasma environments like ATS-6, Worst-case, and 4 Sept 97.

Figure 3-2 shows the potential distribution over all the surface elements of the spacecraft in the worst-case environment in non-eclipse conditions. The plot on left shows, how the maximum, minimum and, chassis potentials (blue, red, and green color respectively) change with time. It can be seen that the potential goes to –24 kV within 30000 seconds (8.33 hours). From the colored spacecraft graphics and scale on the right it is clear that the minimum potential –24 kV is at the spacecraft chassis and at the antennas. The maximum potential of –6 kV is observed at the outer ends of both the solar arrays. This view of spacecraft is from the side opposite to the sun.

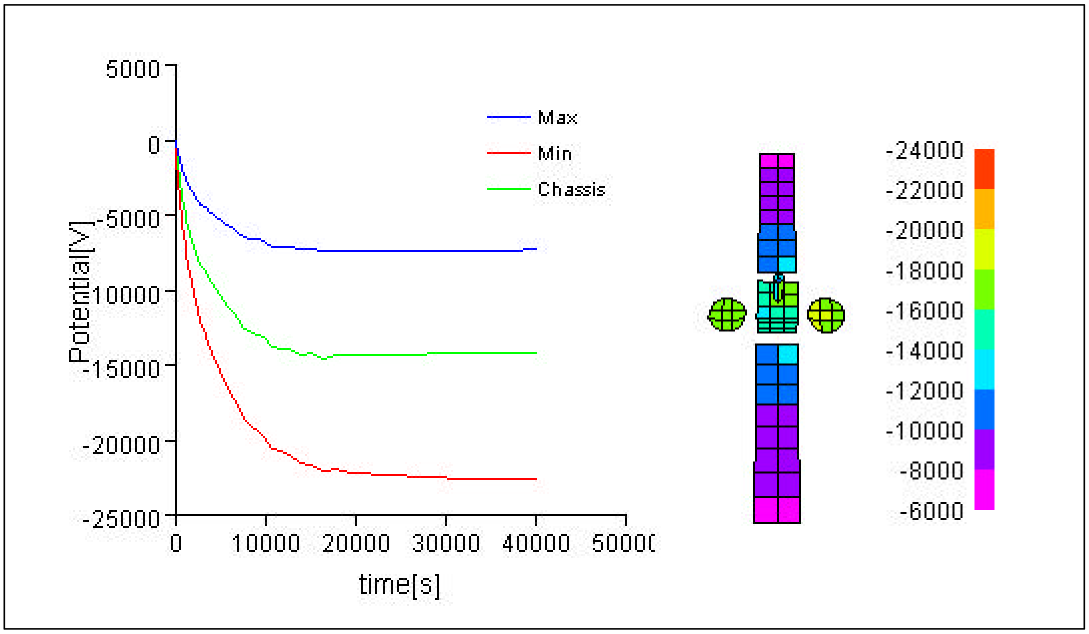

Figure 3-2. Potentials on the external surfaces of the spacecraft in the Worst-case environment in non-eclipse conditions

Figure 3-3 shows that in eclipse conditions the minimum potential of –24 kV is on the sun side of the chassis and antennas. The maximum potential of –10 kV is on the sun side of the outer ends of the solar arrays.

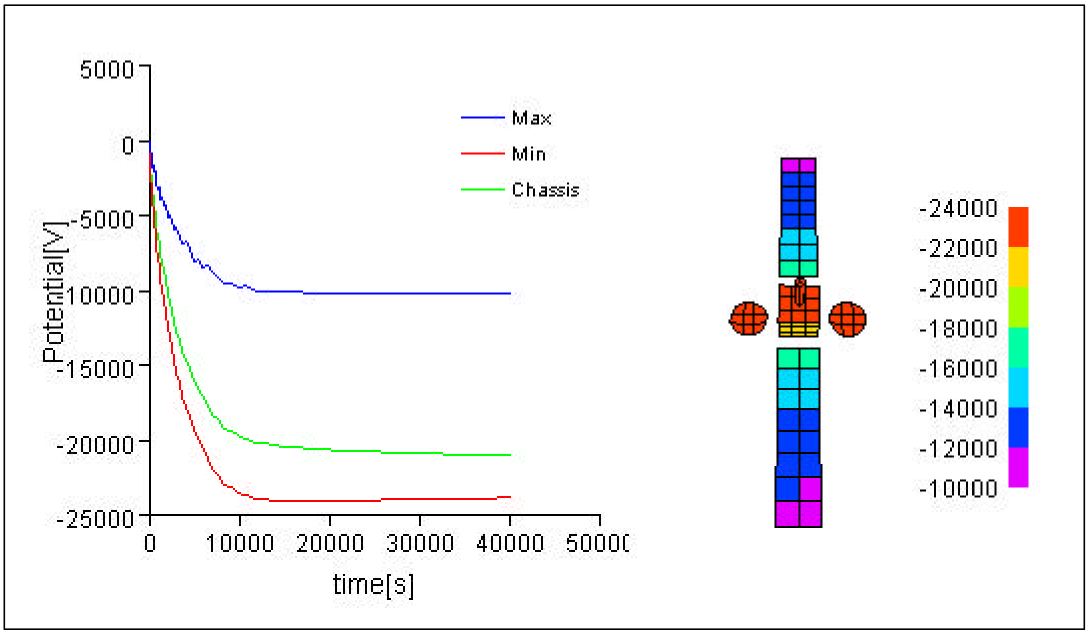

Figure 3-3. Potentials on the external surfaces of the spacecraft in the Worst-case environment in eclipse conditions

Figure 3-4 shows that in the ATS-6 environment in non-eclipse conditions, potential goes to –30 kV at the chassis and the maximum potential is –10 kV at the outer ends of the solar arrays. Both of these potentials are on the side of spacecraft, which is opposite to the sun.

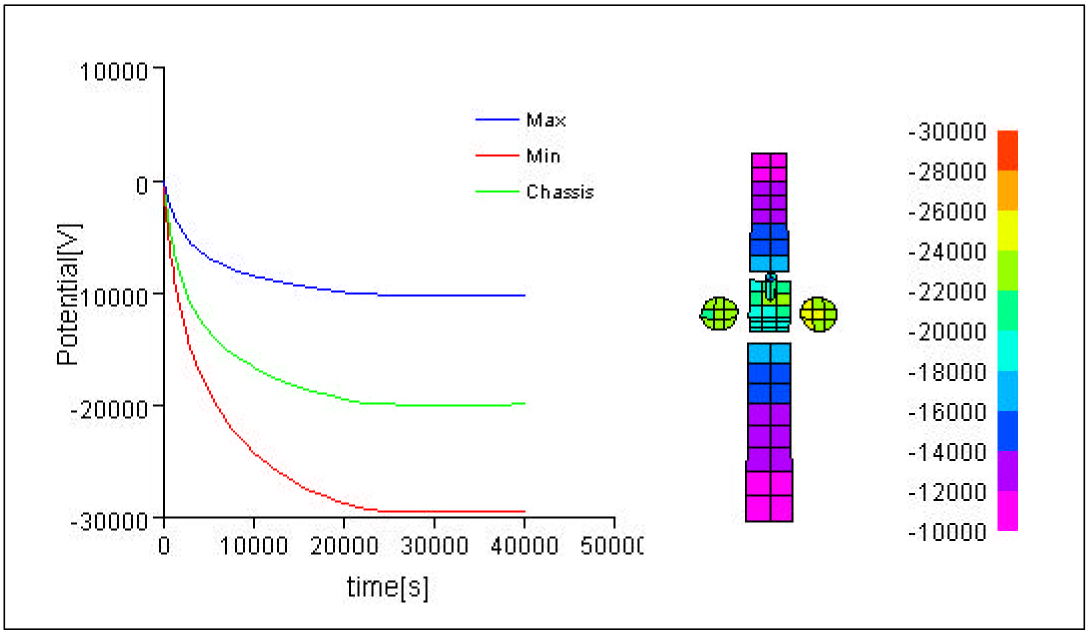

Figure 3-4. Potentials on the external surfaces of the spacecraft in the ATS-6 environment in non-eclipse conditions

Figure 3-5 shows that in the ATS-6, eclipse environment the minimum potential at the sun side of the chassis goes to –32 kV.

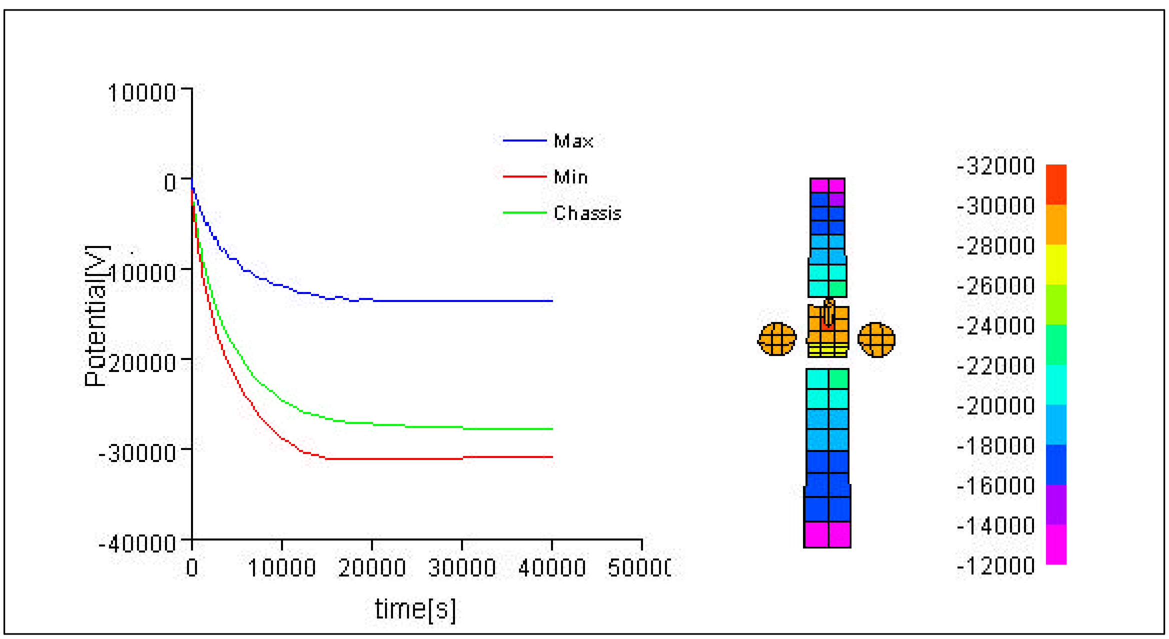

Figure 3-5. Potentials on the external surfaces of the spacecraft in the ATS-6 environment in non-eclipse conditions

Figure 3-6 shows the surface potential distribution of a spacecraft in 4 Sept 97, non-eclipse environment. The maximum potential is –1.6 V while the minimum potential is –4.4 V.

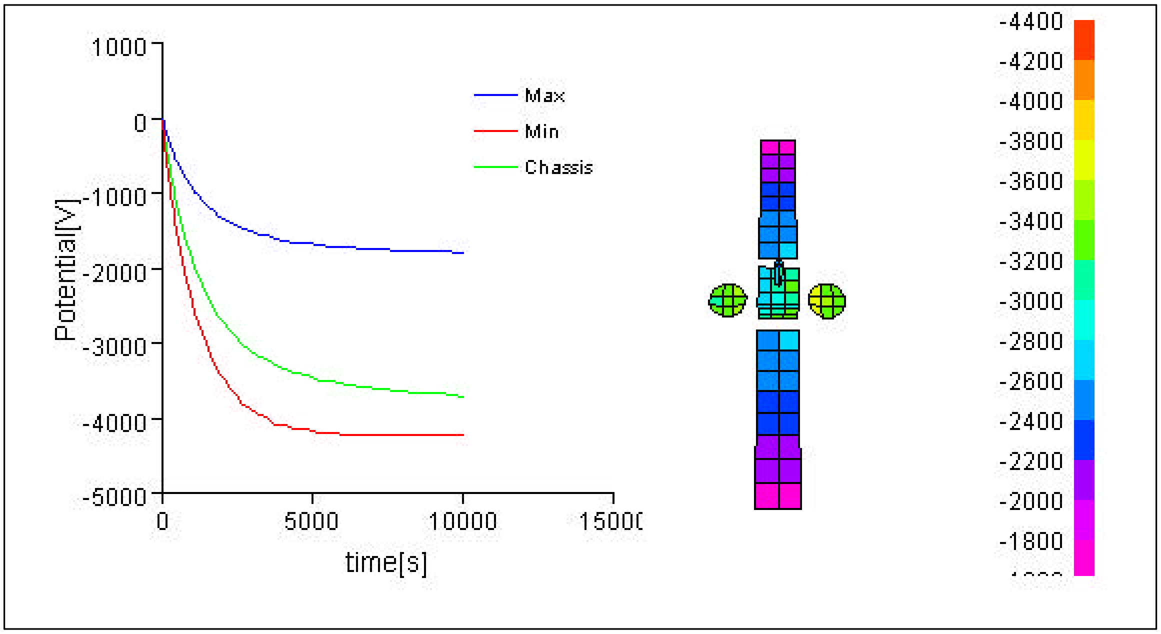

Figure 3-6. Potentials on the external surfaces of the spacecraft in the 4 Sept 97 environment in non-eclipse conditions.

Figure 3-7 shows the surface potential distribution in the 4 Sept 97, eclipse environment. The potential remains high as compared to the other two environments. The minimum potential is –4.2 kV at the chassis on the sun side of the spacecraft, and the maximum potential is –1.6 kV , at the outer ends of the solar arrays, as usual.

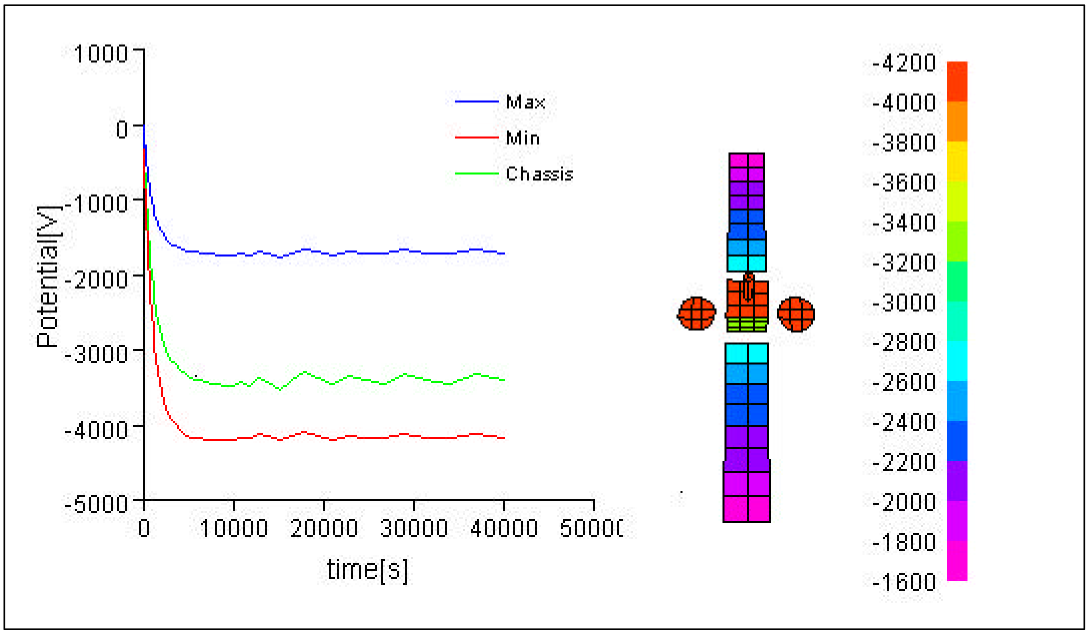

Figure 3-7. Potentials on the external surfaces of the spacecraft in the 4 Sept 97 environment in eclipse conditions.

3.2. Calculation of Dipole Moment

The output of SEE program is the potential at each of the surface elements and the position vector of the center of each surface element. Using Eqn. 3-1, we can calculate the equivalent point charge, q_i, at the center of each element.

The dipole moment of the i^th surface element of spacecraft can be written as,

Eqn. 3-2 $$\vec{p}_i = q_i \vec{r}_i$$

Total dipole moment of the spacecraft becomes,

Eqn. 3-3 $$\vec{p} = \sum_j q_j \vec{r}_j$$

Where j is the total number of surface elements created by the SEE program.

3.3. *Interactions between Two Spacecraft Flying in Formation at GEO*

Lets assume that two identical spacecraft SC_A and SC_B are flying together as shown in Figure 3-8 with their center of mass following the Geosynchronous Earth Orbit.

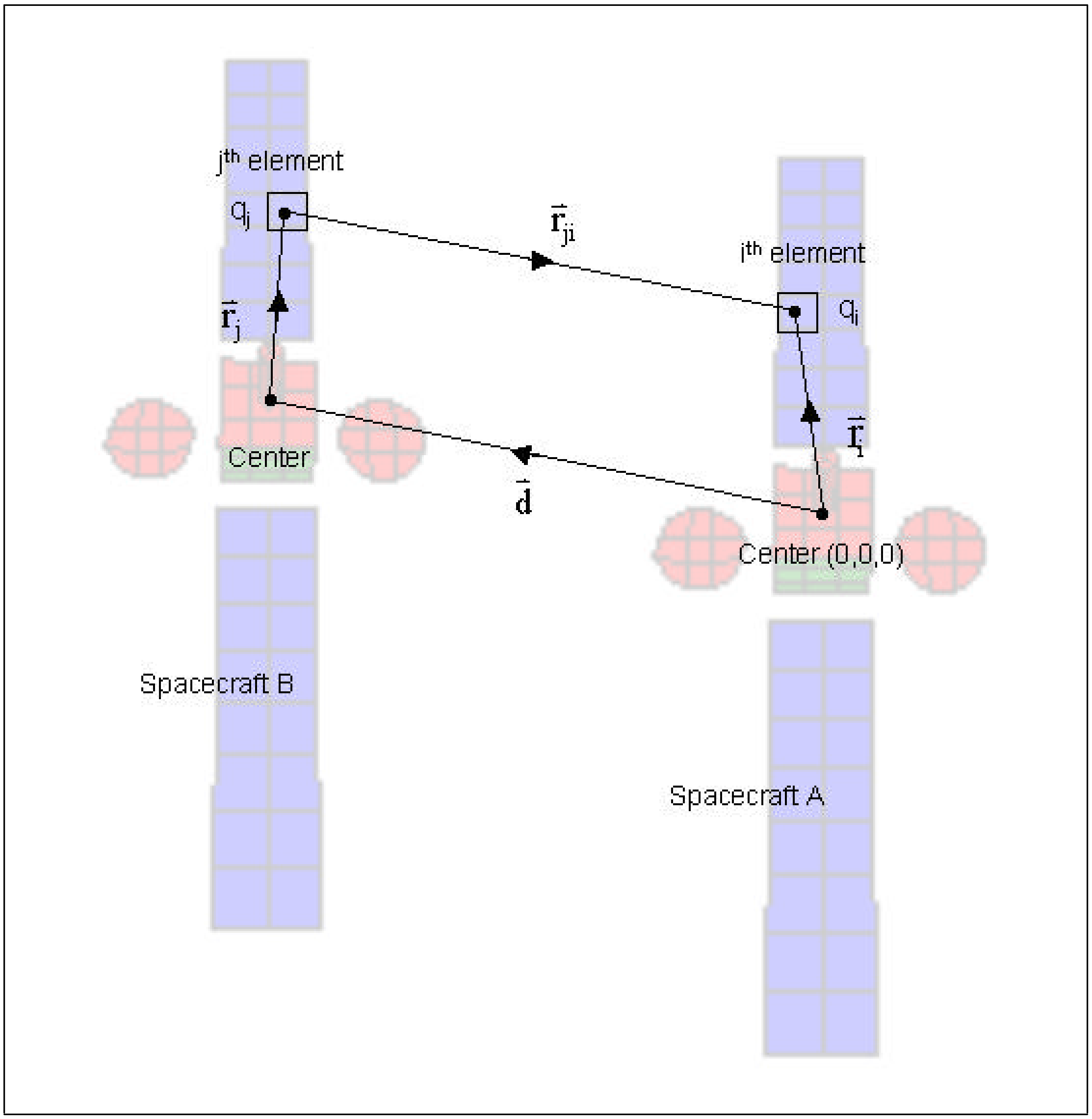

Figure 3-8. Vector diagram showing two spacecraft separated by distance $|\vec{d}|$

Where i (j) is the index number of surface elements on spacecraft A (B), N_A (N_B) is the number of total surface elements on spacecraft A (B), q_i (q_j) is the equivalent point charge at the center of ith (jth) element of spacecraft A (B), $\vec{r}_i$ ($\vec{r}_j$) is the position vector of ith (jth) element of spacecraft A (B), $\vec{d}$ is position vector of the center of spacecraft B w.r.t. the center of spacecraft A (0,0,0), and $\vec{r}_{ji}$ is the vector directed from the center of jth element of spacecraft B to the center of ith element of spacecraft A.

Total electric field $\vec{E}_i$ at the center of the ith element of spacecraft A due to charge distribution on the surface of spacecraft B can be given by,

Eqn. 3-4
$$\vec{E}_i = \frac{1}{4 p e_0} \sum_{j=1}^{N_B} \frac{q_j \, \vec{r}_{ji} \, e^{\frac{-|\vec{r}_{ji}|}{?_d}}}{|\vec{r}_{ji}|^3},$$

Where $?_d$ is the ambient plasma Debye length defined in Eqn. 2-7.

From Eqn. 3-2, the dipole moment of the ith element of spacecraft A will be

Eqn. 3-5
$$\vec{p}_i = q_i \vec{r}_i \, .$$

The force acting on ith element of spacecraft A due to the total charge on spacecraft B will be,

Eqn. 3-6
$$\vec{F}_i = q_i \vec{E}_i$$

Total force acting on spacecraft A due to charge on spacecraft B will be,

Eqn. 3-7
$$\vec{F} = \sum_{i=1}^{N_A} \vec{F}_i$$

The torque acting on ith element of spacecraft A due to charge on spacecraft B will be,

Eqn. 3-8
$$\vec{T}_i = \vec{p}_i \times \vec{E}_i$$

So the total torque acting on spacecraft A, i.e. $\vec{T}$, due to the charge on spacecraft B will be,

Eqn. 3-9
$$\vec{T} = \sum_{i=1}^{N_A} \vec{T}_i$$

Using the surface potentials calculated in the SEE code (see Figure 3-2 to Figure 3-7) and Eqn. 3-1 to Eqn. 3-9, we can calculate the net Coulomb force and torque due to two (or more) spacecraft separated by some distance $|\vec{d}|$. In order to estimate the magnitude of Coulomb force and torque within a close formation, this section assumes that two identical spacecraft are separated by a distance $|\vec{d}|$ in the orientation shown in Figure 3-9. The two vehicles are assumed to be in GEO orbit with the environmental conditions shown in Table 3-1.

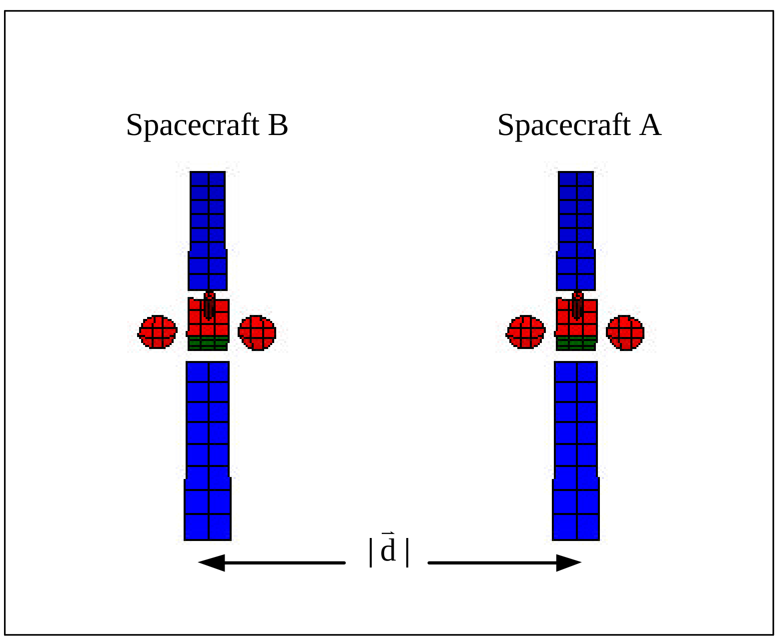

Figure 3-9. Two identical spacecraft separated by distance $|\vec{d}|$

Figure 3-10 shows the force and torque between spacecraft A and B due to charge on both of them as a function of the separation between these two spacecraft and the plasma environment. They are calculated using the SEE program and the Matlab-6.0 program (given in Appendix) implementing Eqn. 3-1 to Eqn. 3-9. For torque calculations, total electric field at the center of spacecraft A ($\vec{E}_{center}$) due to charge distribution over the surface of spacecraft B, and the total dipole moment of spacecraft A ($\vec{P}_{total}$) were calculated. The torque on spacecraft A will be maximum when the angle between $\vec{E}_{center}$ and $\vec{P}_{total}$ is 90 or 270 degrees. This maximum torque was considered wherever Coulomb torque between spacecraft A and B was required.

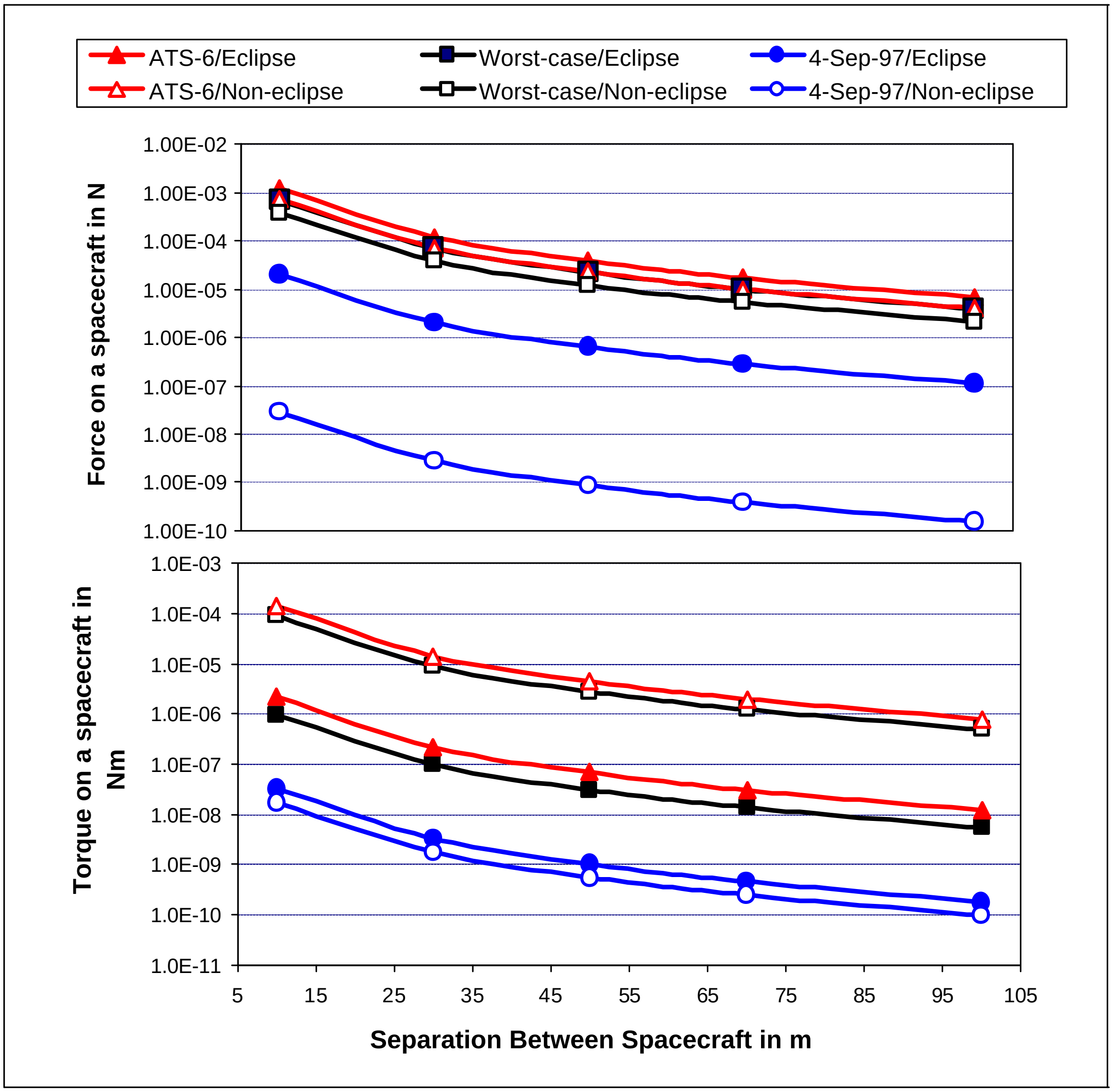

Figure 3-10. Plots of the electric force and torque between spacecraft A ad B Vs separation between them in different plasma conditions.

Thus it can be seen that the Coulomb force between spacecraft is as high as a millinewton in the ATS-6 environment in eclipse conditions. It reduces to 10^{-7} mN in the 4 Sept 97 environment in Non-eclipse conditions. The torque on the spacecraft is as high as 10^{-4} Nm in the ATS-6 environment in Non-eclipse conditions. It reduces to 10^{-10} Nm in the

4 Sept 97 environment in eclipse conditions. The Coulomb force and torque are in decreasing order in the ATS-6, Worst-case and 4 Sept 97 environment. For the same kind of environment, the Coulomb force is more in Eclipse conditions than that in Non-eclipse conditions while the torque is more in Non-eclipse conditions than that in eclipse conditions (exception: for the 4 Sept 97 environment, the torque in Eclipse condition is more than that in Non-eclipse condition).

3.4. Propulsion Requirements to Maintain Formation

Electric thrusters can be used to compensate for the electric force and torque explained in Section 3.3. The candidate microsatellite thruster technologies considered here are MicroPPT, Colloid Thrusters and FEEP. These technologies are discussed in detail in Section 5.1.

3.4.1. Mission Parameter Calculations for Thruster Technologies

Suppose the thruster is mounted at one corner of the chassis ($1\text{m} \times 1\text{m} \times 1\text{m}$) of spacecraft A as shown in the figure Figure 3-11. The maximum thrust $\vec{F}_{max}$ that this thruster should produce to compensate for the torque acting on spacecraft A, will be,

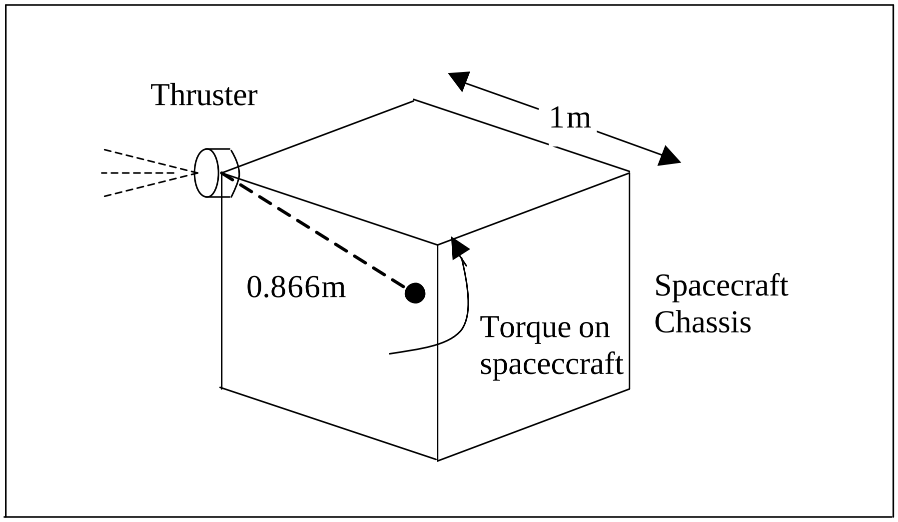

Figure 3-11. Thruster mounted on the corner of spacecraft chassis to compensate for the electric torque acting on it.

Eqn. 3-10
$$\vec{F}_{max} = \frac{\text{Max.Torque on Spacecraft A}}{0.866}$$

where 0.866 m is the length of moment arm. The maximum thrust $\vec{F}_{max}$ to be produced by the thruster to compensate for the Coulomb force between the spacecraft will be equal and opposite to the Coulomb force on these individual spacecraft. As seen in the Figure 3-10, for a specific plasma environment, the Coulomb force was more in eclipse conditions as compared to non-eclipse conditions while the Coulomb torque was more in non-eclipse conditions as compared to eclipse conditions. Therefore, while calculating maximum power, or inert mass requirements respective conditions should be taken in to account to find $\vec{F}_{max}$.

Maximum power requirement P_{max}, for an electric thruster to compensate for the maximum torque acting on spacecraft A, in a specific plasma environment is given by, Eqn. 3-11 $$P_{max} = \frac{|\vec{F}_{max}|\, g_0 I_{sp}}{?}$$

where $\vec{F}_{maz}$ is given by Eqn. 3-10, g_0 is gravitational constant, and ? is the thruster effciencey. The power supply (inert) mass of the thruster required to compensate for torque becomes,

Eqn. 3-12 $$m_{inert} = ßP_{max} = \frac{ß|\vec{F}_{max}|\, g_0\ I_{sp}}{?}$$

Where ß is power-specific mass of the thruster in kg / W.

The required propellant mass can be calculated from the total impulse needed during the mission. As the satellite will be in eclipse conditions for half of the mission lifetime t , and in non-eclipse conditions for the other half of the mission lifetime. So total impulse $\vec{I}_{Total}$, necessary to be generated by the thruster to compensate for torque will be,

Eqn. 3-13 $$|\vec{I}_{Total}| = \frac{t}{2}\left(|\vec{F}_{max(eclipse)}| + |\vec{F}_{max(non-eclipse)}|\right)$$

Mass of the propellant required for the thruster to compensate for torque will be,

Eqn. 3-14 $$m_{prop} = \frac{|\vec{I}_{Total}|}{g_0 I_{sp}} = \frac{t\left(|\vec{F}_{max(eclipse)}| + |\vec{F}_{max(non-eclipse)}|\right)}{2\, g_0 I_{sp}}$$

Total mass of the propulsion system to compensate for parasitic Coulomb torque becomes,

Eqn. 3-15 $$\begin{aligned} m_{sys} &= m_{inert} + m_{prop} \\ &= \frac{ß|F_{max\,(non\text{-}eclipse)}|\, g_0\ I_{sp}}{?} + \frac{t\left(|\vec{F}_{max(eclipse)}| + |\vec{F}_{max(non-eclipse)}|\right)}{2\, g_0 I_{sp}} \end{aligned}$$

To compensate for the Coulomb force acting on the spacecraft the maximum thrust will be equal to the maximum force on the spacecraft A during eclipse conditions, which should be considered while calculating maximum power requirement and inert mass.

3.4.2. Comparative Mission Trade Study

The candidate thruster technologies considered here i.e. MicroPPT, Colloid thruster, and FEEP are compared for the mission parameters discussed in Section 3.4.1. The maximum power and total mass of electric propulsion system required to compensate for Coulomb force and torque are plotted against the spacecraft separation for different electric propulsion technologies in the ATS-6 and 4 Sept 97 plasma environments as shown in Figure 3-12. The Coulomb force and torque observed in the Worst-case environment are a little bit less than those observed in the ATS-6 environment. Therefore, the power and mass of electric propulsion systems required in the Worst-case environment are just less than those required in the ATS-6 environment. Hence, the parameters in the Worst-case environment are not plotted to avoid complexity.

Figure 3-12(a) shows that the maximum power P_{max} required to compensate for the Coulomb force. It is as high as 150 Watts for MicroPPT in the ATS-6 environment for a separation of 10 m between the spacecraft. It reduces to almost a miliwatt for Colloid thruster in the 4 Sept 97 environment for separation of 100 m between the spacecraft. P_{max} is in decreasing order for MicroPPT, FEEP, and Colloid thruster for the same type of environment and the same spacecraft separation. Also P_{max} is in decreasing order for the ATS-6, Worst-case and 4 Sept 97 environment for the same type of thruster and the same spacecraft separation. P_{max} goes on decreasing with increase in the spacecraft separation for the same kind of electric thruster and the plasma environment. For any environment, the Coulomb force is more in eclipse conditions than that in non-eclipse conditions, so maximum power is calculated considering force in eclipse conditions.

Figure 3-12(b) shows plot of P_{max} of thruster to compensate for torque Vs separation between spacecraft. It is as high as 15 Watts for MicroPPT in the ATS-6 environment for a separation of 10 m between the spacecraft. It reduces to almost a microwatt for Colloid thruster in the 4 Sept 97 environment for separation of 100 m between the spacecraft. The plots show a trend, which is very similar to that seen in Figure 3-12 (a). Also as the Coulomb torque is more in non-eclipse conditions than that in eclipse conditions (4 Sept 97 environment is an exception), maximum power is calculated considering the torque in non-eclipse conditions.

Figure 3-12(c) shows plot of electric propulsion system mass m_{sys} to compensate for the Coulomb force on a spacecraft Vs the separation between spacecraft. Propellant mass required for 10 years mission is considered while calculating this m_{sys}. m_{sys} required is about 100 kg for MicroPPT in the ATS-6 environment for a separation of 10 meters. It is a little bit less than 10^{-3} kg for Colloid thruster in the 4 Sept 97 environment for a separation of 100 meters. For the same type of electric thruster and plasma environment, m_{sys} goes on decreasing with increase in the separation between spacecraft. m_{sys} is in decreasing order for the ATS-6, Worst case and 4 Sept 97 environment for the same type of thruster and the same spacecraft separation. Also it is in decreasing order for MicroPPT, FEEP and Colloid thruster for the same kind of plasma environment and the same spacecraft separation.

Figure 3-12(d) shows plot of m_{sys} to compensate for the Coulomb torque on a spacecraft Vs spacecraft separation. m_{sys} is more than 10 kg for MicroPPT in the ATS-6 environment for a separation of 10 meters. It is less than a milligram for Colloid thruster in the 4 Sept 97 environment for a separation of 100 meters. It shows the same trends seen in Figure 3-12(c).

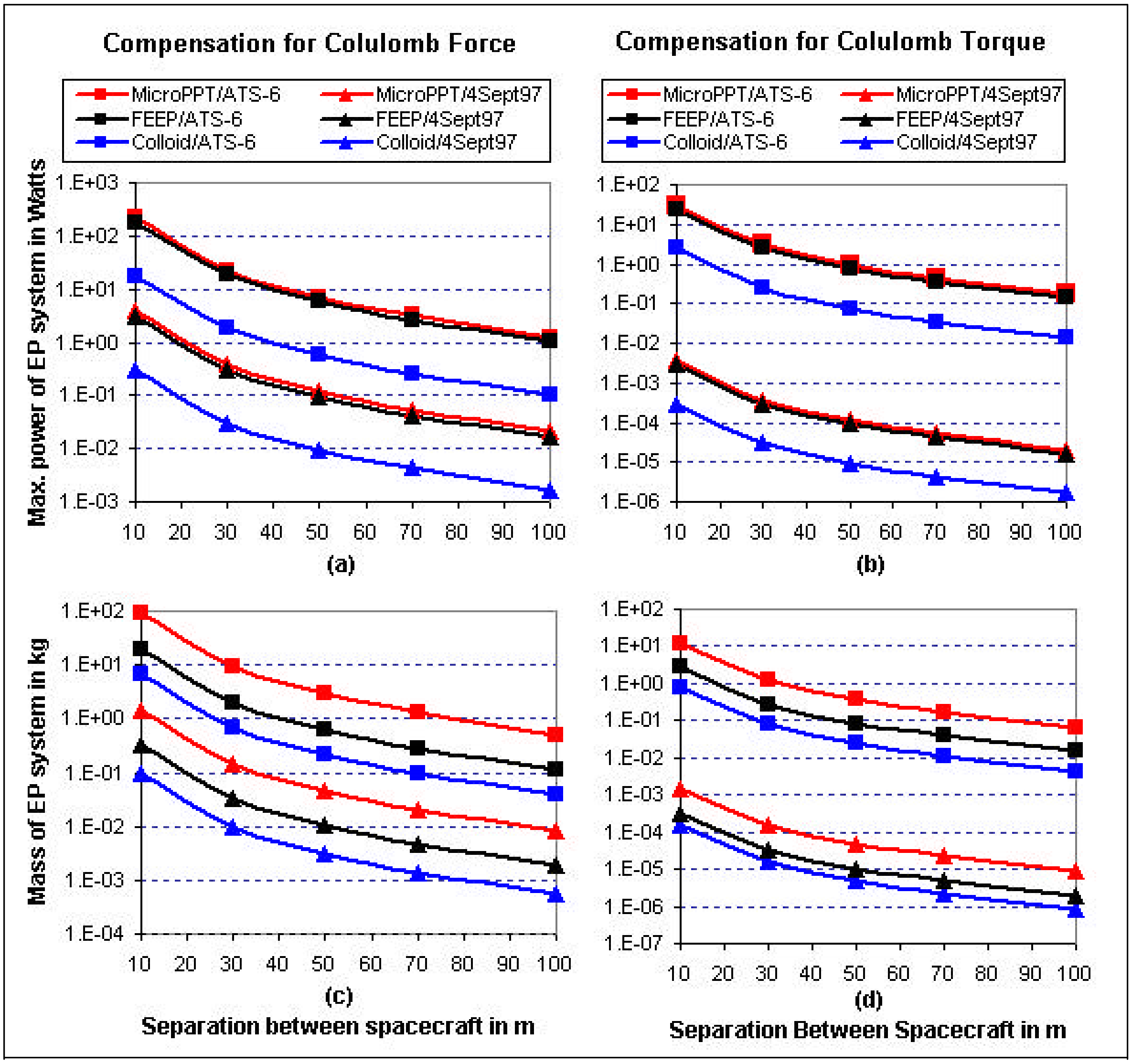

Figure 3-12. Plots of maximum power and mass of propulsion system required compensating for the Coulomb force and torque Vs spacecraft separation, for different electric propulsion systems in the ATS-6 and 4 Sept 97 environment.

Figure 3-13 shows plots of the total power and total electric propulsion (EP) system mass, to compensate for both the Coulomb force and torque acting on a spacecraft Vs spacecraft separation. The total power is the sum of powers of EP systems required to compensate for the Coulomb force and torque. Similarly total EP system mass is the sum of masses of EP systems required to compensate for the Coulomb force and torque.

.

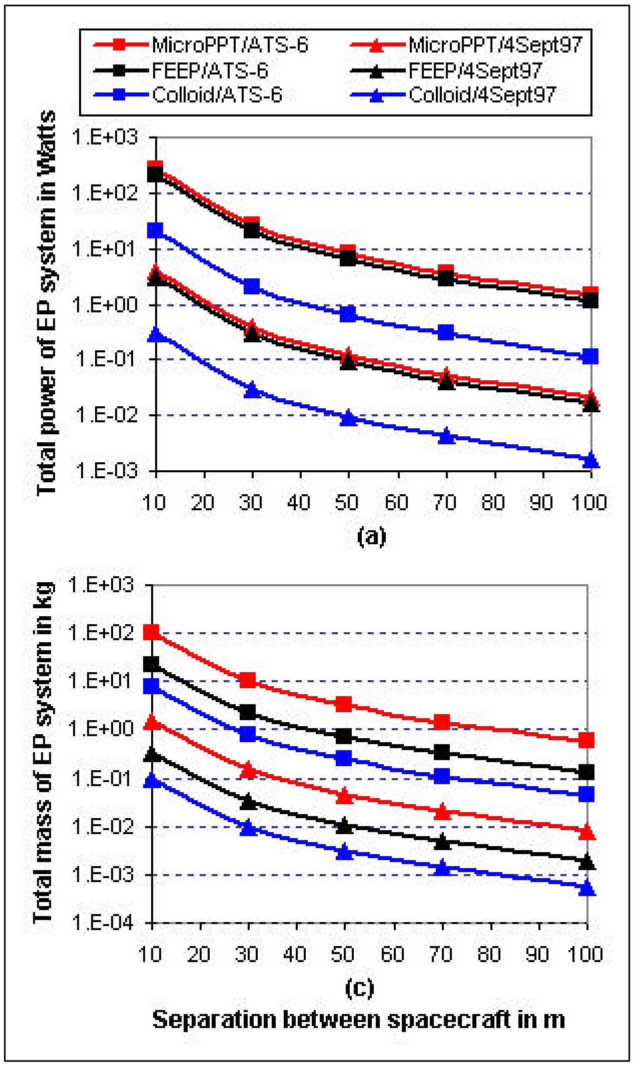

Figure 3-13. Plots of total power and total mass of EP system required compensating for both the Coulomb force and torque Vs spacecraft separation, for different EP systems in the ATS-6 and 4 Sept 97 environment.

4. Active Coulomb Control System

The innovative concept of Coulomb control system will be discussed in detail. The spacecraft configurations considered while developing this idea will be explained. Performance of the Coulomb control system in terms of input power, propulsion system mass, and specific impulse will be evaluated for two body as well as multi body formations.

4.1. Coulomb Control Concept

4.1.1. Objective of the Coulomb control technology

All spacecraft propulsion systems flown to date operate according to the rocket principle: mass is ejected from a vehicle to affect momentum transfer and propulsive force. Varieties on this principle utilize chemical reactions to accelerate the mass as well as electromagnetic forces, however the thruster lifetime is fundamentally constrained by the amount of mass (propellant) available on board.

The goal of this research is to investigate the feasibility of achieving nearly propellantless control of satellites in a formation using Coulomb forces between vehicles. This concept will rely on interaction with ambient space plasma and the active emission of electric charge from the vehicle to control spacecraft charging. Attractive and repulsive Coulomb forces between vehicles can be adjusted to maintain the relative cluster formation. This novel propulsive scheme may utilize a negligible amount consumables, enable high-precision close-formation flying superior to conventional thruster technology, eliminate thruster plume exhaust contamination of neighboring spacecraft, and provide a mechanism for configuring a formation into a "safe" collision-avoidance mode in the event of position uncertainty.

4.1.2. Existing Technology

Formation flying will require a propulsion system, which can impart highly controllable, repeatable, and low level thrust to the individual microspacecraft for formation keeping and attitude control. Even with the high specific impulse available from conventional electric propulsion thrusters, maintaining a formation by forcing individual satellites to occupy non-Keplerian orbit paths will require continuous thrusting over the lifetime of the mission. Over a five- to ten-year mission, such continuous thrust requirements will place heavy demands on thruster reliability and operational lifetime.

For widely spaced formations (inter-spacecraft separation on the order of 100 m or more), the fine-positioning requirements may be met with conventional electric propulsion thrusters. However, for very closely spaced swarms, current propulsive systems are not well suited to perform precision formation flying. For space interferometry, configurations are envisioned where the inter-satellite spacing is less than ten meters. In such a tight swarm, precision formation keeping will be extremely difficult. Existing thruster technologies that have been identified as the most promising tools for accomplishing such tight-formation flying include micro pulsed-plasma thrusters (micro PPT's), field-emission electric propulsion (FEEP) thrusters, and colloid thrusters.[21] Although all of these thrusters are technologically immature, each device is capable, in principle, of generating controllable micro-Newton levels of thrust.

Propellant-emitting thrusters will pose a spacecraft integration/contamination problem for tight satellite formations. Each of the thruster technologies currently under development will exhaust damaging propellant. For many spacecraft operating in close proximity, the microthruster propellant (vaporized Teflon for PPT's, liquid cesium for FEEP, and NaI-doped liquid glycerine for colloid) has a high likelihood of contaminating sensitive spacecraft surfaces, optics, and other instruments on neighboring craft. Such contamination would be incompatible with high-resolution imaging systems. In addition to material contamination problems, the potential exists for exhaust plume impingement forces to be transmitted from one spacecraft in the constellation to another, greatly complicating the fine position control.

4.1.3. Overview of Coulomb Concept

The concept proposed in this thesis uses the principle of Coulomb attraction/repulsion between charged bodies to control the spacing between nodes of a microsatellite cluster. The Coulomb control principle is most easily conveyed by examining the interaction between two neighboring bodies capable of transferring electric charge. Much more detailed analysis of the physical processes will be presented in later sections.

Consider, for instance, two vehicles separated by a distance *d* in space. Initially, both spacecraft are electrically neutral, i.e., the amount of negative charge (electrons) is equal to the amount of positive charge producing a net vehicle charge of zero and no interaction between the craft. Now, allow one craft to change its charge state through the emission of electrons. This is a trivial process utilizing an electron-gun or similar cathode device. If the electron beam is used to transfer an amount of negative charge, q_{SC}, from spacecraft 1 (SC1) to spacecraft 2 (SC2), the net negative charge of SC2 will equal the net postive charge remaining on SC1, producing an attractive force between the spacecraft given by

Eqn. 4-1

$$F_0 = \frac{1}{4 p e_0} \frac{q_{SC}^2}{d^2} .$$

where e_0 is the permittivity of free space. The charge required to produce a 10 μN attractive force at a spacecraft separation of d = 10 m is $q_{SC} = 3.3x10^{-7}$ C. Thus, using a 1-mA electron beam current, this charge can be transferred in only 330 μsec.

For discussion purposes, consider 1-m spherical spacecraft (radius of 0.5 m). The potential of the charged-spacecraft surface can be evaluated from Gauss' law as:

Eqn. 4-2

$$V_{SC} = \frac{1}{4 p e_0} \frac{q_{SC}}{r_{SC}} ,$$

where V_{SC} is the spacecraft potential in volts and r_{SC} is the spacecraft radius. For a charge of $q_{SC} = 3.3x10^{-7}$ C and radius of r = 0.5 m, the surface of SC1 will assume a positive potential of 6 kV, while V_{SC2} = -6 kV. Thus, a 12-kV electron beam must be used in order to allow the charge from SC1 to "climb the hill" and reach the surface of SC2. The minimum power required to generate a 10 μN attractive force in 330 μsec between the spacecraft separated a distance d = 10 m is then only 12 Watts. This power can be reduced if longer charging time is acceptable.

It is perhaps more intuitive to discuss inter-spacecraft Coulomb forces in terms of the spacecraft potential in volts, V_{SC}. By combining the above equations, the Coulomb force between two spacecraft can be written as

Eqn. 4-3

$$F_0 = 4 p e_0 \frac{r_{SC1} r_{SC2} V_{SC1} V_{SC2}}{d^2} .$$

Spacecraft charging has historically been associated with negative impacts on satellite payloads. Arcs and other breakdown phenomena arising from such differential charging can wreak havoc on sensitive electronics. Differential charging results when some regions of a spacecraft assume electric potentials drastically different from other regions of the same vehicle. The induced intra-vehicle electric fields can cause spontaneous interruption of payload functions. In this proposal, *absolute* spacecraft charging is proposed as a formation controlling method. If adjusted uniformly over a vehicle, the spacecraft absolute potential with-respect-to space, V_{SC}, can be driven to large values (such as many kilo-volts) with no impact to spacecraft functions and no risk of arc or spontaneous failure.

4.1.4. <u>Supporting Flight Heritage</u>

A wealth of pertinent data and experience is available from the results of the SCATHA flight experiment. The SCATHA satellite was launched in January, 1979 with the goal of measuring the build-up and breakdown of charge on various spacecraft components and to characterize the natural environment at GEO altitudes.[71]

The satellite potential with respect to space plasma potential was monitored on the SCATHA craft. During passive operation of the satellite, the spacecraft potential was seen to vary from near ground to many kilovolts negative. This is a common occurrence. An isolated passive body immersed in plasma will accrue a net negative charge due to the higher mobility of electrons as compared to heavy ions. For hot plasma such as that found at MEO-GEO, this negative charge is substantial. One goal of the SCATHA mission was to test the validity of actively controlling the spacecraft potential by emitting charge through an electron beam. To this end, an electron gun was used to transfer charge from SCATHA to the space plasma at various current and voltage levels up to 13 mA and 3 kV.

Due to the plasma environment, spacecraft routinely charge to negative voltages. However, a very important result, as reported by Gussenhoven, et al., was that, "*the electron beam can achieve large, steady-state changes in the vehicle potential and the returning ambient plasma*."[72] In fact, Gussenhoven found that when a 3 kV electron beam was operated, "*the satellite became positively charged to…a value approaching beam energy for 0.10 mA*" emission current. Similarly, Cohen, et al. report that "*spacecraft frame and surfaces on the spacecraft went positive with respect to points 50 meters from the satellite when the gun was operated. Depending upon ejected electron currents and energies, spacecraft frame-to-ambient-plasma potential differences between several volts and 3 kV were generated*."[73]

For rough estimation, we can approximate the SCATHA spacecraft as a sphere with a diameter of 1.7 m.[74] If an identical SCATHA spacecraft had been in orbit simultaneously, the satellite potential control demonstrated on this 1979 mission would have been sufficient to actively generate attractive and repulsive forces between the vehicles with magnitudes up to almost 10 μN over 10 meters, at a power expense of only 3 Watts. In addition to the SCATHA data, during a separate flight-experiment the ATS-6 spacecraft demonstrated charging as high as 19 kV.[75,76] Assuming a spacecraft diameter on the order of 1 meter, findings hint at the possibility to generate and control forces of hundreds of μN.

4.2. *Formation Geometries Considered in Study*

Although the Coulomb control concept explored in this thesis could conceptually be used for any mission requiring close formation flying, the strengths of the concept strongly coincide with the needs for interferometric imaging as outlined in the previous section. As such, the formation geometries studied in the reported work were slanted towards interferometry applications.

Based on discussions in Section 1.2, visible interferometry involving full, instantaneous u-v coverage can be said to have two overarching requirements: 1) the vehicles must fly in close formation, with spacing on the order of the vehicle dimension, and 2) the optical path length between any collector and the combiner must be equal. Based on these rough guidelines, four fundamental formation geometries of increasing sophistication were studied in the context of Coulomb control. The geometries will be summarized here, with more details provided in Section 5.2.

4.2.1. Earth Orbiting 3-Satellite Formation

The first set of formations studied included only three spacecraft. Conceptually, the formation can be thought of as two collectors and a single combiner. The vehicles were constrained to a straight line, with the combiner located midway between the collectors, flying in formation in Earth orbit. Three variations on this formation, depending upon the relation between the formation axis and the orbital velocity vector, were studied to investigate the fundamental nature of Coulomb control on a simplified system. Schematics of the various three-spacecraft formations can be found in Section 5.2.1.

4.2.2. *Earth Orbiting 5-Satellite Formation*

In an incremental increase in the complexity of the formation, a geometry of four collector vehicles surrounding a single combiner satellite was considered within Earth orbit. A diagram of this formation is shown in Figure 5-7. The 5-satellite formation maintained geometrical simplicity, while retaining the two overarching constraints for full, instantaneous u-v coverage. The orientation of the formation was chosen to loosely represent a visible Earth observing array operating from geosynchronous orbit.

4.2.3. *Earth Orbiting 6-Satellite Formation*

The first step towards analyzing a sophisticated, yet practical, interferometry configuration was performed by analyzing the dynamics of a 6-Satellite formation. The geometry of the formation was chosen to represent the optimized five-aperture (pentagonal) Cornwell array of Figure 1-3, with a central combiner included in a free orbit. The entire formation was analyzed in an Earth orbital environment, representative of either a visible Earth imager or an astronomical platform.

4.2.4. *Rotating 5-Spacecraft Formation*

The final formation geometry analyzed was chosen in order to analyze the suitability of Coulomb control for the Terrestrial Planet Finder (TPF) mission under consideration by NASA. For the TPF mission, an array of four collectors and a single combiner are planned. The entire five-vehicle formation is constrained to a straight line, rotating rigidly about the center vehicle. Rather than operating within Earth orbit, the TPF mission has been designed to occupy one of the Earth-Sun Lagrange points, thus the formation local dynamics can ignore gravity. Design variations on the formation have previously been investigated for either structurally connected vehicles via a central truss, or separated spacecraft using electric propulsion thrusters to maintain uniform circular motion. In this study, we will add to the comparison by considering a Coulomb control system for formation keeping.

4.3. Performance Evaluation of a Coulomb System

The purpose of this section is to evaluate some fundamental performance metrics of a Coulomb control system on a spacecraft formation. Aspects such as control force, input power, required consumable mass, and environment interaction will be calculated first for a simple two-spacecraft system, then later extended to a multiple-vehicle formation.

4.3.1. Two Body Analysis

Consider two spherical spacecraft having radii of r_{sc1}, r_{sc2}, separated by a distance of d from each other in a vacuum as shown in Figure 4-1. Each vehicle uses some amount of active on-board power P, to generate a charge of q_{sc1} and q_{sc2} respectively. The spacecraft will then interact according to Coulomb's Law.

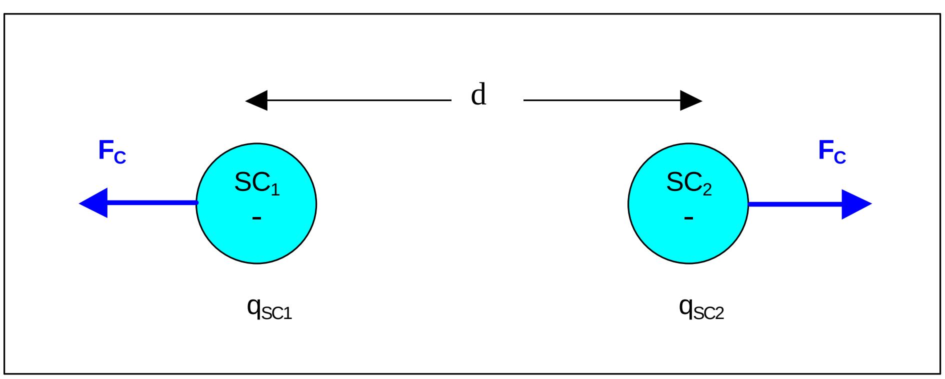

Figure 4-1. Schematic of two-vehicle interaction

We can express Coulomb's Law[77] as an equation giving the magnitude of the electric force between point charges.

Eqn. 4-4
$$F_o = \frac{1}{4\pi\varepsilon_0}\frac{|q_{SC1}||q_{SC2}|}{d^2}$$

where q_{SC1}, q_{SC2} are point charges at the centers of the spacecraft.

The potential of the spacecraft surface due to the internal charge can be easily evaluated from Gauss's law according to

Eqn. 4-5
$$V_{SC} = \frac{1}{4\pi\varepsilon_0}\frac{q_{SC}}{r_{SC}}\,.$$

By combining Eqn. 4-4 and Eqn. 4-5 we can write the magnitude of electric force between two spacecraft in vacuum as ,

Eqn. 4-6
$$F_0 = 4\pi\varepsilon_0\frac{r_{SC1}r_{SC2}|V_{SC1}||V_{SC2}|}{d^2}\,.$$

For vehicles immersed in plasma, we must modify the vacuum force F_o, to account for the shielding effect of the free charges according to Eqn. 2.8 as follows,

Eqn. 4-7
$$F_c = F_0 e^{-d/\lambda_d}\,.$$

Combining Eqn. 4-6 with Eqn. 4-7 we get,

Eqn. 4-8
$$F_c = 4\pi\varepsilon_0 e^{-d/\lambda_d}\frac{r_{SC1}r_{SC2}|V_{SC1}||V_{SC2}|}{d^2}\,.$$

Where λ_d is the Debye length.

Power Required for Coulomb Force

As discussed previously in Section 2.2, an isolated spacecraft will assume an equilibrium potential (voltage) such that the net environmental current due to plasma and photoelectron emission is zero. It is possible to change the vehicle potential by emitting charge from the spacecraft. For example, if it is desired to drive the spacecraft potential lower than equilibrium (more negative), the emission of positive charge from the vehicle will cause a net surplus of on-board electrons and a lowering of the potential. In order to emit such a current, the charges must be ejected from the vehicle with sufficient kinetic energy to escape the spacecraft potential well. Thus, if the vehicle as at a (negative) potential $-V_{SC}$, then ions must be emitted from a source operating at a power supply voltage, V_{PS}, greater than $|-V_{SC}|$. This is illustrated schematically in Figure 4-2.

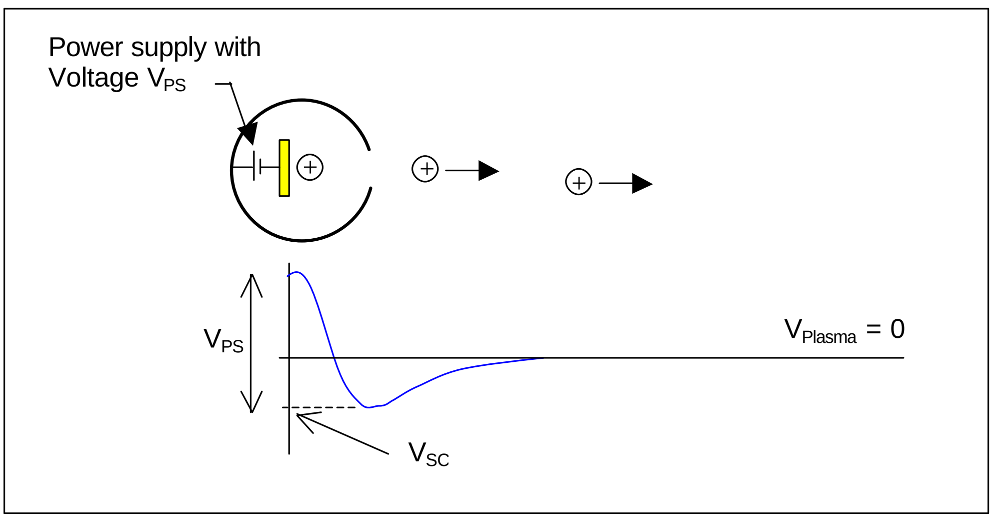

Figure 4-2. Schematic showing required voltages for charge emission from spacecraft. V_{PS} is the voltage of the on-board power supply. Top portion of figure represents ion emission system within spherical spacecraft, while bottom portion shows an aligned plot of electric potential on vertical axis with distance on horizontal axis.

While V_{PS} is greater than $|-V_{SC}|$ ions are able to escape the spacecraft, the net current to the spacecraft is *not* zero, and the potential of the vehicle will change. Once the spacecraft reaches a potential where $V_{SC} = -V_{PS}$, the emitted ions have insufficient energy to escape the spacecraft (they can't climb the potential hill) and the current is returned. This is demonstrated in Figure 4-3.

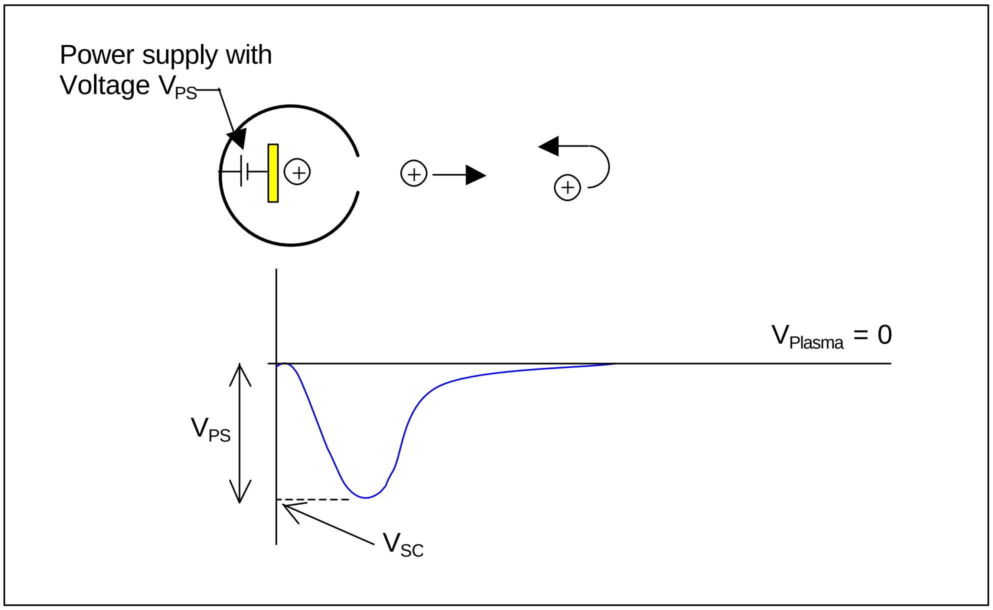

Figure 4-3. Vehicle potential will stabilize when V_{SC} reaches the value of $-V_{PS}$. Top portion of figure represents ion emission system within spherical spacecraft, while bottom portion shows an aligned plot of electric potential on vertical axis with distance on horizontal axis.

The spacecraft potential will thus stabilize at $V_{SC} = -V_{PS}$. At this increased negative potential, the vehicle will attract a larger amount of ion plasma current from the environment. If the increased ion current from the plasma reaches the spacecraft, the vehicle potential will increase slightly (become more positive), allowing some of the emitted ion current to escape the vehicle and restore the potential to the more negative value. Thus the emitted ion current, I_e, must be at least as large as the environmental ion current, $I_{environ}$, to maintain the vehicle at the steady state potential. If I_e were less than

$I_{environ}$, the vehicle power supply would be insufficient to maintain the spacecraft potential at $V_{SC} = -V_{PS}$. The above discussion could easily be extended to include electron emission raising the vehicle potential to some positive value.

Basic concepts can be used to calculate the power required to maintain the spacecraft at some steady state potential. To maintain the spacecraft at a voltage of $|V_{SC}|$, current must be emitted in the amount of $|I_e| = 4pr^2|J_p|$, where J_P is the current density to the vehicle from the plasma, using a power supply having voltage of at least $|V_{PS}| = |V_{SC}|$. Quantitatively,

Eqn. 4-9 $$P = |V_{SC} I_e|.$$

For a two-spacecraft system with each vehicle using Power P, the total system power is just the sum of the individual power to each vehicle. Combining Eqn. 4-9 with Eqn. 4-8 gives,

Eqn. 4-10 $$F_C = 4p\epsilon_0 e^{-d/?d} \frac{r_{SC1} r_{SC2} P^2}{d^2 I_{e1} I_{e2}}.$$

Eqn. 4-10 shows how to determine the required system power to maintain a steady-state Coulomb force in a given plasma environment. Since the space environment is constantly changing due to solar events and other phenomena, we must calculate the transient response characteristics of the Coulomb control force. To simplify the analysis we will eliminate the solar array from the equivalent circuit in the SEE program and assume that the spacecraft (i.e. just chassis) is just a sphere of radius r m. The circuit diagram is shown in Figure 4-4. Thus we have eliminated the node, which was at potential V_B i.e. cover glass potential and in turn the capacitances C_B and C_{AB}, current I_B in the SEE program model. Now we have only two nodes: ground, which is at plasma potential V_p (i.e. V = 0 in the SEE program model) and spacecraft chassis, which is at potential V_{SC} (i.e. V_A in the SEE program model). C (i.e. C_A in SEE program model) is capacitance of the spacecraft. It is given by

Eqn. 4-11
$$C = 4\,p\,e_0\,r$$

where r is the radius of the spacecraft. I (i.e. I_A in SEE program model) is the resultant net current to the spacecraft. It is the sum of ion current, electron current, photoelectron current and control current (or emission current). It is given by

Eqn. 4-12
$$I = 4\,p\,r^2\,J_P + I_e$$

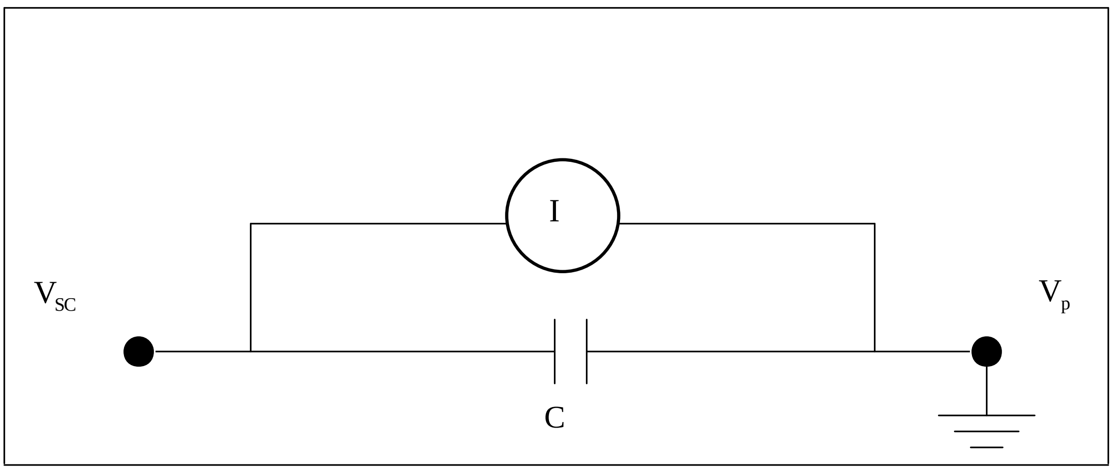

Figure 4-4. Equivalent circuit model for spacecraft and surrounding plasma

If this sum is zero, then the net current is zero; there will not be any change in the spacecraft potential because

Eqn. 4-13
$$\frac{dV_{SC}}{dt} = \frac{4\,p\,r^2\,J_p + I_e}{C}\,.$$

So if we adjust the control current $I_{control}$ such that dV/dt is not zero, we can change the potential of the spacecraft and thus dither the control force. From the above circuit, Eqn. 2-17, and Eqn. 2-18, we can write the governing equation for the spacecraft potential:

Eqn. 4-14 If $V_{SC} < 0$,

$$\frac{dV_{sc}}{dt} = \frac{I}{C} = \frac{I_e + 4\pi r^2 J_p}{4\pi\varepsilon_0 r}$$

$$= \frac{I_e + 4\pi r^2 \left\{ J_{e0} \exp\left[\frac{-e|V_{sc}|}{k_B T_e}\right] - J_{i0}\left[1 + \frac{e|V_{sc}|}{k_B T_i}\right] - J_{pe0} \right\}}{4\pi\varepsilon_0 r}$$

Eqn. 4-15 If $V_{SC} > 0$,

$$\frac{dV_{sc}}{dt} = \frac{I}{C} = \frac{I_e + 4\pi r^2 J_p}{4\pi\varepsilon_0 r}$$

$$= \frac{I_e + 4\pi r^2 \left\{ J_{e0}\left[1 + \frac{eV_{sc}}{k_B T_e}\right] - J_{i0} \exp\left[\frac{-eV_{sc}}{k_B T_i}\right] - J_{pe0} \exp\left[\frac{-eV_{sc}}{k_B T_{pe}}\right]\left[1 + \frac{eV_{SC}}{k_B T_{pe}}\right] \right\}}{4\pi\varepsilon_0 r}$$

Where J_{e0}, J_{i0} and J_{pe0} can be calculated from Eqn. 2-13, Eqn. 2-14, and Eqn. 2-15 respectively. We can solve this equation numerically to calculate the transient charging response of the spacecraft. If V_f is the desired final voltage, then the emission current must be emitted with energy at least equal to V_f. Once the vehicle reaches $V_{sc}=V_f$ the emission current will be extinguished and the potential will stabilize. Thus, the emission current can be written in terms of the emission power supply voltage $I_e=P_{ps}/V_f$. Consider a simple spherical spacecraft of radius 0.5 m, with V_f=6kV and exposed to average GEO plasma. A typical photoelectron current J_{pe0} is on the order of 10 µA/m^2 and temperature of photoelectrons on the order of spacecraft material work function (around 4.5 eV for most materials). The spacecraft potential V_{SC} is plotted against time at various levels of power P_{PS} of the emission system assuming the initial potential to be zero as shown in Figure 4-5. It can be seen that for only 200 mW of system power the vehicle can be charged to a potential of 6 kV within 8 msec. Faster charging times are enabled with a larger power investment.

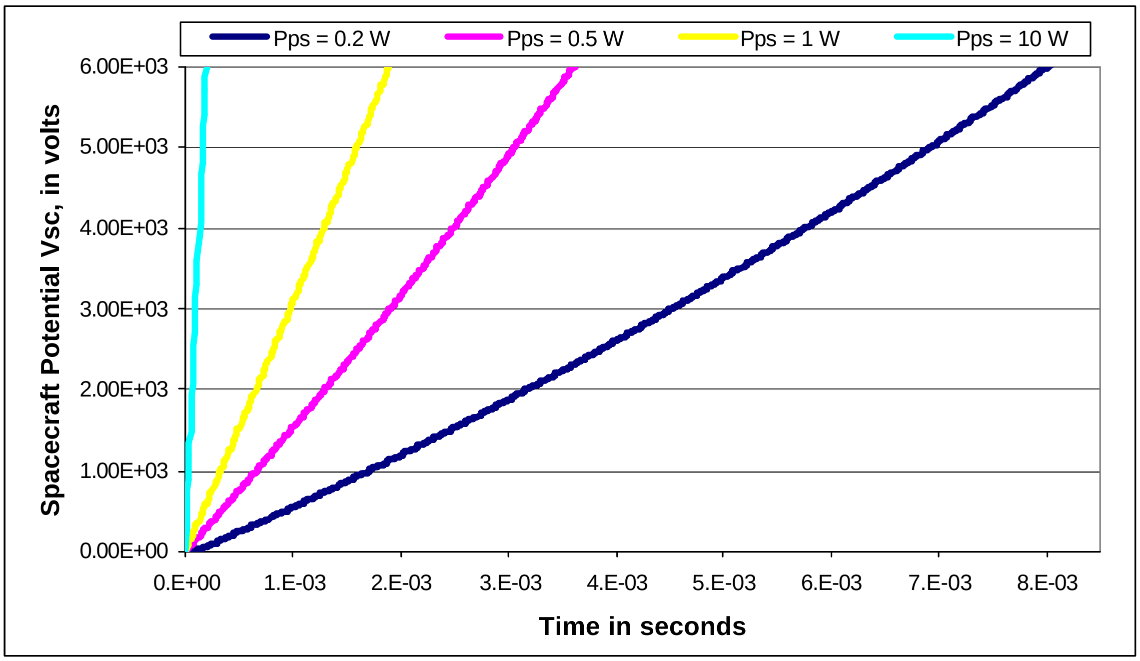

Figure 4-5. Plot of spacecraft potential V_{SC} against time, at different levels of power of the ion emitting gun P_{PS}.

<u>Mass Flow Rate For Coulomb Control System</u>

Coulomb control is fundamentally a propellantless concept. However, vehicle charge control will require some amount of consumables. For instance, driving the spacecraft charge negative requires the active emission of positive charge. This is accomplished by a beam of gaseous ions.

Mass flow rate is then the mass of gaseous ions expelled out per unit time to maintain potential of the SC. As electrons have negligible mass we can say that mass flow rate of electrons is negligible and thus driving the potential positive requires zero mass flow. If I_e is the emission current constituting ions, m_{ion} is the mass of ion, and q_{ion} is the charge, then mass flow rate is given by,

Eqn. 4-16
$$\dot{m} = \frac{I_e m_{ion}}{q_{ion}}.$$

Since the only purpose of the ion emission is to carry charge form the vehicle, it makes sense to use the least massive ions that are practical.

For the two spacecraft combination, propellant mass flow rate $\dot{m}_{Total}$, will be the sum of mass flow rates for individual spacecraft ($\dot{m}_{SC1}$ and $\dot{m}_{SC2}$).

Eqn. 4-17
$$\begin{aligned}\dot{m}_{Total} &= \dot{m}_{SC1} + \dot{m}_{SC2} \\ &= \frac{I_{e1}\, m_{ion}}{q_{ion}} + \frac{I_{e2}\, m_{ion}}{q_{ion}}\end{aligned}$$

$$\dot{m}_{Total} = \frac{m_{ion}}{q_{ion}}\left(I_{e1} + I_{e2}\right).$$

where I_{e1} (I_{e2}) is the emission current for SC_1 (SC_2).

Specific Impulse of a Coulomb System

A common performance parameter used for propulsion systems is specific impulse I_{sp} This parameter compares the thrust derived from a system to the required propellant mass flow rate.[78] Although I_{sp} is traditionally used as a parameter to evaluate momentum transfer (rocket) systems, we can use the formal definition to compare the Coulomb system. For a Coulomb control system the specific impulse I_{sp} is given by

Eqn. 4-18
$$I_{sp} = \frac{F}{\dot{m}_{Total} g_0}$$

Since Coulomb force calculations are meaningless for a single vehicle, we will treat the system as two separate vehicles, each subject to a force of F_c given by Eqn. 4-10, so that the sum of the forces experienced by all spacecraft in the formation is $F=2F_c$.

Eqn. 4-19
$$I_{sp} = \frac{8\ p\ e_0\ e^{-d/?_d}\ q_{ion}}{g_0\ m_{ion}} \frac{r_{SC1}\ r_{SC2}\ P^2}{d^2\ I_{e1}\ I_{e2}\ (I_{e1} + I_{e2})}$$

where g_0 is the gravitational constant. If $r_{sc1} = r_{sc2} = r_{sc}$, and $I = I_{e1} = I_{e2}$, then Eqn. 4-19 becomes,

Eqn. 4-20
$$I_{sp} = \frac{4\, p\, e_0 e^{-d/?_d} q_{ion}}{g_0 m_{ion}} \frac{r^2{}_{SC} P^2}{d^2 I_e^3}.$$

Note that, unlike a rocket system, the definition of I_{sp} of a coulomb system is meaningless for a single vehicle. For a two spacecraft formation, Eqn. 4-20 indicates that the specific impulse of the formation is a function of the radii of the spacecraft, power supplied to the ion (electron) gun, the separation between the two spacecraft, the emission currents of both vehicles, and the mass of the charge carriers, m_{ion}.

Consider a two-spacecraft formation with identical 0.5-m-radius vehicles in the average GEO plasma environment charged to the same negative potential. In order to reach and maintain this negative potential, the vehicles must emit an ion current. Consequently, the spacecraft will attract ion saturation current I_{i0}, from the plasma, so I_e must be equal to I_{i0} for steady state. It is apparent that light ions will provide the most efficient I_{sp}, so assume that the emitted species is H^+. Calculated values of specific impulse for each vehicle in the formation are shown in Figure 4-6 for various system input power levels. For 1 mW systems with vehicle separation on the order of 20 m, I_{sp} values of 10^4 seconds are obtained, with values increasing to 10^{10} sec for just 1 W of power. It should be noted that for a positive vehicle potential, the emitted species would be electrons and, thus, the calculated values of I_{sp} would be a factor of 2,000 greater.

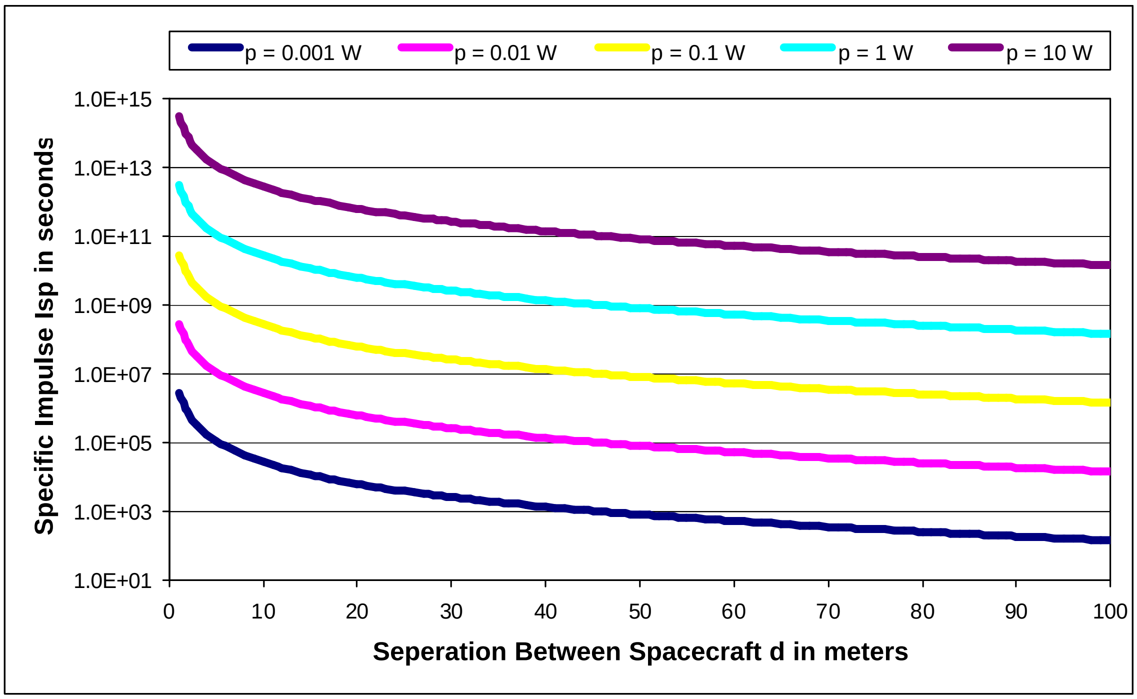

Figure 4-6. Graph of specific impulse for a 2 spacecraft formation as a function of spacecraft separation at different values of input power.

Emission Current Jet Force

Generating usable net charge on a spacecraft for Coulomb force requires the emission of current. In principle, the charge will be carried away from the vehicle by particles with non-zero mass. Such mass ejection will result in a momentum jet force on the vehicle as in a traditional electric propulsion thruster. In the case of electron emission, the mass of the charge carriers is insignificant and the resulting jet force is negligible. Ion emission, however, may produce a significant reaction force. It is instructive to consider how the Coulomb force between spacecraft compares with the momentum reaction on the vehicle induced by the beam of ion current.

The reactive thrust force F_j, of an ejected mass flow is computed as

Eqn. 4-21
$$F_J = \dot{m}u_e ,$$

where $\dot{m}$ is the ejected mass flow rate and u_e is the exhaust velocity at which the mass is emitted. Assuming steady state Coulomb force generation, the ions will be electro-statically accelerated through a potential of V_{SC}, such that

Eqn. 4-22
$$u_e = \sqrt{\frac{2q_{ion}V_{SC}}{m_{ion}}} .$$

With this simplification and recognizing that the mass flow is related to the emission current via Eqn. 4-16, the momentum jet force of the emitted ion current is

Eqn. 4-23
$$F_J = I_e\sqrt{\frac{2m_{ion}V_{SC}}{q_{ion}}} .$$

The jet force can also be written in terms of the input power to the emission system as

Eqn. 4-24
$$F_J = \sqrt{\frac{2m_{ion}PI_e}{q_{ion}}} .$$

We can compare the magnitude of the jet reaction force with the induced Coulomb force between two vehicles. Assume identical spacecraft charged to the same value of V_{SC}. From Eqn. 4-10 and Eqn. 4-24 we can write the ratio of F_C/F_J (taking F_c as the total Coulomb force on both vehicles) in terms of the input power as

Eqn. 4-25 $$\frac{F_C}{F_J} = 4\sqrt{2}\, p\, e_0 \sqrt{\frac{q_{ion}}{m_{ion}}}\, \frac{r_{SC1}\, r_{SC2}\, P^{3/2}\, e^{\frac{-d}{?_d}}}{I_{e1}\, I_{e2}\, (I_{e1} + I_{e2})\, d^2}\,.$$

If $r_{sc1} = r_{sc2} = r_{sc}$, and $I = I_{e1} = I_{e2}$ then Eqn. 4-25 becomes,

Eqn. 4-26 $$\frac{F_C}{F_J} = 2\sqrt{2}\, p\, e_0 \sqrt{\frac{q_{ion}}{m_{ion}}}\, \frac{r_{SC}{}^2\, P^{3/2}\, e^{\frac{-d}{?_d}}}{I_e{}^3\, d^2}\,.$$

For a formation of two spacecraft, we find that the F_C/F_J ratio is a function of the radii of the spacecraft, power supplied to the ion (electron) gun, the separation between the two spacecraft, and the emission currents of both of them. Similar to the calculations for specific impulse, if we consider formation of two identical spacecraft in GEO having same radii of 0.5 m, charged to same high negative voltage V_{SC} and provided with same power P for each of them, they will draw same ion saturation current from the ambient plasma. So the (ion) emission current I_e will be also same. Figure 4-7 shows the ratio of Coulomb to jet force assuming hydrogen ion emission in average GEO plasma.

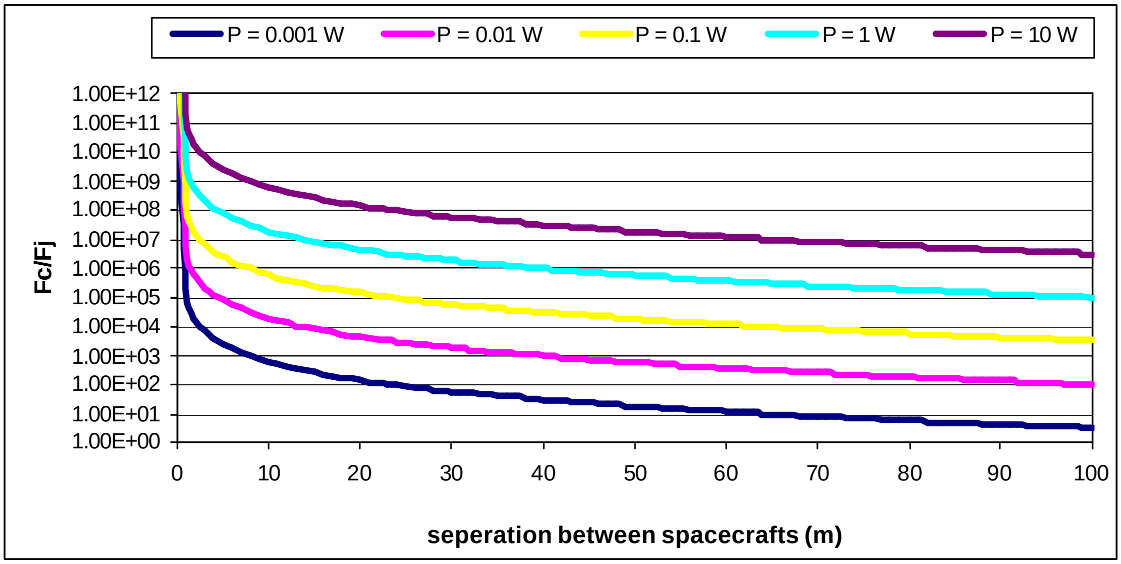

Figure 4-7. Graph of F_C/ F_J Vs separation between spacecraft for 2 spacecraft formation at different levels of system power.

It can be seen that for separations up to 100 m and system power greater than 1 mW the Coulomb force is considerably higher than the jet force. This implies two conclusions: 1) the Coulomb force is a much wiser use of power than a mass-emitting electric propulsion thruster, and 2) the directional jet force will not be a significant perturbation to the Coulomb control system.

4.3.2. Multi-body Analysis

In this section, we will see how to calculate the various parameters in section 4.3.1 for a general case with more than two spacecraft. Suppose we have n spacecraft. Let's assume that q_i are the charges on the spacecraft, r_i are the radii of the spacecraft, $d_{i,j}$ is the distance from spacecraft$_i$ to spacecraft$_j$, V_i are the voltages of the spacecraft; $\hat{d}_{i,j}$ is the unit vector along the line joining the centers of spacecraft$_i$ and spacecraft$_j$, directed from spacecraft$_j$ to speraft$_i$.

For steady state operation, the emission current from each vehicle must balance the environmental current to maintain desired potential:

Eqn. 4-27 $$I_{(e)\,i} = I_{(environ)\,i}$$

where $I_{(e)i}$ ($I_{(environ)I}$) is the emission (environmental) current of spacecraft$_i$. The total power required for the entire system to maintain steady state is,

Eqn. 4-28 $$P_{(input)Total} = \sum_{i=1}^{n} P_{(input)i} = \sum_{i=1}^{n} |\, V_{(SC)\,i} \,|\, I_{(e)\,i}$$

Where $P_{(input)}$ is the input power for spacecraft$_i$. The sum of coulomb forces F_i, acting on any spacecraft SC_i in the formation can be written as the vector sum,

Eqn. 4-29 $$F_i = F_{i,1} + F_{i,2} + \ldots\ldots\ldots + F_{i,n} = \sum_{\substack{j=1 \\ j\neq i}}^{n} F_{i,j}$$
$$= \frac{q_i}{4\pi\varepsilon_0} \sum_{\substack{j=1 \\ j\neq i}}^{n} \frac{q_j}{d^2_{\,i,j}} \hat{d}_{i,j} e^{\frac{-d_{i,j}}{\lambda_d}}$$

The total Coulomb force F_C in the formation will be sum of all such F_i's,

Eqn. 4-30 $$F_C = \sum_{i=1}^{n} |\, F_i \,| = \frac{1}{4\pi\varepsilon_0} \sum_{i=1}^{n} \left| q_i \sum_{\substack{j=1 \\ j\neq i}}^{n} \frac{q_j}{d^2_{\,i,j}} \hat{d}_{i,j} e^{\frac{-d_{i,j}}{\lambda_d}} \right|.$$

As an upper bound for calculating the amount of consumables needed, we will assume all vehicles must emit ions. If emitting ions mass flow rate of any spacecraft F_i is given by Eqn. 4-16. For a formation, total mass flow rate for the coulomb control system becomes,

Eqn. 4-31 $$\dot{m}_{Total} = \sum_{i=1}^{n} \dot{m}_i = \frac{m_{ion}}{q_{ion}} \sum_{i=1}^{n} I_{(e)\,i}$$

where $\dot{m}_i$ is the mass flow rate for spacecraft$_i$.

4.3.3. *Specific Impulse of The Entire Coulomb System*

Referring to Eqn. 4-30 and Eqn. 4-31, the specific impulse of entire coulomb formation, $I_{(sp)Total}$ will be,

Eqn. 4-32
$$I_{(sp)Total} = \frac{\sum_{i=1}^{n} |F_i|}{g_0 \sum_{i=1}^{n} \dot{m}_i}$$

$$I_{(sp)Total} = \frac{q_{ion}}{g_0\ m_{ion}\ 4\pi\varepsilon_0} \frac{\sum_{i=1}^{n} \left| q_i \sum_{\substack{j=1 \\ j\neq i}}^{n} \frac{q_j}{d^2_{i,j}} \hat{d}_{i,j} e^{\frac{-d_{i,j}}{\lambda_d}} \right|}{\sum_{i=1}^{n} I_{(e)i}}$$

4.3.4. *Propulsion System Mass*

In order to evaluate the utility of a Coulomb control system for a given mission, we must calculate the propulsion system mass required. System mass can be broken down into two categories: inert mass due to electrical power supplies, and propellant mass due to ion beam gas supply (if needed).

Inert mass of the Coulomb Control System is mass of power supply; electron, ion guns etc. We assume that inert mass of the Coulomb control system m_{inert}, is proportional to the power P of power supply.

Eqn. 4-33
$$\begin{aligned} m_{inert} &\propto P \\ \therefore m_{inert} &= \beta P \end{aligned}$$

Where β is the constant of proportionality. It is the ratio of the mass of the coulomb control system m_{inert} to the input power required and it is measured in kg/W. ß is known as the specific mass of the coulomb control system. Eqn. 4-28 gives us the power required $P_{(input)\ Total}$, to keep the spacecraft voltages at steady state. So the inert mass of the coulomb formation is given by

Eqn. 4-34 $$m_{inert} = ßP_{(input)Total} = ß\sum_{i=1}^{n} P_{(input)i} = ß\sum_{i=1}^{n} | V_{(SC)\,i} \,|\, I_{(e)\,i}$$

If τ is the mission lifetime, from Eqn. 4-31 the total mass of fuel (propellant) required m_{fuel}, becomes,

Eqn. 4-35 $$m_{fuel} = t\ \dot{m}_{(fuel)Total} = t\sum_{i=1}^{n} \dot{m}_{(fuel)\,i} = \frac{t\ m_{ion}}{q_{ion}} \sum_{i=1}^{n} I_{(e)\,i}$$

Where $\dot{m}_{(fuel)\,i}$ is the mass flow rate of $spacecraft_i$.

The total mass of Coulomb control propulsion system m_{prop}, is the sum of inert mass of the coulomb control system m_{inert} and mass of fuel m_{fuel} required over mission lifetime τ . Thus, we can write,

Eqn. 4-36
$$\begin{aligned} m_{prop} &= m_{inert} + m_{fuel} \\ &= ß\sum_{i=1}^{n} | V_{(SC)\,i} \,|\, I_{(e)\,i} + \frac{t\ m_{ion}}{q_{ion}} \sum_{i=1}^{n} I_{(e)\,i} \\ &= \sum_{i=1}^{n} \left\{ I_{(e)\,i} \left[ß\,| V_{(SC)\,i} \,| + \frac{t\ m_{ion}}{q_{ion}} \right] \right\} \\ &= \sum_{i=1}^{n} \left\{ I_{(e)\,i} \left[\frac{ß\,| q_i \,|}{4\,p\,e_0 r_i} + \frac{t\ m_{ion}}{q_{ion}} \right] \right\} \end{aligned}$$

5. Comparative Mission Analyses

The purpose of this chapter is to compare the performance of the Coulomb control system with more traditional electric propulsion thrusters under consideration for formation flying missions. The formations discussed in this study, namely three-spacecraft, five-spacecraft, and six-spacecraft Earth orbiting along with five-spacecraft rotating formation at a libration point will be analyzed. Performance parameters such as total propulsion system mass, input power, and specific impulse will be compared.

5.1. Conventional Electric Propulsion Systems

The most likely thruster candidates for planned formation flying missions are micro pulsed-plasma thrusters (MicroPPT), Colloid thrusters, and Field-emission Electric Propulsion (FEEP) thrusters. A brief overview of the operating principles for each technology will be presented.

5.1.1. Micro Pulsed Plasma Thruster

MicroPPT is essentially an electromagnetic accelerator, which uses solid Teflon (Polytetrafluoroethylene-PTEE) bars as propellant. It is a pulsed thruster with characteristically very short pulse width of the order of tens of microseconds. The minimum amount of impulse that can be imparted to a spacecraft in one pulse (the impulse bit) can be as small as 2 micronewton-seconds. MicroPPTs can be characterized by I_{sp} = 500 sec, η = 2.6%, and power-specific mass of β = 0.37 kg/W.[21,79]

The most common types of PPTs are breech-fed, side-fed, and co-axial versions. Here we will focus on simple and more general breech-fed type, as shown in Figure 5-1. In order to fire a PPT, a capacitor is discharged, creating a large potential across the space between an anode and a cathode. This potential causes a surface breakdown (which is initiated at a semiconducting spark plug surface) on the face of a solid bar of Teflon propellant, ablating it and allowing an arc to pass through the outer, gaseous layer, ionizing it. This large current carrying arc induces a magnetic field around itself. So the Lorentz force (I × B) acting on the ions upstream of the arc accelerates them downstream. In addition, there is a gas dynamic effect caused by the heating of the ablated Teflon by the arc.[80]

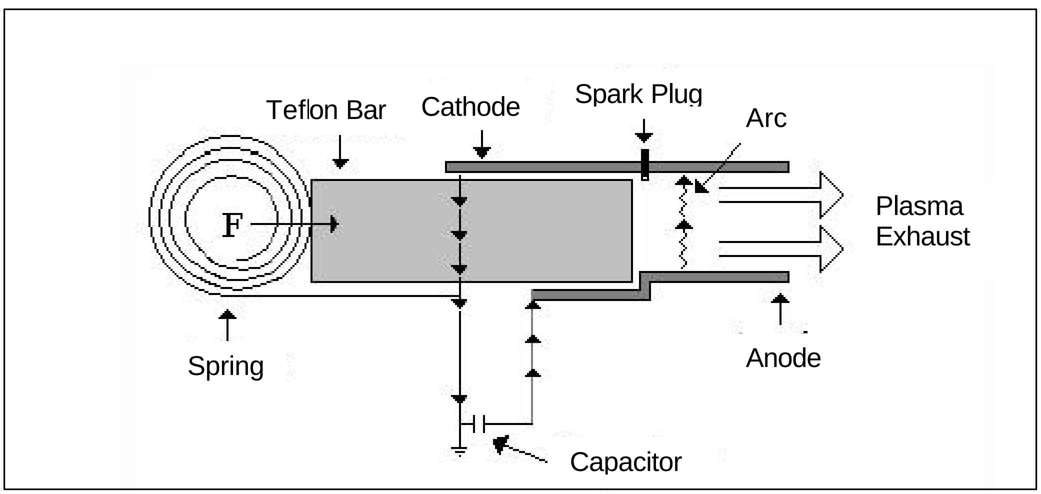

Figure 5-1. Breech-fed pulsed plasma thruster schematic.[80]

5.1.2. <u>Colloid Thruster</u>

A colloid thruster extracts charged droplets (and/or free ions) from an electrolytic liquid using strong electric fields. Common examples of propellant mixtures include combinations of formamide or glycerol as solvents and sodium iodide (NaI) or lithium chloride (LiCl) as solutes. Figure 5-2 shows a schematic of a single needle colloid emitter's main elements.

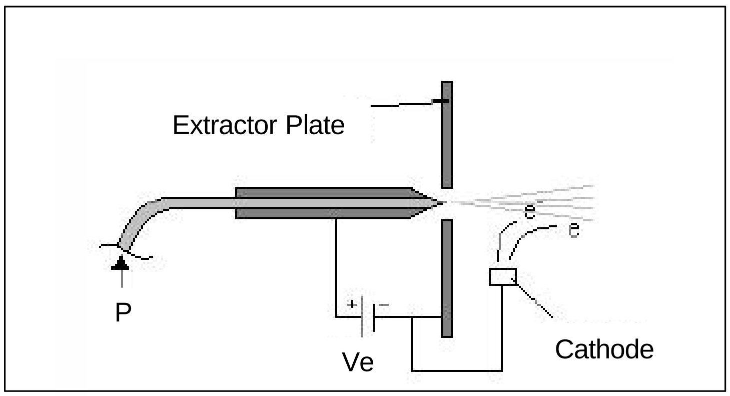

Figure 5-2. Single-needle colloid thruster schematic.[80]

The lightest gray shading represents the propellant, while the annular extracting plate and conducting needle are shown in a darker gray. A power supply is used to establish a voltage difference V_e between the extractor and needle creating an electrostatic attraction force on the surface of the fluid meniscus that forms at the needle exit. This force, balanced with the fluid surface tension and possible back pressure on the fluid results in the formation of a cone that emits a jet of droplets at its vertex. Then, these droplets are accelerated through the potential V_e to a high speed. Colloid thruster performance can be characterized by I_{sp} = 1,000 sec, efficiency η = 65%, and power-specific mass β = 0.216 kg/W.[21]

5.1.3. *Field Emission Electric Propulsion Thruster (FEEP)*

Similar to the colloid thruster, the FEEP device extracts charged particles from a liquid propellant. The difference is in the propellant used and operating voltage range. Instead of electrolytic fluid, FEEP uses liquid phase metal, like cesium or indium because of their low ionization potential, high atomic weight, and low melting point. Ions are directly extracted by field emission and subsequently accelerated down the electric potential. In order to overcome the ionization potential they need to be operated at higher voltages than the colloid thrusters.

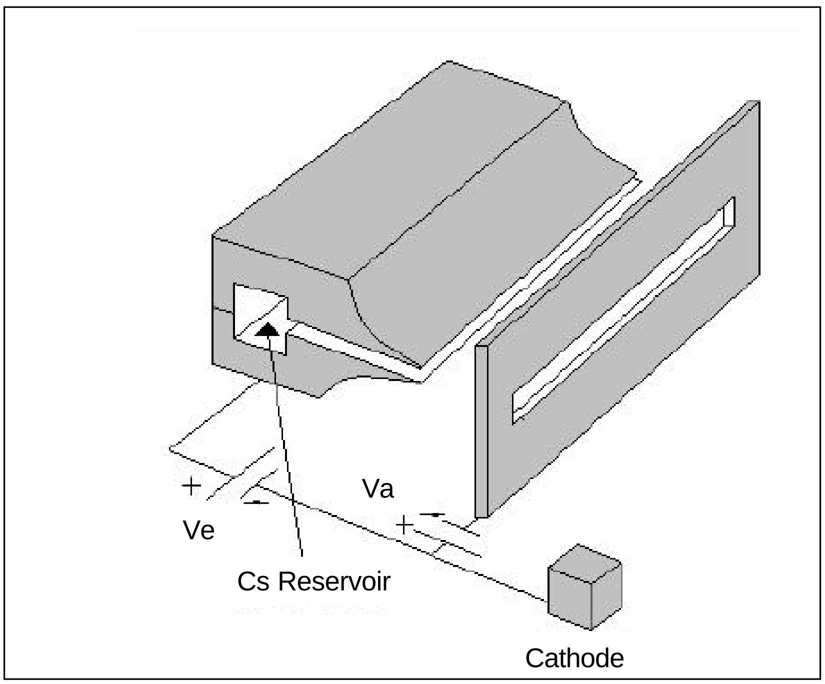

Figure 5-3. Schematic of Cesium FEEP thruster.[80]

The cesium FEEP thruster shown in Figure 5-3 consists of a slit shaped emitter which contains a propellant reservoir. Generally the slit is 1-2 microns high and 1 mm to several cm long. The extractor plate is biased at a negative potential of several kilovolts.

The distance between the emitter and the extractor is greatly exaggerated for clarity. A neutralizer is also necessary since the beam consists only of ions.[80] The FEEP technology can be characterized with performance parameters of I_{sp} = 10,000 sec, efficiency η = 65%, and power-specific mass β = 0.11 kg/W.[21]

5.1.4. *Mission Parameter Calculations for Thruster Technologies*

Using traditional thruster performance parameters, we can calculate the propulsion system design metrics for the electric propulsion technologies. Of particular importance to any mission is the input power required by the system, the propellant mass, and the inert mass (consisting of power supplies, thruster hardware, etc.) necessary to maintain a formation. Considering n spacecraft in a formation, each using an electric propulsion thruster to maintain the formation by exerting a thrust force T_i, the total thrust T_{Total} for the formation is,

Eqn. 5-1
$$T_{Total} = \sum_{i=1}^{n} |T_i|$$

The input power P_{input} can be calculated knowing the force required of each thruster, the efficiency of the thruster in converting electrical power to kinetic thrust power, and the specific impulse of the device. For the entire formation, the total power is

Eqn. 5-2
$$P_{(input)Total} = \sum_{i=1}^{n} P_{(input)i} = \sum_{i=1}^{n} \frac{|T_i| g I_{(sp)i}}{h_i}$$

where g is the gravitational constant, $I_{(sp)i}$ is the specific impulse of individual thruster, η_i is the efficiency of individual thrusters.

The inert mass of the thruster system m_{inert} is proportional to the power P of power supply.

Eqn. 5-3
$$m_{inert} \propto P$$
$$\therefore m_{inert} = ßP$$

Where β is a constant of proportionality known as the power-specific mass measured in kg/W. Eqn. 5-2 gives us the power required $P_{(input)\ Total}$ for the formation, so the inert mass of the thruster system is given by,

Eqn. 5-4
$$m_{inert} = ßP_{(input)Total} = ß\sum_{i=1}^{n} P_{(input)i} = ßg\sum_{i=1}^{n} \frac{|T_i|\, I_{(sp)i}}{?_i}$$

If the mission lifetime is t, total impulse I_{Total} in the formation becomes,

Eqn. 5-5
$$I_{Total} = t\,T_{Total}$$
$$= \sum_{i=1}^{n} t\,|T_i|$$

The total mass of fuel required for the formation m_{fuel} for lifetime t will be,

Eqn. 5-6
$$m_{fuel} = \frac{I_{Total}}{g_0 I_{sp}}$$
$$= \frac{t}{g_0}\sum_{i=1}^{n} \frac{|T_i|}{I_{(sp)i}}$$

The total mass m_{prop} for the electric thruster system will be sum of mass of fuel m_{fuel} and inert mass m_{inert},

Eqn. 5-7
$$m_{prop} = \sum_{i=1}^{n} |T_i| \left(\frac{ßgI_{(sp)i}}{?_i} + \frac{t}{gI_{(sp)i}} \right)$$

5.2. Formation Geometries

Four formations were considered in this study. Three of them

- 3 Satellites in a line (1 combiner, 2 collectors)
- 5 satellites in a plane (1 combiner, 4 collectors)
- 6 satellites in a plane (1 combiner, 5 collectors)

were assumed to have a combiner in a circular orbit (shown in Figure 5-4) with collector satellites positioned relative to it. The fourth case consisted of 5 satellites (1 combiner and 4 collectors) in a line located at a stable earth-sun Libration point. In the remainder of this section, the 4 formations are described in detail with specific attention given to the parameters defining their configuration.

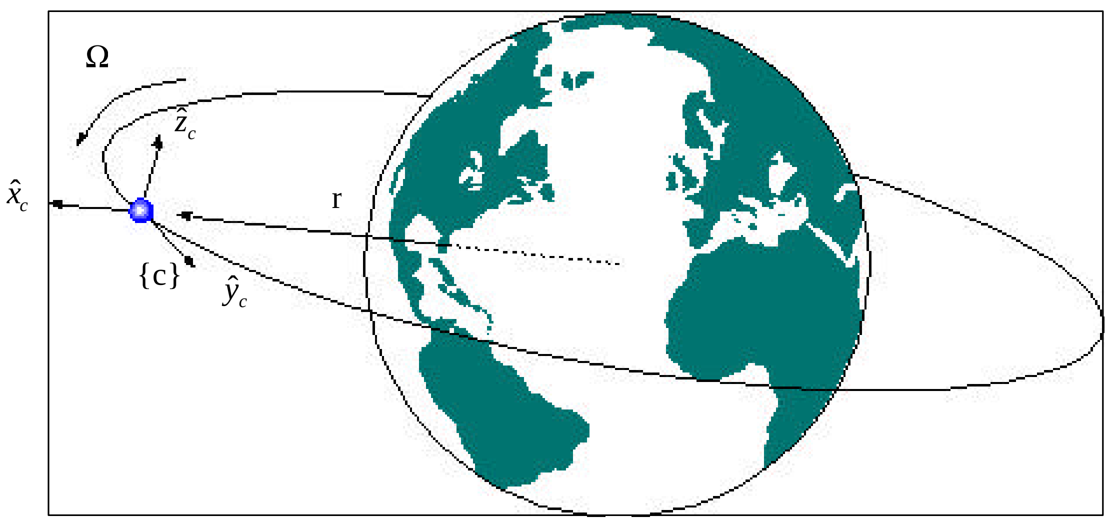

Figure 5-4. Combiner and its fixed frame, {c}, in a circular orbit.

5.2.1. <u>*Earth Orbiting Three Satellite – Geometry*</u>

Three different 3-satellite formations were considered. In each case the combiner (denoted with a 0 subscript) was assumed to maintain a circular orbit with radius r and true anomaly q . The combiner-fixed rotating reference frame, denoted {c} and shown in Figure 5-4, was used to describe collector motion relative to the combiner.

Spacecraft charges were analytically computed such that the 3 satellites formed a line shown in Figure 5-5, where M_i are spacecraft masses, q_i are spacecraft charges and L is the separation between the combiner (blue) and either collector (yellow). The distinguishing feature of the formations was their axis alignment.

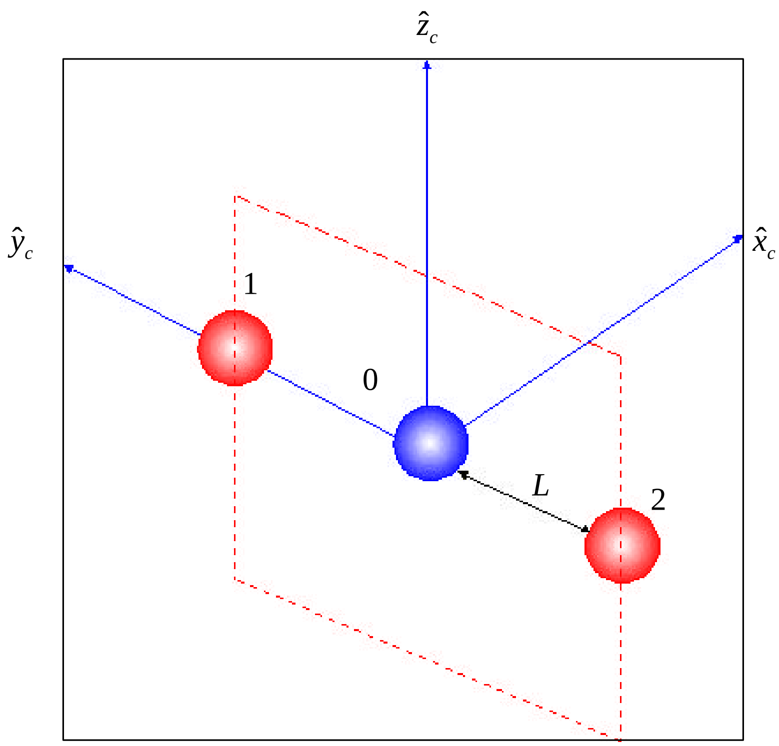

Figure 5-5. Three satellite formation.

Figure 5-6 shows the 3 cases examined with spacecraft aligned along the combiner fixed frame, x, y, and z axes. These 'virtual tether' formations have little imaging use, but, provided insight into the solutions of the more complicated formations considered later.

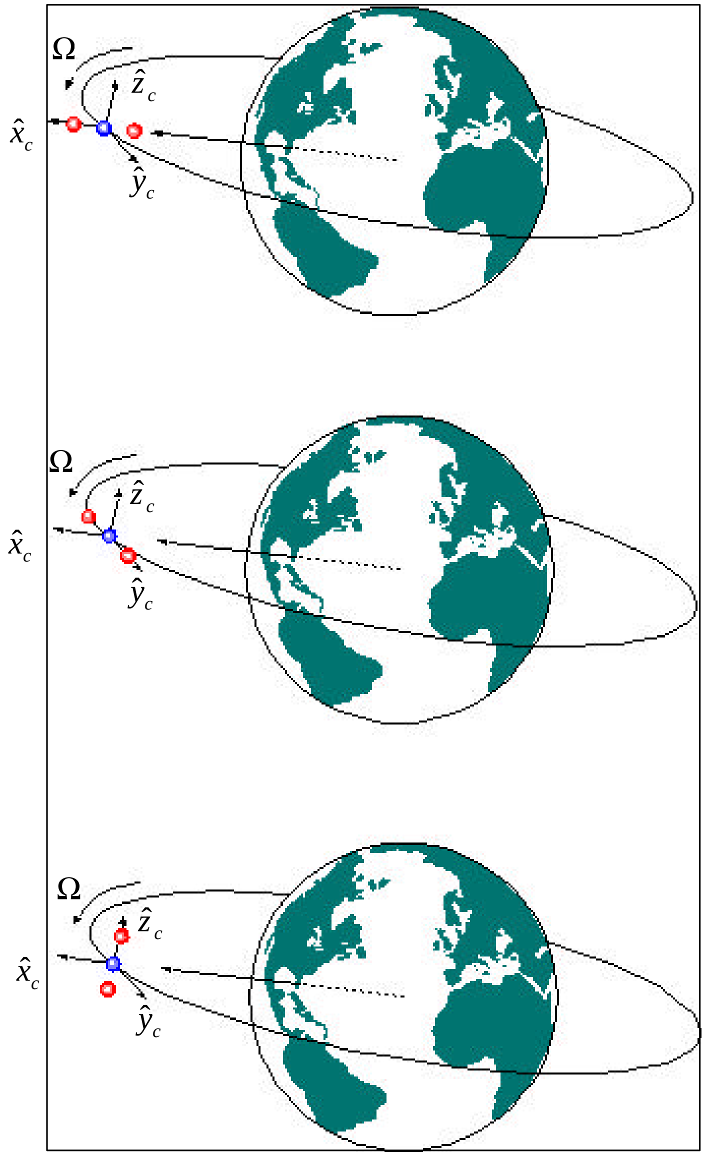

Figure 5-6. The three 3-satellite formations aligned along the x, y, and z {c} frame axes .

5.2.2. *Earth Orbiting Five Satellite - Geometry*

As in the previous formation, the combiner was assumed to have a circular orbit with radius r and true anomaly q . Spacecraft charges were analytically determined such that the four collectors formed a square in the combiner fixed $\hat{y}_c - \hat{z}_c$ plane with side length

$2L$ as shown in Figure 5-7. Charges are again denoted q_i and masses as m_i. Although this formation could be used for imaging it is not optimal due to U-V plane overlap.

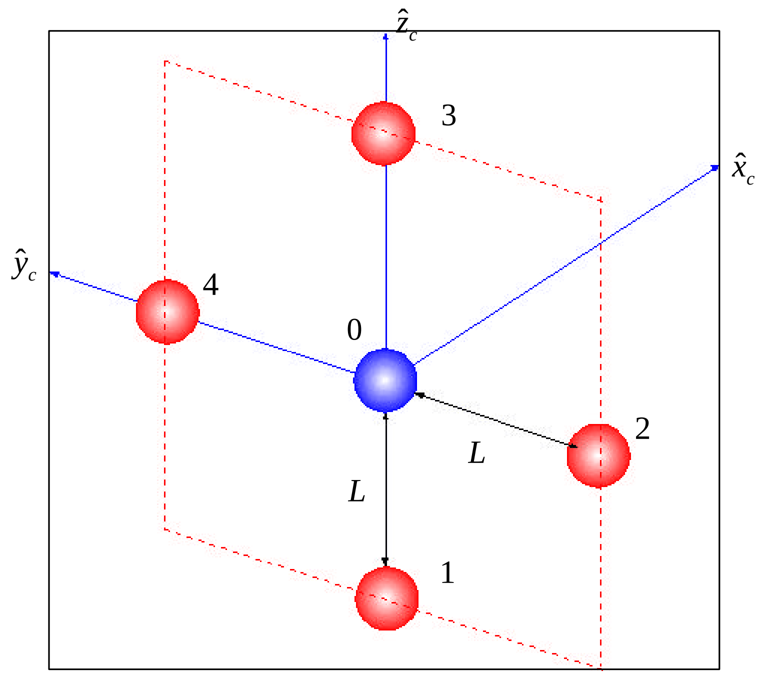

Figure 5-7. The five-satellite formation geometry.

5.2.3. *Earth Orbiting Six Satellite - Geometry*

Again, the combiner was assumed to be in the circular orbit with radius r and true anomaly ? . Spacecraft charges were computed numerically such that the 5 collectors were in a circle of radius L about the combiner, in its Y-Z plane. In addition, the goal was to maintain a pentagon formation, shown in Figure 5-8, as that is optimal from an imaging perspective.

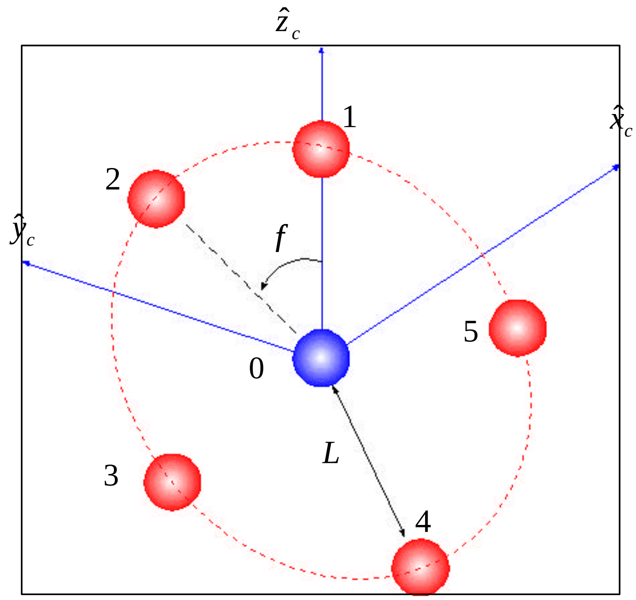

Figure 5-8. In-plane pentagon satellite formation configuration

5.2.4. *Libration Point Five Satellite – Geometry*

The five satellites were assumed to be at a stable Earth-Sun Libration point aligned as shown in Figure 5-9. Charges were analytically computed such that collectors `1' and `3' had a combiner separation of L_1 and collectors `2' and `4' had a separation of L_1+L_2. In addition, the system was assumed to rotate about the combiner fixed y-axis with angular rate of Ω.

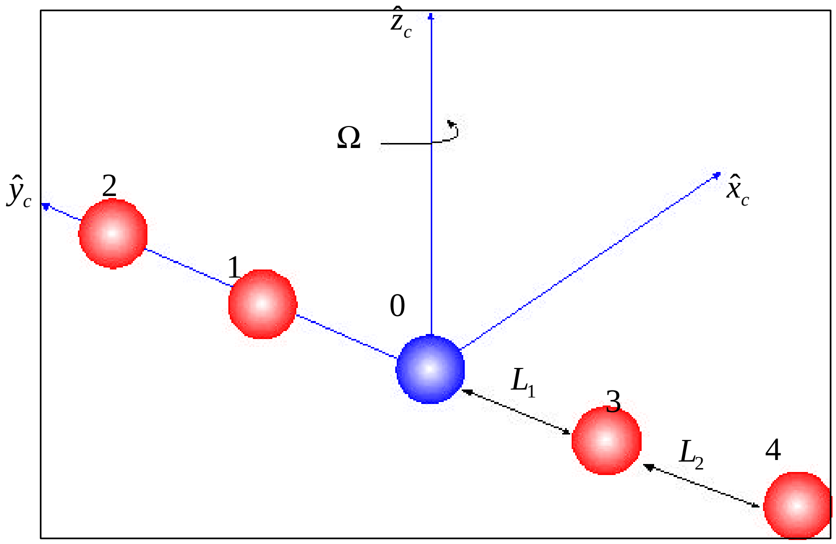

Figure 5-9. Rotating five-satellites formation configuration

5.3. *Equilibrium Solutions*

The charge needed to be maintained on each spacecraft in the formations discussed in Section 5.2, was found in related work by Chong et al[81,82,83]. Summary of this work will be given here for reference.

5.3.1. *Dynamic Equations*

The combiner at the center is assumed to be following a circular Keplerian orbit. Hill's equations were used to describe the motion of the collectors with respect to the combiner. Only the combiner is having its own station keeping system but the collectors are not. So only axial forces are possible for formation keeping by Coulomb control technology for the formations under consideration. If we consider a formation of n vehicles, the motion of ith spacecraft with respect to the combiner in Hill's system can be described as follows:

Eqn. 5-8

$$
\begin{aligned}
\ddot{x}_i - 2\Omega\dot{y}_i - 3\Omega^2 x_i &= \frac{k_c}{m_i}\sum_{j=0}^{n}\frac{(x_i - x_j)}{\left|\vec{p}_i - \vec{p}_j\right|^3} q_i q_j \\
\ddot{y}_i + 2\Omega\dot{x}_i &= \frac{k_c}{m_i}\sum_{j=0}^{n}\frac{(y_i - y_j)}{\left|\vec{p}_i - \vec{p}_j\right|^3} q_i q_j \\
\ddot{z}_i + \Omega^2 z_i &= \frac{k_c}{m_i}\sum_{j=0}^{n}\frac{(z_i - z_j)}{\left|\vec{p}_i - \vec{p}_j\right|^3} q_i q_j \\
i = 1,\ldots,n &\text{ and } i \neq j
\end{aligned}
$$

where $\vec{p}_i$ is the position vector of the i^{th} spacecraft, m_i is its mass, Ω is the orbital angular velocity, q_i is the spacecraft charge in Coulombs, and $k_c = 1/4\pi\varepsilon_0$ is the Coulomb's constant. As shown in the Figure 5-10, the y direction is along the orbital velocity vector, x is in the zenith-nadir direction, and z is normal to the orbit plane.

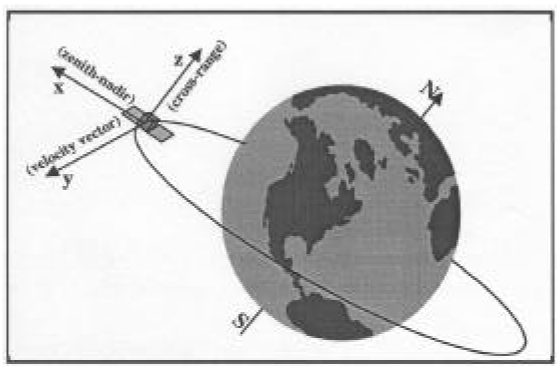

Figure 5-10. Illustration of combiner-fixed relative coordinate system used in the Hill's equation formulation[15]

Each spacecraft in a static formation should have zero relative velocity and acceleration i.e. it should satisfy the condition $\dot{x} = \ddot{x} = \dot{y} = \ddot{y} = \dot{z} = \ddot{z} = 0$ in the Hill's system. So the equilibrium system of equations in Eqn. 5-8 becomes

$$-3O^2 x_i = \frac{k_c}{m_i}\sum_{j=0}^{n}\frac{(x_i - x_j)}{\left|\vec{p}_i - \vec{p}_j\right|^3} q_i q_j$$

$$0 = \frac{k_c}{m_i}\sum_{j=0}^{n}\frac{(y_i - y_j)}{\left|\vec{p}_i - \vec{p}_j\right|^3} q_i q_j$$

Eqn. 5-9

$$O^2 z_i = \frac{k_c}{m_i}\sum_{j=0}^{n}\frac{(z_i - z_j)}{\left|\vec{p}_i - \vec{p}_j\right|^3} q_i q_j$$

$$i = 1,\ldots,n \text{ and } i \neq j$$

5.3.2. Equilibrium Formation Solutions

While finding the set of equilibrium solutions for the formations, the geometry of formation and masses of the spacecraft were fixed and the set of equations in Eqn. 5-9 was solved for the charges on the spacecraft by forcing the position and velocity constraints. Parameter $V_n r$ (= $q_n/4\pi\varepsilon_0$), which is defined as an equivalent normalized charge, is used to express the optimum charges on the n^{th} spacecraft. V_n is the normalized spacecraft surface potential while r is the radius of spacecraft. The mass m of each spacecraft was taken to be 150 kg and radius r was taken to be 1m. The spacecraft separation L was taken to be 10 m wherever necessary unless specified. The optimal reduced charges in equilibrium were calculated by minimizing the sum of squares of charges on all the spacecraft in a formation.

Earth Orbiting Three Satellite Formation – Equilibrium

Figure 5-11 shows the collector normalized voltages V_{1n} and V_{2n} as a function of combiner normalized voltage V_{0n} for the x-axis aligned, y-axis aligned and z-axis aligned formations. The angular rate Ω for GEO is taken to be 7.2915×10^{-5} rad/s. One of the interesting results is that one solution for the y-axis aligned formation is keeping all the spacecraft uncharged. In the z-axis aligned formation the central combiner can be kept uncharged. However, in the x-axis aligned formation all the spacecraft need to be charged.

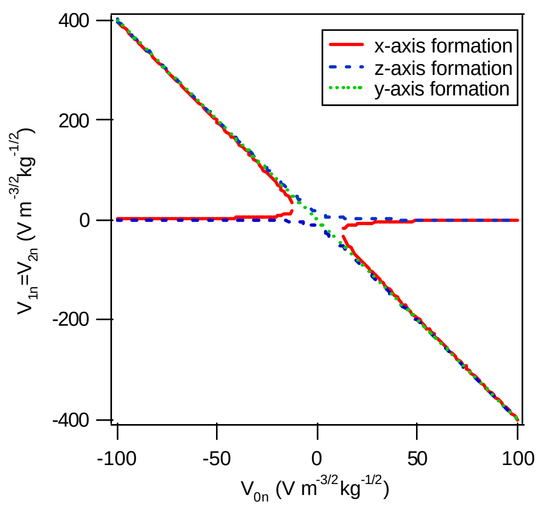

Figure 5-11 Analytic solution set for equilibrium three-spacecraft linear formations

In table 5-1 the optimum normalized spacecraft reduced charges in equilibrium conditions for the three-satellite formations aligned along x-axis and y-axis are given. In y-axis aligned formation the spacecraft do not need to be charged as they are following Keplerian orbit.

Cases	**Optimal Reduced Charges (kV m)**		
	V_0r	V_1r	V_2r
x-axis aligned	5.34	-5.34	-5.34
z-axis aligned	± 2.39	± 2.39	± 2.39

Table 5-1 Spacecraft reduced charges in equilibrium conditions for the three-satellite formations in GEO for 150 kg spacecraft separated by L = 10m.

Earth Orbiting Five Satellite Formation – Equilibrium

Two families of equilibrium solutions were obtained for the five satellite formation shown in Figure 5-7. The first one was obtained by setting $q_2 = q_4 = 0$, resulting in the formation which is same as the z-axis aligned three satellite formation. The second set of solutions is shown in Figure 5-12. It shows two sub-sets of solutions for V_{0n}, V_{1n} and V_{3n} corresponding to a range of V_{2n} (= V_{4n}). For example, if V_{2n} is selected to be 50 V(kgm)$^{-1/2}$, then $V_{1n} = V_{3n} = 46$ V(kgm)$^{-1/2}$ and $V_{0n} = -47.6$ V(kgm)$^{-1/2}$, or $V_{1n} = V_{3n} = 2.6$ V(kgm)$^{-1/2}$ and $V_{0n} = -14.3$ V(kgm)$^{-1/2}$.

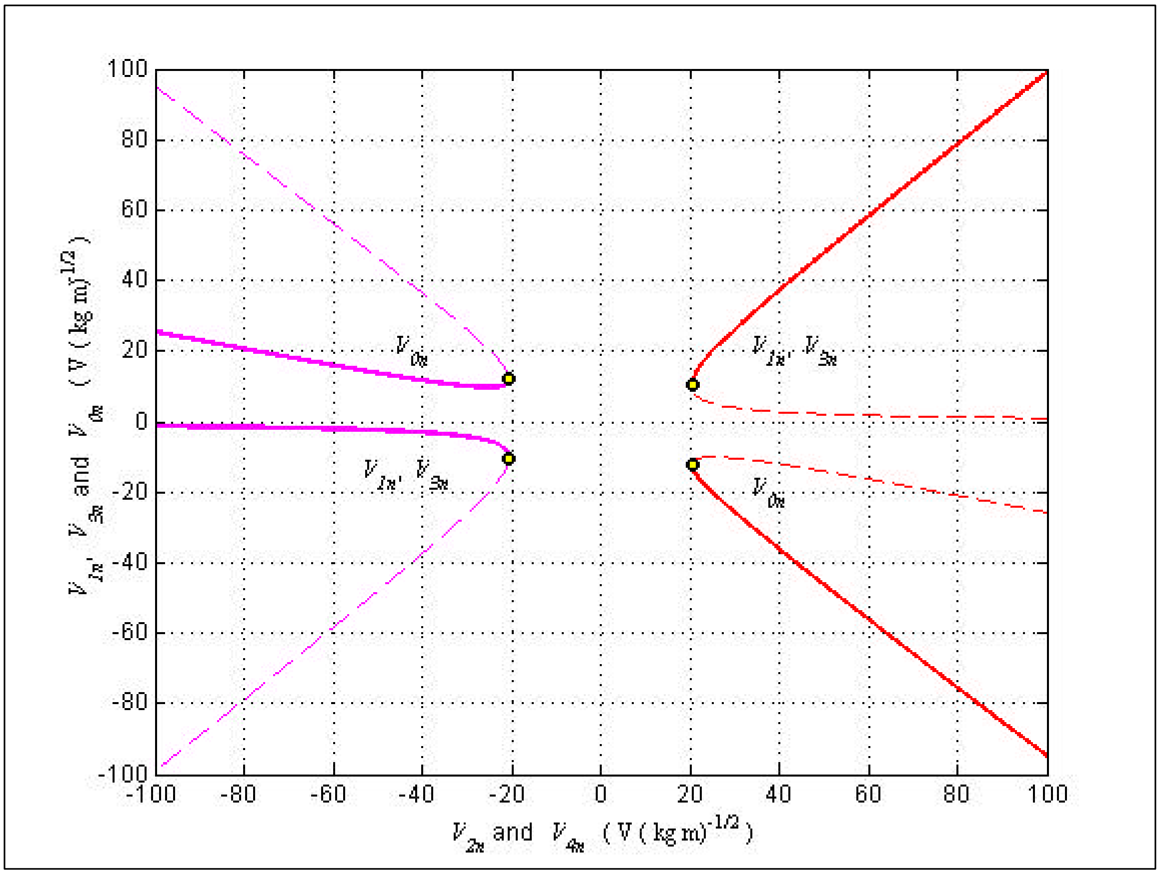

Figure 5-12. Second set of solutions for equilibrium five-spacecraft two-dimensional formation.

The optimal reduced charges on all the satellites are given in Table 5-2

	Optimal Reduced Charges (kV m)		
Spacecraft	V_{1n}, V_{3n}	V_{2n}, V_{4n}	V_{0n}
Voltage (kV)	+/- 3.96	+/- 7.92	-/+ 4.78

Table 5-2 Optimal reduced charges for equilibrium five-spacecraft two-dimensional formation.

Earth Orbiting Six Satellite Formation- Equilibrium

The reduced charges for spacecraft were found numerically, which are listed in Table 5-3.

	Optimal Reduced Charges (kV m)					
Spacecraft	V_0 r	V_1 r	V_2 r	V_3 r	V_4 r	V_5 r
Voltage (kV m)	8.47	-5.21	-7.55	-6.33	-6.33	-7.55

Table 5-3. Equilibrium solution spacecraft reduced charges for 6 spacecraft formation

Libration Point five Satellite Formation-Equilibrium

This formation, shown in Figure 5-9 is at an Earth-Sun Libration point. Unlike other formations this formation does not orbit around Earth but it is rotating about the z_c axis with an angular rate of Ω. The equilibrium solution spacecraft reduced charges for the collector 2 & 4 were found for a range of the collector 1 & 3 voltages were found, as shown in Figure 5-13. L_1 and L_2 were taken to be 12.5 m and 25 m respectively. Three formation spin rates (Ω) 0.5 rev/hr, 0.005rev/hr and 0.005 rev/hr were considered. The solutions are shown in Figure 5-13, Figure 5-14 and Table 5-4.

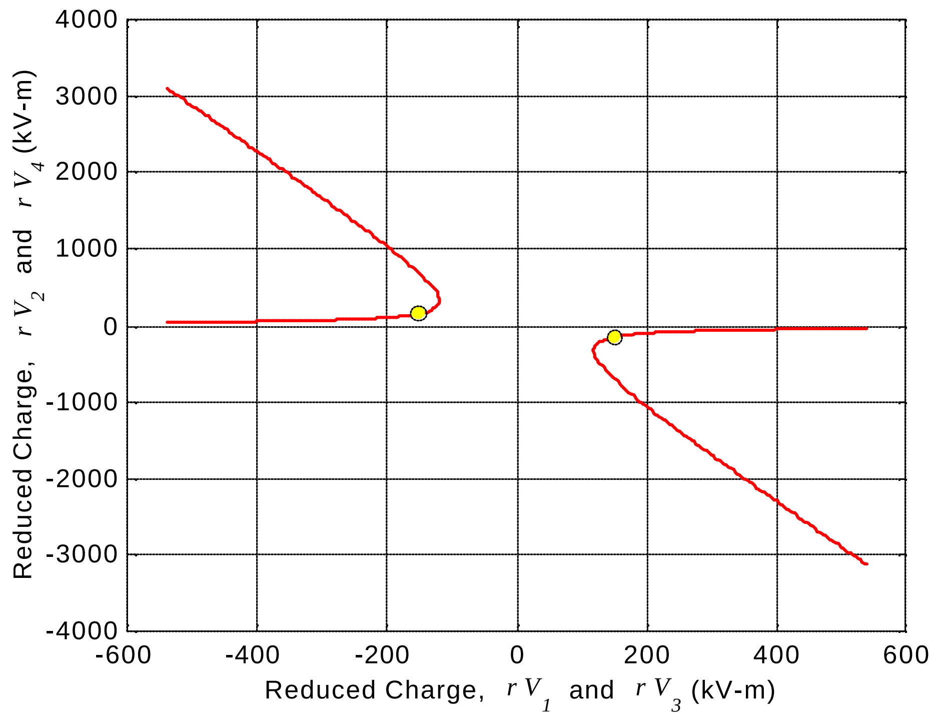

Figure 5-13. Sets of equilibrium solution reduced charges on the collector 2 and 4 for a range of charges on the collector 1 and 3 when the spin rate is 0.5 rev/hr. The optimal solutions giving smallest charges on all the spacecraft are indicated by yellow dots.

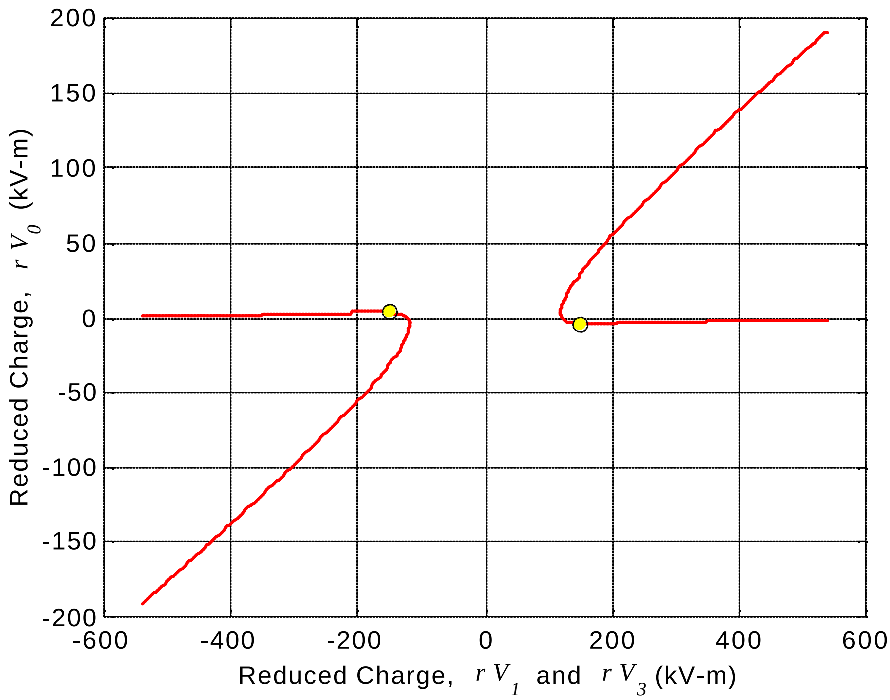

Figure 5-14. Sets of equilibrium solution reduced charges on combiner for a range of the collector 1 and 3 charges when the spin rate is 0.5 rev/hr. The optimal solutions giving smallest charges on all the spacecraft are indicated by yellow dots.

The optimal reduced charges for all the spacecraft in the Libration point 5 spacecraft formation are listed in Table 5-4 for different spin rates.

Spin Rate (rad /s)	**Optimal Reduced Charges (kV m)**				
	V_0 r	V_1 r	V_2 r	V_3 r	V_4 r
8.73E-06	3.73E-02	-1.52E+00	1.52E+00	-1.52E+00	1.52E+00
8.73E-05	3.73E-01	-1.52E+01	1.52E+01	-1.52E+01	1.52E+01
8.73E-04	3.73E+00	-1.52E+02	1.52E+02	-1.52E+02	1.52E+02

Table 5-4. Optimal reduced charges for all the spacecraft in the Libration point 5 spacecraft formation

5.4. *Comparative Mission Trade Study*

Six basic formation geometries were considered in this study (Section 5.2) namely, three variations of three-satellite linear formations, one configuration consisting of five satellites in a plane, one configuration of five satellites in a pentagon formation with a center vehicle, and one rotating linear set of five spacecraft. For each of these formations, the required absolute potential (electric charge) to maintain a static formation using the Coulomb control was computed by Chong et al. We can use these solutions to compare the performance of the Coulomb system with the three canonical electric propulsion thrusters described in Section 5.1. The operating time for a mission τ, is taken to be 10 years.

Using the Hill's equations to predict the required equilibrium formation forces and the performance characteristics of the three electric propulsion technologies, the relations in Eqn. 5-2, Eqn. 5-4, and Eqn. 5-6 can be used to calculate the input power needed by the electric propulsion system, the inert mass required for the mission, and the propellant mass.

For the Coulomb system comparison, the fuel mass can be easily calculated from Eqn. 4-35 if the required emission current, I_e, is known. The emission current is chosen to balance the environmental current (net vehicle current equals zero) in order to maintain a steady potential on the spacecraft. The required vehicle potential for a given formation is found from the solution methods of Section 5.3. Since very general solutions were found for most cases, the "charge optimal" solutions represented by the yellow marker dots on the plots of equilibrium solutions were used to compute mission parameters (for instance, see Figure 5-12 for five-spacecraft two dimensional formation). Using the required vehicle potential, the net environmental current from the plasma is computed according to Eqn. 2-17 and Eqn. 2-18 assuming average GEO plasma conditions as outlined in Table 2-1, a photoelectron current density $J_{pe0} = 10\ \mu A/m^2$, and a photoelectron temperature on the order of 5eV.

With the required emission current for each vehicle, $I_{(e)i}$, and vehicle potential, $V_{(sc)i}$, known, the system input power for each vehicle using Coulomb control is simply $P_i = I_{(e)i} V_{(sc)i}$. In order to calculate the inert mass of the Coulomb system, it is necessary to know the value of the power-specific mass, β, in kg/W. Since the Coulomb technology does not yet exist, this number had to be estimated. Based on the similarity of the Coulomb system to the basic principles of electrostatic emission, such as that used in the Colloid thruster and FEEP, a value of β was chosen to be the average of the Colloid and the FEEP technologies, namely $\beta_{Coulomb} = 0.165$ kg/W. As the Coulomb system does not need to convert electrical power to kinetic thrust power, the efficiency parameter η is not applicable. Although there will be some power loss in the controlling electronics, the amount is believed to be very small and thus an efficiency of unity is applied when calculating the Coulomb input power.

5.4.1. Earth Orbiting Three Spacecraft Formation

In order to investigate the dynamics of a Coulomb formation, very simple three-spacecraft geometries were studied. Three different combinations were specified depending upon the axis along which the spacecraft are aligned 5.2.1. In case a, the spacecraft are aligned along X axis as shown in Figure 5-15. The combiner spacecraft SC_0 is at the center of the Hill's coordinate frame and follows constant equatorial circular orbit. The collectors, i.e. SC_1 and SC_2, are along the X axis at a distance L=10 m from the combiner.

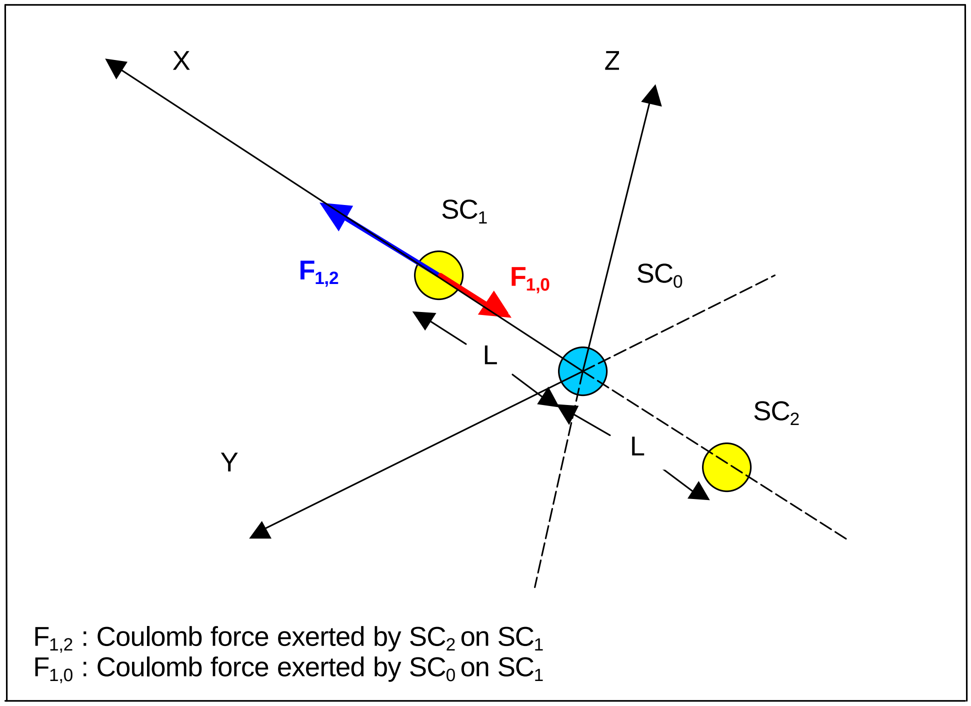

Figure 5-15. Coulomb forces acting on SC_1 in the 3 satellite formation aligned along x axis with respect to Earth. (Diagram not drawn to scale)

The Coulomb performance metrics are listed in Table 5-5 for each spacecraft in the formation case ‘a’. Mission parameters of the entire formation using Coulomb control are compared to those using three canonical electric propulsion technologies in Table 5-6. Graphical comparison between the total propulsion system mass as well as required input power is presented in Figure 5-16 and Figure 5-17.

As discussed in Section 5.3.2, the three-spacecraft case ‘b’ permitted trivial solutions where the vehicles remained uncharged and no formation control force was required. However, an identical mission analysis is presented for the three-spacecraft case ‘c’ in Table 5-7, Table 5-8, Figure 5-18, and Figure 5-19.

Parameters	**Numerical Values For Spacecraft**		
	SC_0	**SC_1**	**SC_2**
1.Charge q_i C	-5.94×10^{-7}	5.94×10^{-7}	5.94×10^{-7}
2.Radius r_i m	0.50	0.50	0.50
3.Emission Current Ie A	3.10×10^{-5}	-3.68×10^{-5}	-3.68×10^{-5}
4.Surface Voltage V_{SC} V	-1.07×10^{4}	1.07×10^{4}	1.07×10^{4}
5.Input Power P_{input} W	3.31×10^{-1}	3.93×10^{-1}	3.93×10^{-1}
6.Propellant Mass Flow Rate $\dot{m}$ kg/s	3.24×10^{-13}	2.09×10^{-16}	2.09×10^{-16}
7.Net Control Force F_i N	0.00	2.27×10^{-5}	2.27×10^{-5}

Table 5-5. Vehicle parameters calculated for the 3-spacecraft formation - Case ‘a’.

Parameters	**Coulomb Control**	**MicroPPT**	**Colloid Thrusters**	**FEEP**
1.Specific Impulse Isp s	1.43×10^{7}	5×10^{2}	1×10^{3}	1×10^{4}
2.Efficiency ? %	N/A	2.6×10^{-2}	6.5×10^{-1}	6.5×10^{-1}
3.Fuel Mass for 10 Years m_{fuel} kg	1.02×10^{-4}	2.91	1.46	1.46×10^{-1}
4.Input Power P_{input} W	1.12	8.55	6.84×10^{-1}	6.84
5.Specific Mass ß kg/W	1.65×10^{-1}	3.70×10^{-1}	2.16×10^{-1}	1.13×10^{-1}
6.Inert Mass m_{inert} kg	1.84×10^{-1}	3.17	1.48×10^{-1}	7.70×10^{-1}
7.Total Mass m_{Total} kg	1.84×10^{-1}	6.08	1.61	9.15×10^{-1}

Table 5-6. Comparison between Coulomb control system and three electric propulsion technologies for the 3-spacecraft formation - Case ‘a’.

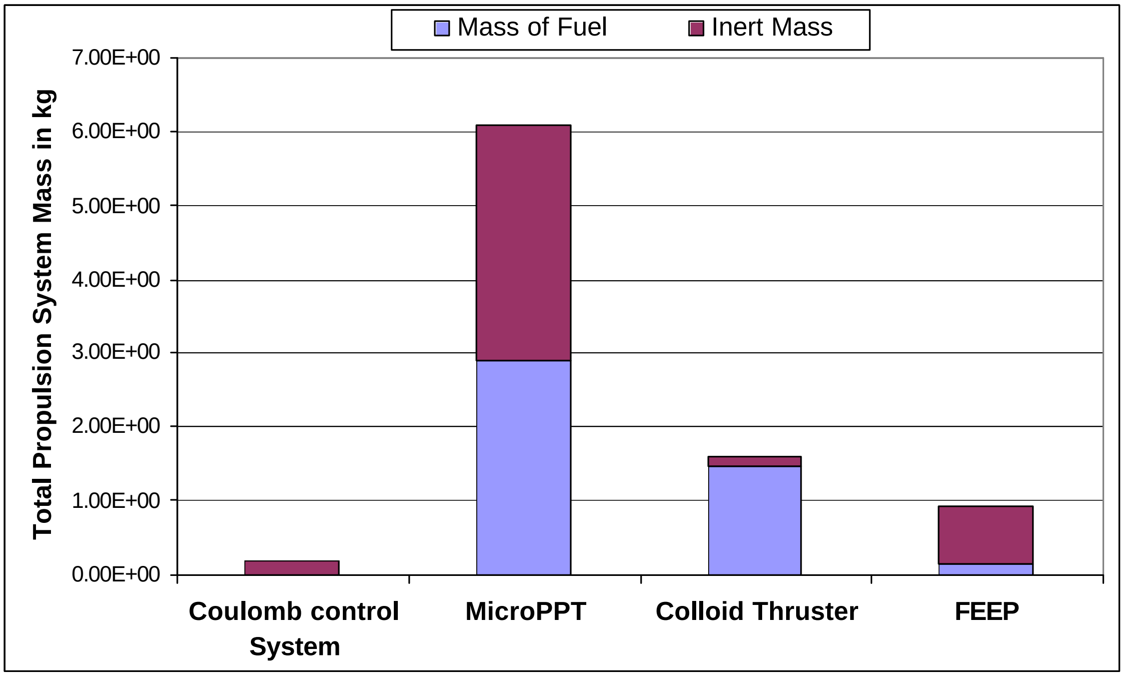

Figure 5-16. Total propulsion system mass for Coulomb control system and three electric propulsion technologies (3 spacecraft formation Case 'a').

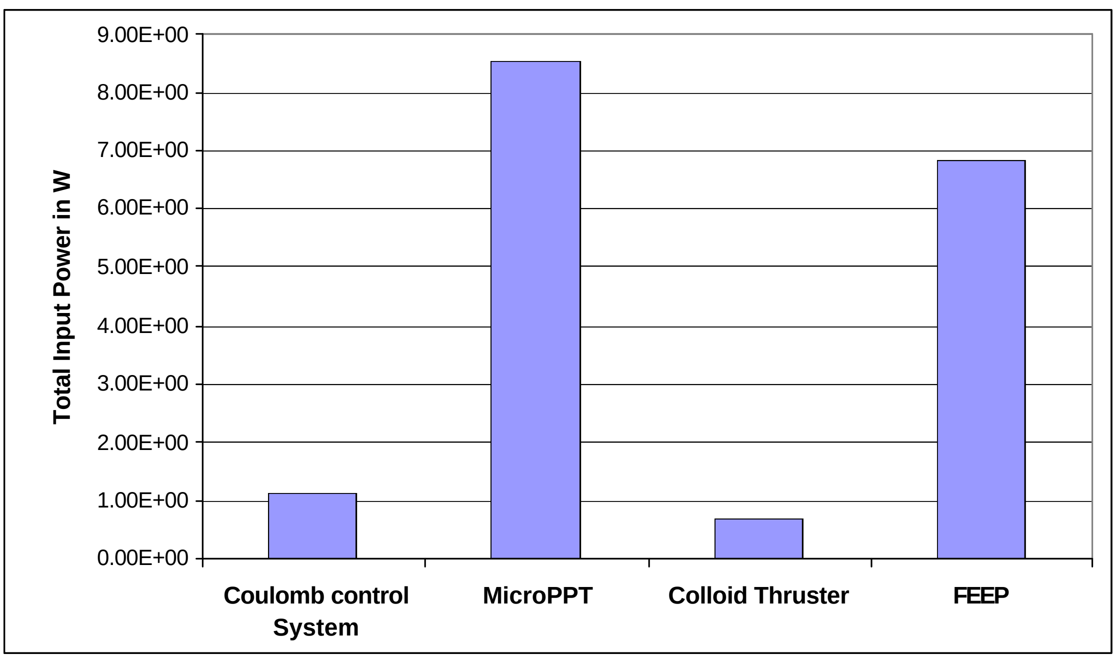

Figure 5-17. Total input power required to maintain formation for Coulomb control and three electric propulsion technologies (3 spacecraft formation Case 'a').

Parameters	**Numerical Values For Spacecraft**		
	SC_0	**SC_1**	**SC_2**
1.Charge q_i C	2.66×10^{-7}	2.66×10^{-7}	2.66×10^{-7}
2.Radius r_i m	0.50	0.50	0.50
3.Emission Current Ie A	-1.86×10^{-5}	-1.86×10^{-5}	-1.86×10^{-5}
4.Surface Voltage V_{SC} V	4.78×10^{3}	4.78×10^{3}	4.78×10^{3}
5.Input Power P_{input} W	8.90×10^{-2}	8.90×10^{-2}	8.90×10^{-2}
6.Propellant Mass Flow Rate $\dot{m}$ kg/s	1.06×10^{-16}	1.06×10^{-16}	1.06×10^{-16}
7.Net Control Force F_i N	0.00	7.30×10^{-6}	7.30×10^{-6}

Table 5-7. Vehicle parameters calculated for the 3-spacecraft formation Case 'c'.

Parameters	**Coulomb Control**	**MicroPPT**	**Colloid Thrusters**	**FEEP**
1.Specific Impulse Isp s	4.68×10^{9}	5×10^{2}	1×10^{3}	1×10^{4}
2.Efficiency ? %	N/A	2.6×10^{-2}	6.5×10^{-1}	6.5×10^{-1}
3.Fuel Mass for 10 Years m_{fuel} kg	1.00×10^{-7}	9.39×10^{-1}	4.69×10^{-1}	4.69×10^{-2}
4.Input Power P_{input} W	2.67×10^{-1}	2.75	2.20×10^{-1}	2.20
5.Specific Mass ß kg/W	1.65×10^{-1}	3.70×10^{-1}	2.16×10^{-1}	1.13×10^{-1}
6.Inert Mass m_{inert} kg	4.41×10^{-2}	1.02	4.76×10^{-2}	2.48×10^{-1}
7.Total Mass m_{Total} kg	4.41×10^{-2}	1.96	5.17×10^{-1}	2.95×10^{-1}

Table 5-8. Comparison between Coulomb control system and three electric propulsion technologies for the 3-spacecraft formation - Case 'c'.

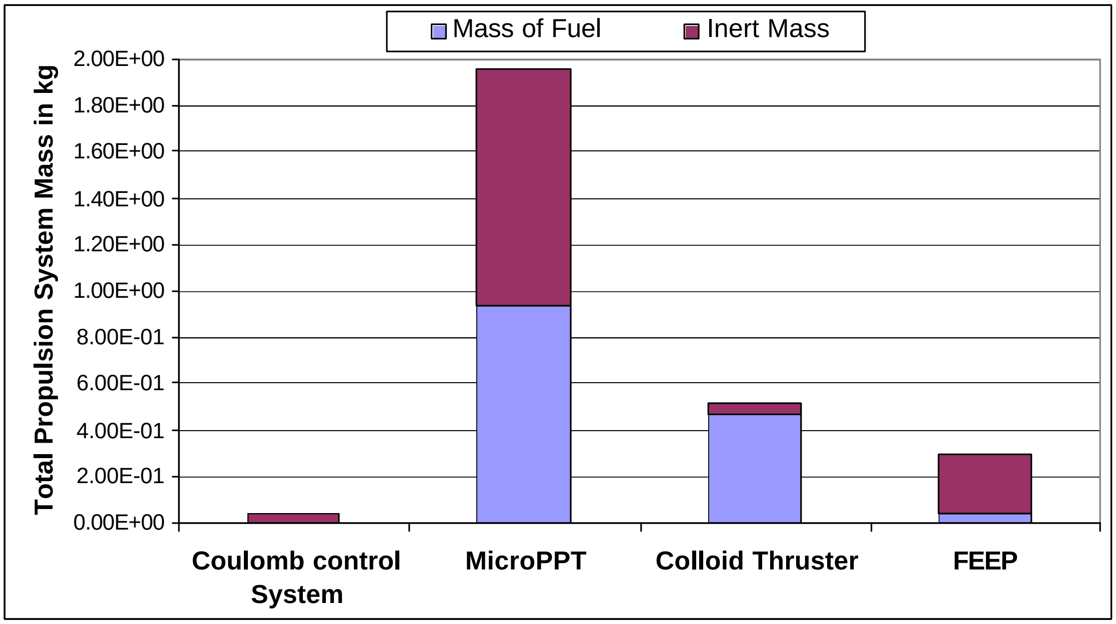

Figure 5-18. Total propulsion system mass for Coulomb control system and three electric propulsion technologies (3 Spacecraft Formation – Case 'c').

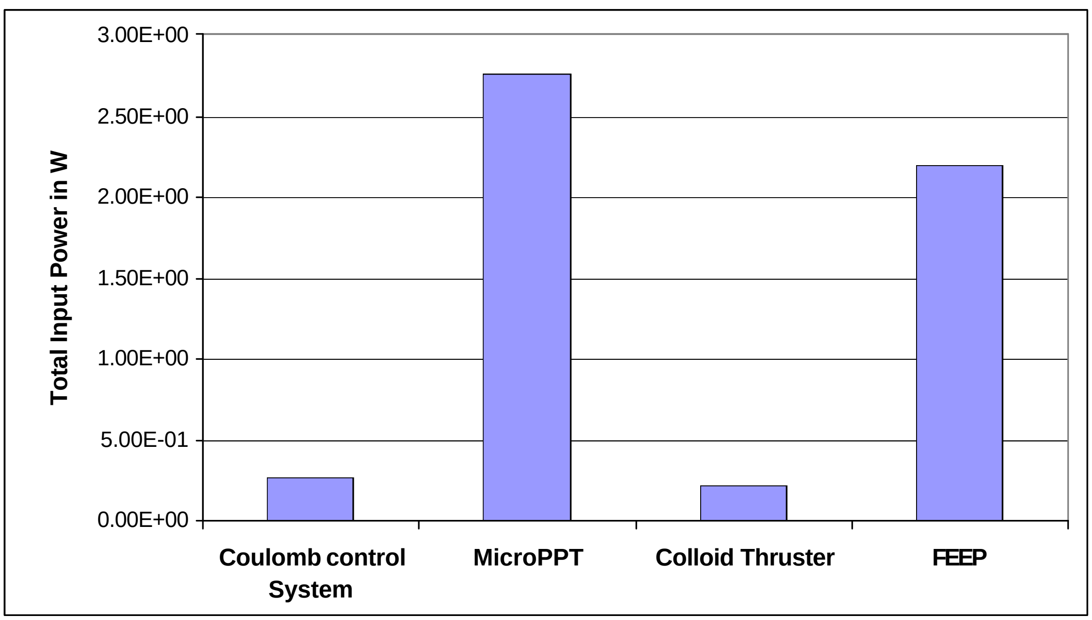

Figure 5-19. Total input power required to maintain formation for Coulomb control and three electric propulsion technologies (3 Spacecraft Formation – Case 'c').

5.4.2. *Earth Orbiting Five Spacecraft Formation*

In an incremental step towards considering practical interferometry formations, a five-spacecraft formation comprised of four collectors and one central combiner was studied and is shown schematically in Figure 5-20. Using techniques identical to those of Section 5.4.1, the Coulomb vehicle parameters for all five spacecraft have been calculated and presented in Table 5-9. Table 5-10 compares the formation performance characteristics using Coulomb control and three canonical electric propulsion technologies. The total system input power and propellant masses are compared in Figure 5-21 and Figure 5-22.

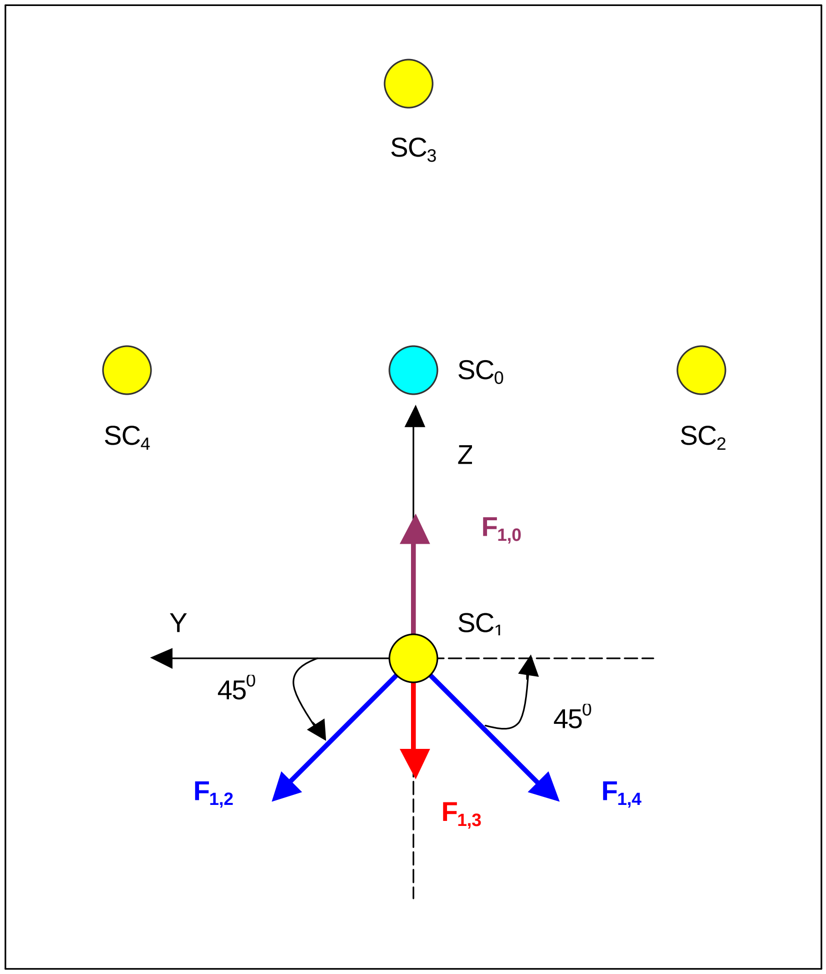

Figure 5-20. Coulomb forces exerted on SC_1 by other 4 spacecraft in five-vehicle Earth-orbiting formation (diagram not drawn to the scale).

Parameters	**Numerical Values For Spacecraft**				
	SC_0	**SC_1**	**SC_2**	**SC_3**	**SC_4**
q_i C	5.32×10^{-7}	-4.40×10^{-7}	-8.81×10^{-7}	-4.40×10^{-7}	-8.81×10^{-7}
r_i m	5.0000×10^{-1}	5.0000×10^{-1}	5.0000×10^{-1}	5.0000×10^{-1}	5.0000×10^{-1}
I_e A	-3.34×10^{-5}	3.07×10^{-5}	3.14×10^{-5}	3.07×10^{-5}	3.14×10^{-5}
$V_{(SC)i}$ V	9.56×10^{3}	-7.92×10^{3}	-1.58×10^{4}	-7.92×10^{3}	-1.58×10^{4}
$P_{(input)i}$ W	3.19×10^{-1}	2.43×10^{-1}	4.98×10^{-1}	2.43×10^{-1}	4.98×10^{-1}
$\dot{m}_i$ kg/s	1.90×10^{-16}	3.20×10^{-13}	3.28×10^{-13}	3.20×10^{-13}	3.28×10^{-13}
F_i N	0.00	7.98×10^{-6}	8.98×10^{-9}	7.98×10^{-6}	8.98×10^{-9}

Table 5-9. Vehicle parameters calculated for the five-spacecraft Earth-orbiting formation.

Parameters	**Coulomb Control**	**MicroPPT**	**Colloid Thrusters**	**FEEP**
1.Specific Impulse Isp s	1.26×10^{6}	5×10^{2}	1×10^{3}	1×10^{4}
2.Efficiency ? %	N/A	2.6×10^{-2}	6.5×10^{-1}	6.5×10^{-1}
3.Fuel Mass for 10 Years m_{fuel} kg	4.09×10^{-4}	1.03	5.13×10^{-1}	5.13×10^{-2}
4.Input Power P_{input} W	1.80	3.02	2.41×10^{-1}	2.41
5.Specific Mass ß kg/W	1.65×10^{-1}	3.70×10^{-1}	2.16×10^{-1}	1.13×10^{-1}
6.Inert Mass m_{inert} kg	2.97×10^{-1}	1.12	5.21×10^{-2}	2.71×10^{-1}
7.Total Mass m_{Total} kg	2.98×10^{-1}	2.14	5.66×10^{-1}	3.23×10^{-1}

Table 5-10. Comparison betwe en Coulomb control system and three electric propulsion technologies for five-spacecraft Earth-orbiting formation.

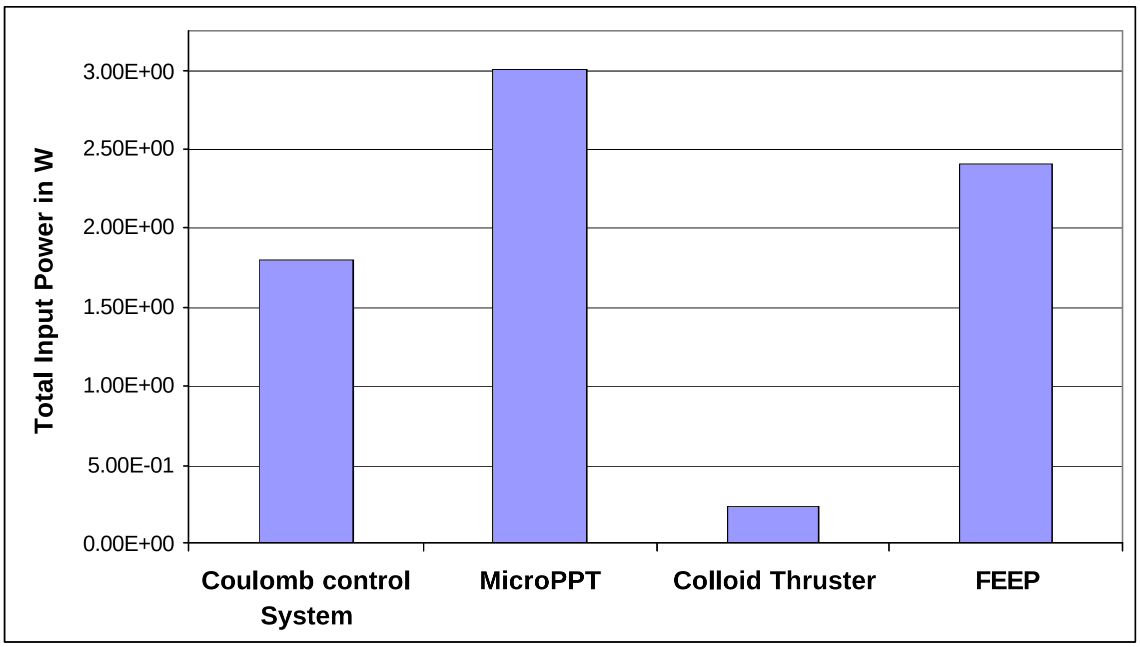

Figure 5-21. Total propulsion system input power required for five-spacecraft formation (Square Planar) using Coulomb control and electric propulsion systems.

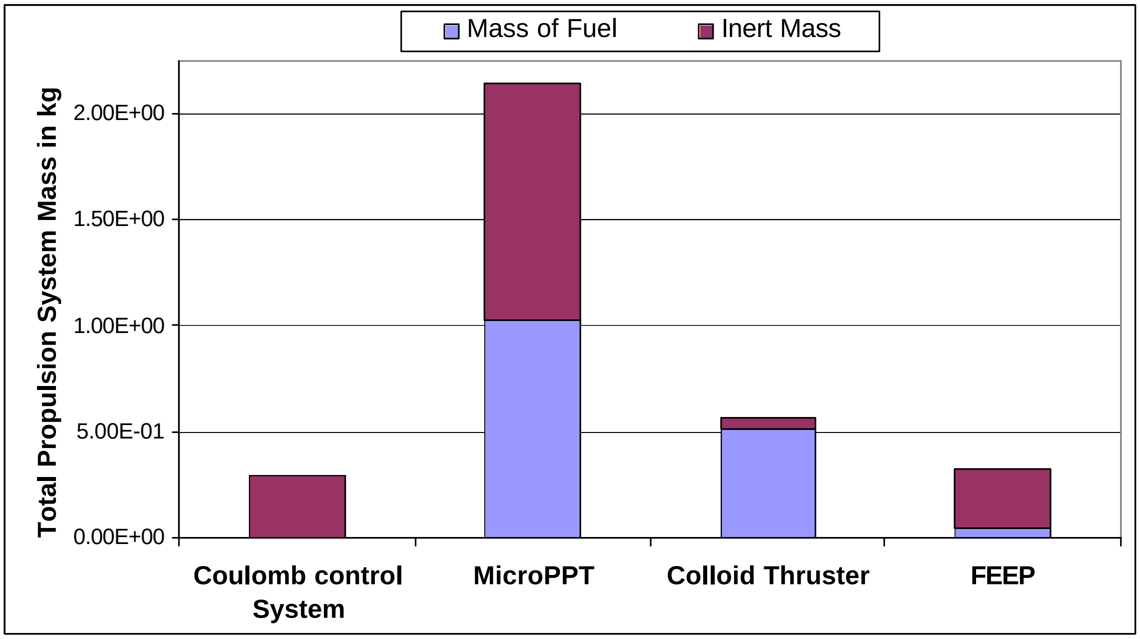

Figure 5-22. Total propulsion system mass for five-spacecraft formation (Square Planar) using Coulomb control and electric propulsion systems.

5.4.3. *Earth Orbiting Six Spacecraft Formation*

The dynamics of a realistic interferometry formation, namely that of a five-vehicle Cornwell array with a central combiner, was studied. Using the "optimal" equilibrium formation potentials (charges) calculated in the numerical solution along with the average GEO plasma conditions, the Coulomb vehicle parameters have been calculated and are presented in Table 5-11, with Table 5-12 comparing the Coulomb control system with three canonical electric propulsion technologies for the same formation. A graphical comparison of total system power and propulsion system mass is presented in Figure 5-23 and Figure 5-24.

Parameters	Numerical Values For Spacecrafts					
	SC_0	SC_1	SC_2	SC_3	SC_4	SC_5
q_i C	9.42	-5.80×10^{-7}	-8.41×10^{-7}	-7.04×10^{-7}	-7.04×10^{-7}	-8.41×10^{-7}
r_i m	5.00×10^{-1}	5.00×10^{-1}	5.00×10^{-1}	5.00×10^{-1}	5.00×10^{-1}	5.00×10^{-1}
I_e A	-5.61×10^{-5}	3.10×10^{-5}	3.14×10^{-5}	3.12×10^{-5}	3.12×10^{-5}	3.14×10^{-5}
$V_{(SC)i}$ V	1.69×10^{4}	-1.04×10^{4}	-1.51×10^{4}	-1.27×10^{4}	-1.27×10^{4}	-1.51×10^{4}
$P_{(input)i}$ W	9.51×10^{-1}	3.23×10^{-1}	4.74×10^{-1}	3.95×10^{-1}	3.95×10^{-1}	4.74×10^{-1}
$\dot{m}_i$ kg/s	3.19×10^{-16}	3.24×10^{-13}	3.28×10^{-13}	3.26×10^{-13}	3.26×10^{-13}	3.28×10^{-13}
F_i N	3.10×10^{-6}	5.39×10^{-6}	8.59×10^{-6}	4.80×10^{-6}	4.81×10^{-6}	8.59×10^{-6}

Table 5-11. Vehicle parameters calculated for the five-spacecraft Cornwell array with central combiner.

Parameters	Coulomb Control	MicroPPT	Colloid Thrusters	FEEP
1.Specific Impulse Isp s	2.21×10^{6}	5×10^{2}	1×10^{3}	1×10^{4}
2.Efficiency ? %	N/A	2.6×10^{-2}	6.5×10^{-1}	6.5×10^{-1}
3.Fuel Mass for 10 Years m_{fuel} kg	5.14×10^{-4}	2.27	1.13	1.13×10^{-1}
4.Input Power P_{input} W	3.01	6.66	5.33×10^{-1}	5.33
5.Specific Mass ß kg/W	1.65×10^{-1}	3.70×10^{-1}	2.16×10^{-1}	1.13×10^{-1}
6.Inert Mass m_{inert} kg	4.97×10^{-1}	2.47	1.15×10^{-1}	5.99×10^{-1}
7.Total Mass m_{Total} kg	4.98×10^{-1}	4.73	1.25	7.13×10^{-1}

Table 5-12. Comparison between Coulomb control system and three electric propulsion technologies for five-spacecraft Cornwell array with central combiner.

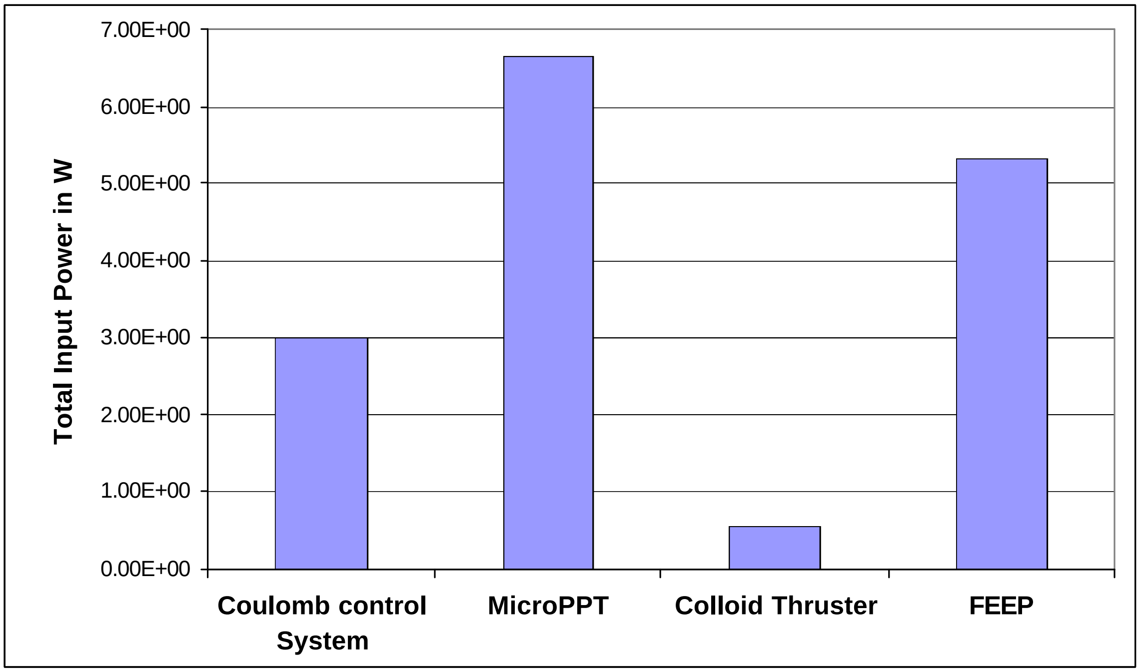

Figure 5-23. Total propulsion system input power for formation calculated for five-spacecraft Cornwell array with central combiner.

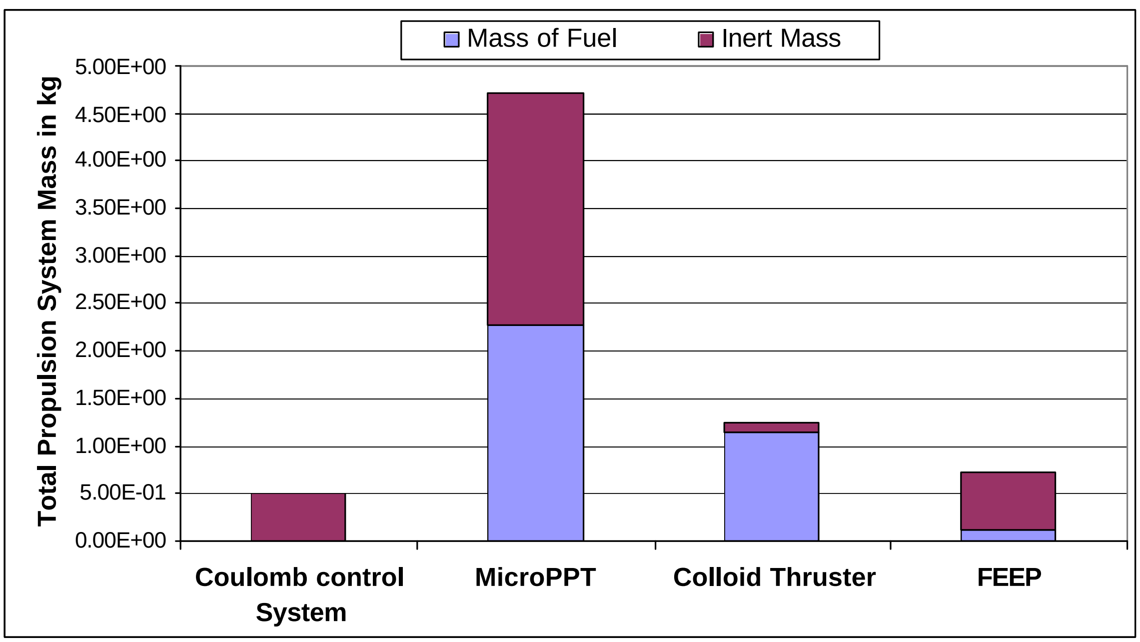

Figure 5-24. Total propulsion system mass required to maintain formation for five-vehicle Cornwell array with central combiner.

5.4.4. *Five-vehicle rotating linear array (TPF)*

The rotating array was chosen for its similarity to the geometric configuration of the Terrestrial Planet Finder (TPF) Mission, for which considerable design analyses have been performed. The TPF formation is assumed to operate outside of a significant gravity well in conditions resembling those found at one of the Earth-Sun Lagrange points. Formation forces are required to hold the collector vehicles in a circular orbit about the central combiner. As mentioned in Section 5.3.2 equilibrium solutions were found for three different rotation rates: 200 hrs/revolution, 20 hrs/revolution, and 2 hrs/revolution. Since the slowest rotation rate considered is impractical for a real mission, the two larger rotation rates are analyzed in this section. Vehicle parameters and system comparisons can be found in Table 5-13, Table 5-14, Figure 5-25, and Figure 5-26 for the 20 hrs/revolution rate, with Table 5-15, Table 5-16, Figure 5-27, and Figure 5-28 representing the 2 hrs/revolution rate.

Parameters	**Numerical Values For Spacecraft**				
	SC_0	**SC_1**	**SC_2**	**SC_3**	**SC_4**
q_i C	4.15×10^{-8}	-1.69×10^{-6}	1.69×10^{-6}	-1.69×10^{-6}	1.69×10^{-6}
r_i m	0.50	0.50	0.50	0.50	0.50
I_e A	-6.18×10^{-6}	3.20×10^{-5}	-9.75×10^{-5}	3.20×10^{-5}	-9.75×10^{-5}
$V_{(SC)i}$ V	7.46×10^{2}	-3.03×10^{4}	3.03×10^{4}	-3.03×10^{4}	3.03×10^{4}
$P_{(input)i}$ W	4.61×10^{-3}	9.72×10^{-1}	2.96	9.72×10^{-1}	2.96
$\dot{m}_i$ kg/s	3.51×10^{-17}	3.34×10^{-13}	5.54×10^{-16}	3.34×10^{-13}	5.54×10^{-16}
F_i N	0.00	5.78×10^{-5}	3.85×10^{-5}	5.78×10^{-5}	3.85×10^{-5}

Table 5-13. Vehicle parameters calculated for the TPF-like rotating five spacecraft linear formation with rotation rate of 0.1×(p/3600) rev/sec.

Parameters	**Coulomb Control**	**MicroPPT**	**Colloid Thrusters**	**FEEP**
1.Specific Impulse Isp s	2.93×10^{7}	5×10^{2}	1×10^{3}	1×10^{4}
2.Efficiency ? %	N/A	2.6×10^{-2}	6.5×10^{-1}	6.5×10^{-1}
3.Fuel Mass for 10 Years m_{fuel} kg	2.11×10^{-4}	1.24×10^{1}	6.19	6.19×10^{-1}
4.Input Power P_{input} W	7.86	3.63×10^{1}	2.91	2.91×10^{1}
5.Specific Mass ß kg/W	1.65×10^{-1}	3.70×10^{-1}	2.16×10^{-1}	1.13×10^{-1}
6.Inert Mass m_{inert} kg	1.30	1.35×10^{1}	6.29×10^{-1}	3.27
7.Total Mass m_{Total} kg	1.30	2.58×10^{1}	6.82	3.89

Table 5-14. Comparison Between Coulomb Control System and Electric Propulsion Systems for TPF-like rotating five spacecraft linear formation with rotation rate of 0.1×(p/3600) rev/sec.

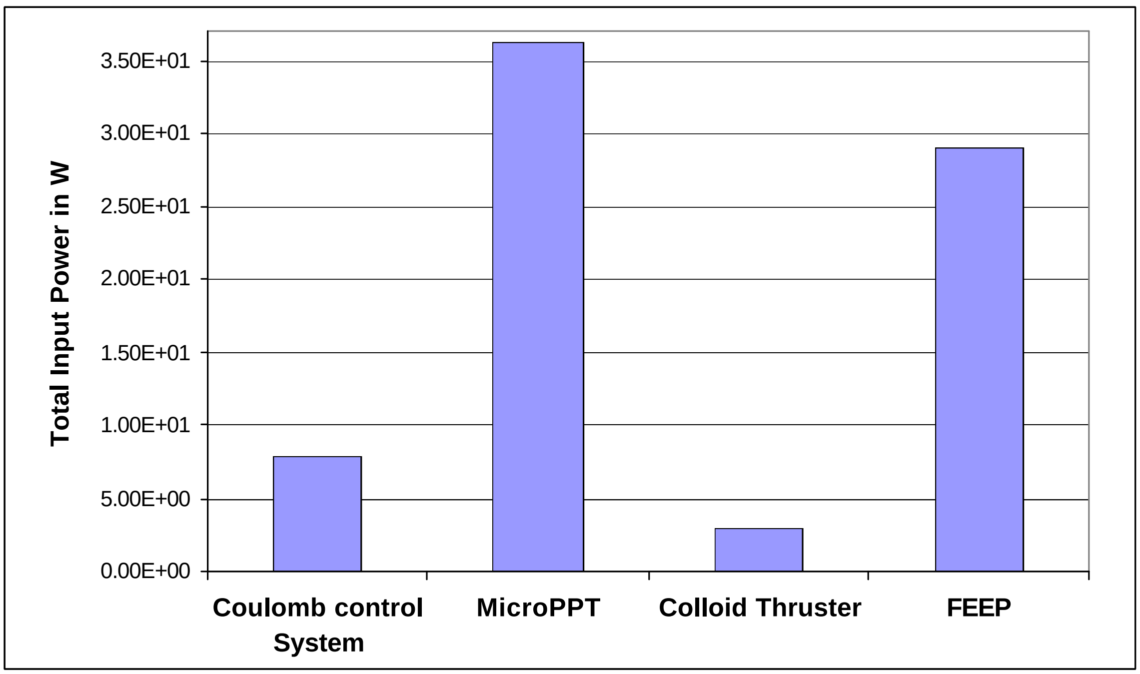

Figure 5-25. Total propulsion system input power for the TPF-like rotating five spacecraft linear formation with rotation rate of 0.1×(p/3600) rev/sec.

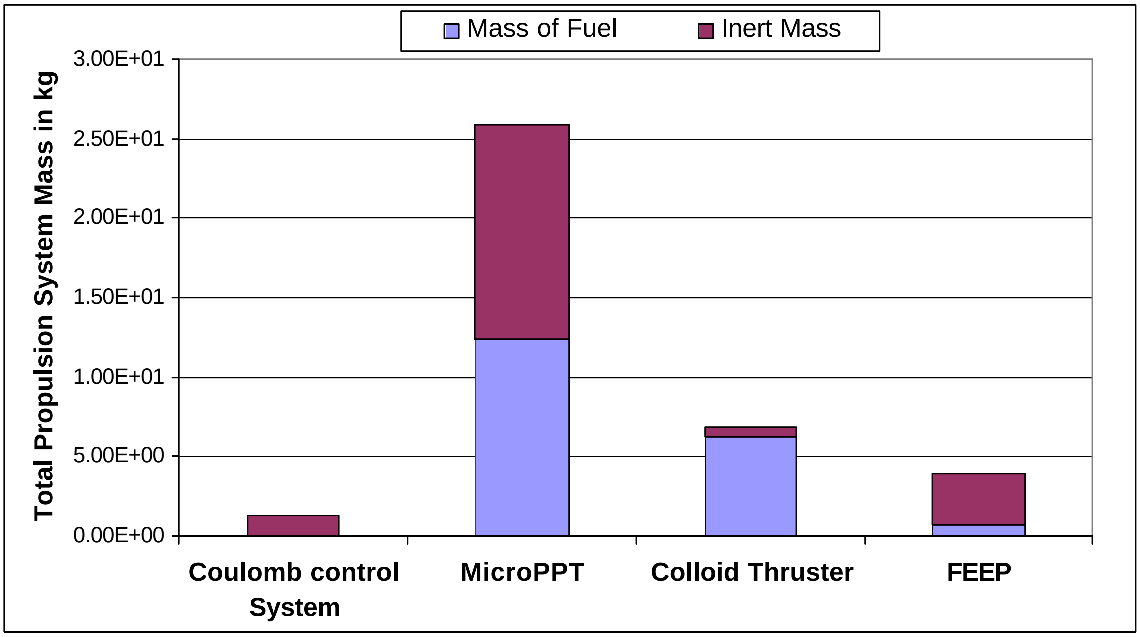

Figure 5-26. Total propulsion system mass required to maintain the TPF-like rotating five-spacecraft linear array with rotation rate of 0.1×(p/3600) rev/sec.

Parameters	**Numerical Values For Spacecraft**				
	SC_0	**SC_1**	**SC_2**	**SC_3**	**SC_4**
q_i C	4.15×10^{-7}	-1.69×10^{-5}	1.69×10^{-5}	-1.69×10^{-5}	1.69×10^{-5}
r_i m	0.50	0.50	0.50	0.50	0.50
I_e A	-2.69×10^{-5}	3.74×10^{-5}	-9.39×10^{-4}	3.74×10^{-5}	-9.39×10^{-4}
$V_{(SC)i}$ V	7.46×10^{3}	-3.03×10^{5}	3.03×10^{5}	-3.03×10^{5}	3.03×10^{5}
$P_{(input)i}$ W	2.01×10^{-1}	1.13×10^{1}	2.85×10^{2}	1.13×10^{1}	2.85×10^{2}
$\dot{m}_i$ kg/s	1.53×10^{-16}	3.90×10^{-13}	5.34×10^{-15}	3.90×10^{-13}	5.34×10^{-15}
F_i N	0.00	5.78×10^{-3}	3.85×10^{-3}	5.78×10^{-3}	3.85×10^{-3}

Table 5-15. Vehicle parameters calculated for the TPF-like rotating five spacecraft linear formation with rotation rate of 1×(p/3600) rev/sec.

Parameters	**Coulomb Control**	**MicroPPT**	**Colloid Thrusters**	**FEEP**
1.Specific Impulse Isp s	2.48×10^{9}	5×10^{2}	1×10^{3}	1×10^{4}
2.Efficiency ? %	N/A	2.6×10^{-2}	6.5×10^{-1}	6.5×10^{-1}
3.Fuel Mass for 10 Years m_{fuel} kg	2.49×10^{-4}	1.24×10^{3}	6.19×10^{2}	6.19×10^{1}
4.Input Power P_{input} W	5.93×10^{2}	3.63×10^{3}	2.91×10^{2}	2.91×10^{3}
5.Specific Mass ß kg/W	1.65×10^{-1}	3.70×10^{-1}	2.16×10^{-1}	1.13×10^{-1}
6.Inert Mass m_{inert} kg	9.78×10^{1}	1.35×10^{3}	6.28×10^{1}	3.27×10^{2}
7.Total Mass m_{Total} kg	9.78×10^{1}	2.58×10^{3}	6.82×10^{2}	3.89×10^{2}

Table 5-16. Comparison Between Coulomb Control System and Electric Propulsion Systems for the TPF-like rotating five spacecraft linear formation with rotation rate of 1×(p/3600) rev/sec.

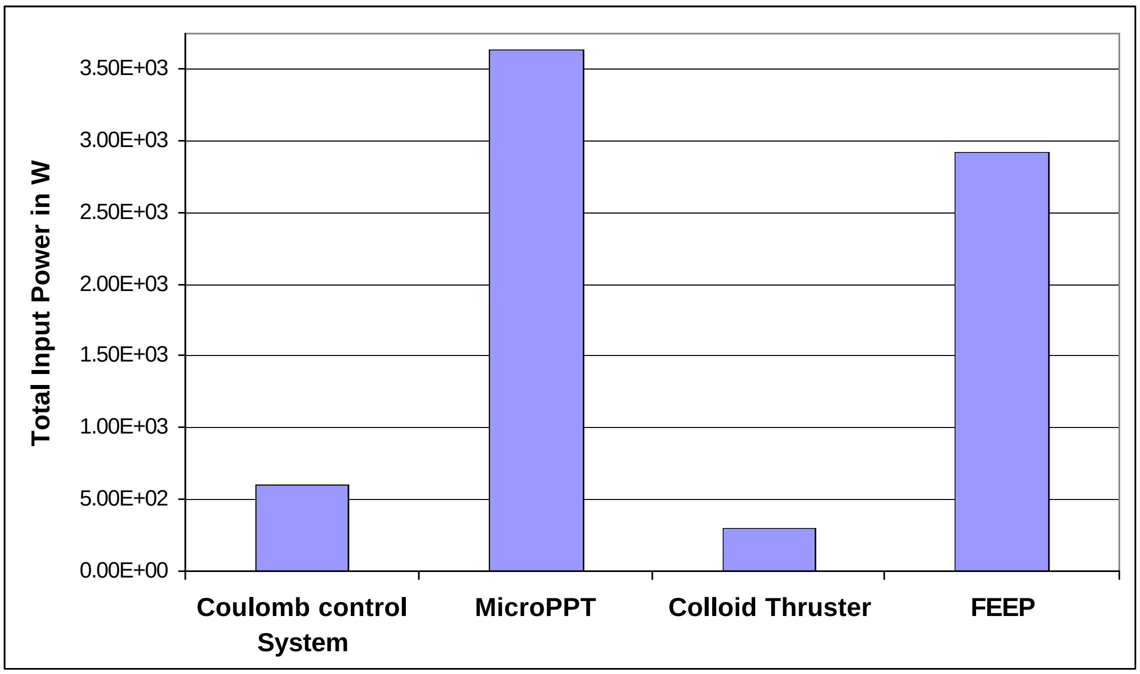

Figure 5-27. Total propulsion system input power for the TPF-like rotating five spacecraft linear formation with rotation rate of 1×(p/3600) rev/sec.

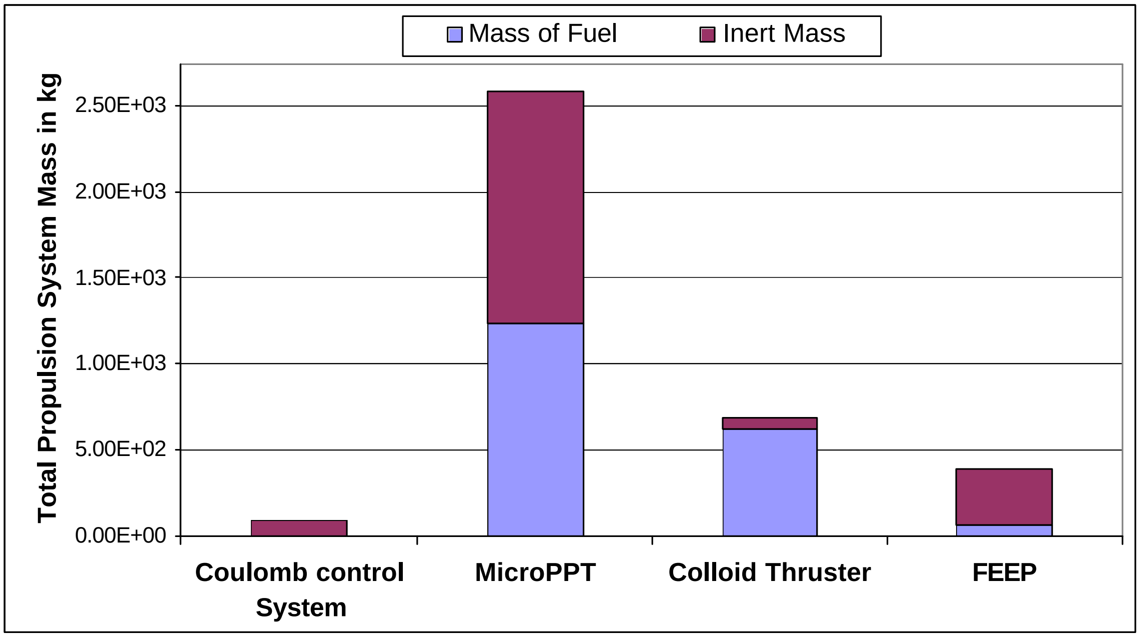

Figure 5-28. Total propulsion system mass required to maintain the TPF-like rotating five-spacecraft linear array with rotation rate of 1×(p/3600) rev/sec.

6. Conclusions and Recommendations

In the final chapter of the thesis, conclusions will be drawn from the research performed on the innovative Coulomb Control Technology. Physical significance of these conclusions will be presented with reference to the propulsion techniques for formation flying. Advantages and limitations of the Coulomb Control Technology will be discussed. NASA and commercial applications of this technology will be presented. Finally future work will be recommended for further development of this technology.

6.1. Conclusions

All the research done so far by the space community on spacecraft charging was focused on mitigating differential charging on single vehicles. Natural charging of spacecraft to potentials of order of kilovolts was detected and analyzed. Proper design guidelines to avoid absolute and differential charging were developed. Control of the spacecraft potential by ion/electron emission was also tested on SCATHA and the international space station.

With the recent advent of spacecraft formation flying concept, propulsion requirements for the formation became a key area of development. An innovative idea of utilizing spacecraft charging to fulfill propulsive requirements of a spacecraft formation was analyzed in this research work. The following technical conclusions can be made based on the present research. The physical significance of these conclusions will be presented shortly.

<u>Conclusion # 1</u>: Coulomb interaction forces as large as 1mN exist between charged vehicles in a formation due to natural charging.

The Coulomb interaction forces were found to be as large as 1 mN for spacecraft 10 m apart in the ATS-6 eclipse environment, with all environments except the 4-Sept.-97 case showing interaction forces greater than 10 μN at the closest spacing. The decay in force with separation is not purely $1/r^2$ due to the finite size effects of the vehicles. At the largest spacing considered (100 m) the inter-spacecraft forces vary from 10^{-10} N up to about 100 nN, depending upon the orbital conditions used in the SEE prediction. The electric-dipole-induced torques were found to be as large as 100 μN-m for the closest spacing in the ATS-6 / Eclipse conditions, falling as low as 10^{-10} N-m for the 4-Sept.-97 case at 100-m spacing.

<u>Conclusion # 2</u>: Coulomb interaction forces resulting from controlled spacecraft charging can be utilized for formation keeping and attitude control.

The Coulomb forces between spacecraft in close formations are found to be comparable to those created by candidate electric propulsion systems. Analytical methods are developed in related research work by Chong et al[81,82,83] to show the existence of static equilibrium formations in Earth orbit, using only Coulomb interaction forces and the charge required to be maintained on each spacecraft in these formations was also found. The spacecraft charge can be varied by active electron or ion emission as per requirement of the different missions discussed in this work. Coulomb forces up to 57.8 μN can be created by maintaining the spacecraft potential at –30.3 kV for a spacecraft separation of 12.5 meters, as shown in Table 5-13 for rotating five spacecraft (TPF like) mission.

<u>Conclusion # 3:</u> *Power levels as low as tens of milliwatts are sufficient to maintain the inter-vehicle Coulomb forces/torques and change their magnitude within milliseconds.*

It was found that with 200 milliwatts of power, the potential of a 1-m-diameter spacecraft in GEO could be varied from 0 to 6kV within 8 milliseconds. Thus the power requirements to maintain the inter spacecraft Coulomb forces are very low and they can be controlled continuously within a time scale of milliseconds.

The surface potential necessary to maintain the inter-spacecraft Coulomb forces for 3 spacecraft formations was found to be a few kilovolts and that required for 6 spacecraft formations was found to be tens of kilovolts, by Chong et al. Power levels as low as tens of milliwatts were found to be sufficient to maintain the required surface potential except the TPF-like rotating five spacecraft linear formation.

<u>Conclusion # 4:</u> *Specific impulse as high as 10^9 sec and propulsion mass saving up to 97% can be attained using Coulomb Control Technology.*

Specific impulse of 10^9 sec was found for Coulomb Control Technology for 3 Spacecraft formation – Case 'c' and TPF like five- spacecraft rotating linear formation. For other formations, it was found to be higher at least by order of two, as compared to candidate electric propulsion technologies. Total propulsion system mass saving was found to be 96- 97% as compared to MicroPPT, for 3 spacecraft formations and 5-spacecraft rotating formations.

6.2. Significance and Advantages of the Research

These findings mark the significance of the revolutionary Coulomb Control Technology within the current spacecraft propulsion research. All the electric propulsion systems flown to date and proposed for future formation flights, operate according to the rocket principle i.e. mass is ejected from a vehicle to affect momentum transfer and propulsive force. Varieties on this priciple utilize chemical reactions to accelerate the mass as well as electromagnetic forces, however the fundamental origin of the thrust is the momentum imparted to the expelled mass. In contrast, the Coulomb Control Technology will rely on the interaction with ambient space plasma and the active emission of electric charge from the vehicle to control spacecraft charging. Attractive and repulsive Coulomb forces between vehicles can be adjusted to maintain the relative cluster formation. This novel propulsive scheme will eliminate thruster plume exhaust contamination of neighboring spacecraft, provide a mechanism for configuring a formation into a "safe" collision-avoidance mode in the event of position uncertainty, utilize less propulsion system mass than competing thruster technologies and possibly enable high-precision close-formation flying due to the high bandwidth at which the Coulomb forces can be varied. A Coulomb control system has the following potentials:

Eliminate spacecraft cross-contamination.

Microthrusters currently envisioned for swarm formation-flying emit propellant such as Teflon or cesium. Many science missions, which benefit from formation flying, will carry sensitive diagnostic equipment. In close proximity operations, propellant exhaust from microthrusters has a high likelihood of adversely impinging upon neighboring craft, and hence disabling diagnostics. The Coulomb control concept will eliminate this limitation.

Improve fine-positioning.

Conventional propulsive devices rely on discrete impulse bits to control fine positioning. Factors limiting the positioning accuracy within a swarm include repeatability of impulse bits, random off-axis thrust components, and resolution of impulse control. Through active feedback, the Coulomb concept can allow continuous, fine-resolution maneuverability, which can greatly improve formation tolerances due to the high bandwidth at which the Coulomb forces can be varied.

Eliminate orbital corrections of the formation.

The application of Coulomb control will modify only the geometry of the formation, but never the center of mass of the formation. Therefore, in case of any perturbations the Coulomb control will reorganize the geometry formation by changing relative positions of the spacecraft in the formation, without altering the center of mass of the formation. This will eliminate the thrust requirements for further correction of the orbit of the formation.

Reduce propulsion system mass.

In a head-to-head comparison of Coulomb control with candidate electric propulsion microthrusters for the SSI missions considered in this study, it was found that the Coulomb system has the potential to reduce the overall spacecraft propulsion system mass by up to 97%. This reduction is enabled due to the low power required by the Coulomb system and nearly propellantless operation with specific impulse values up to 10^9 seconds possible.

Provide assured collision avoidance.

For the class of missions considered requiring close formations in high orbits, the risk of collision is unsettling. Coupled with the earth-to-satellite telecommunications delay time associated with high orbits, loss of position knowledge for any of the vehicles in the formation could be disastrous for the mission. In the Coulomb scheme, simultaneous charging of all of the vehicles to the same polarity would provide assured collision avoidance in a "panic" mode. Even if position knowledge is absent for all of the vehicles, mutual Coulomb repulsion would assure that all vehicles repel each other.

6.3. Applications

The Coulomb Control Technology is ideally suited for high-precision position maintenance of spacecraft in close formations. A unique and important class of missions, that involving meter-level resolution planetary imaging from high orbits, has been presented in some detail in Section 1.2. Such missions would have benefit for Earth climate observation and planetary science, military reconnaissance, and personnel or municipal crisis monitoring/rescue coordination with rapid response time. The ability to view any region on the earth's surface within a hemisphere with meter-level resolution would undoubtedly find many NASA, military, and commercial applications. It is likely that other classes of science and non-science missions would be enabled with the proposed technology.

6.4. *Recommendations:*

The Coulomb Control concept may be a promising propulsion technology for upcoming age of formation flying. In order to exploit this concept, the following study should be performed and the technology should be ground and flight-tested.

Determination of the intra-vehicle response to a charge-changing event:.

The transient response of a spacecraft in natural plasma environment was determined in the present research for simple spacecraft geometry available in Spacecraft Charging Handbook. The transient response of a spacecraft with realistic geometry should be determined during active ion/electron emission. The variables may include vehicle geometry, input power and voltage to charge emission system, physical location of this system on the spacecraft and material properties.

Determination of change in inter-vehicle Coulomb force and torque with time:

Inter-vehicle Coulomb force and torque due to natural charging in the specified plasma environments were determined in the present work. The change in inter-vehicle Coulomb force and torque with charge changing event should be determined, varying emission current, spacecraft power, surface potential, and plasma environment.

Development of centralized Coulomb control strategy:

One of the unique attractive features of Coulomb forces is that they are internal to the formation. They do not cause change in the center of gravity of formation. In traditional electric propulsion technology, if one spacecraft is displaced from its position, only that spacecraft is moved back to its original position. However, in case of Coulomb control, position of all the spacecraft will get affected due to such event. Hence a fully centralized control system should be developed, so that all the spacecraft can be moved to an equivalent formation. This will result in equivalent expenditure of resources from all the spacecraft.

Integration of Coulomb Control Technology and Electric Propulsion technology:

Coulomb Control Technology is best for closely spaced formations while electric propulsion technologies are suited for widely separated formations. Both of these technologies can be utilized in Separated Spacecraft Interferometry formations with varying baseline. It is necessary to research on proper integration of both these technologies so that they are used in the operational envelope in which they work best.

References

[1] Pollard, J.E., Chao, C.C., and Janson, S.W., “Populating and maintaining cluster constellations in low-earth orbit,” AIAA-99-2878, AIAA Meeting Papers on Disk Vol. 4, No. 3, Proc. Of 35th AIAA/ASME/SAE/ASEE Joint Propulsion Conference, June 20-24, 1999, Los Angeles, CA.

[2] Walker, J.G., “The geometry of cluster orbits,” J. Brit. Interplan. Soc., Vol. 35, 1982, p. 345.

[3] Murdoch, J. and Pocha, J.J., “The orbit dynamics of satellite clusters,” Paper IAF-82-54, 33rd International Astronautical Congress, Sept. 27-Oct. 2, 1982, Paris, France.

[4] Micci, M.M. and Ketsdever, A.D., Micropropulsion for Small Spacecraft, Progress in Astronautics and Aeronautics Vol. 187, AIAA Press, Reston VA, 2000, pp. 3-22.

[5] Hoskins, W.A., Wilson, M.J., Willey, M.J., Meckel, N.J., Campell, M., and Chung, S., “PPT development efforts at Primex Aerospace Company,” Paper AIAA-99-2291, AIAA Meeting Papers on Disk Vol. 4, No. 3, Proc. Of 35th AIAA/ASME/SAE/ASEE Joint Propulsion Conference, June 20-24, 1999, Los Angeles, CA.

[6] Chao, C.C., Pollard, J.E., and Janson, S.W., “Dynamics and control of cluster orbits for distributed space missions,” Paper AAS-99-126, Space Flight Mechanics Meeting, Feb. 7-10 1999, Breckenridge, CO.

[7] Kong, E.M.C., Miller, D.W., and Sedwick, R.J., “Exploiting orbital dynamics for aperture synthesis using distributed satellite systems: Applications to a visible Earth imager system,” Paper AAS-99-122, Space Flight Mechanics Meeting, Feb. 7-10 1999, Breckenridge, CO.

[8] Sedwick, R., Miller, D., and Kong, E., “Mitigation of differential perturbations in clusters of formation flying satellites,” Paper AAS-99-124, Space Flight Mechanics Meeting, Feb. 7-10 1999, Breckenridge, CO.

[9] Miller, D.W. and Spores, R.A., “Proceedings of the Formation Flying and Micropropulsion Workshop,” unpublished, Oct. 20-21 1998, available from Dr. Ronald Spores, Air Force Research Laboratory, Edwards AFB, CA.

[10] Micci, M.M. and Ketsdever, A.D., Micropropulsion for Small Spacecraft, Progress in Astronautics and Aeronautics, Vol. 187, AIAA Press, Reston, VA, 2000.

[11] Corazzini, T., Robertson, A., Adams, J.C., Hassibi, A., and How, J.P., "GPS sensing for spacecraft formation flying," Proceedings of the 10th International Technical Meeting, ION/GPS, Sept. 16-19 1997, Kansas City, MO.

[12] Vassar, R.H. and Sherwood, R.B., "Formationkeeping for a pair of satellites in a circular orbit," Journal of Guidance, Control, and Dynamics, Vol. 8, No. 2, 1985.

[13] Leonard, C.L., "Fuel penalty of using ballistic coefficient control for satellite formationkeeping," AAS 13th Annual Guidance and Control Conference, Keystone, CO, Feb. 1990.

[14] Jilla, Cyrus D., Separated Spacecraft Interferometry – System Architecture Design and Optimization, Master's Thesis, Dept. of Aeronautics and Astronautics, Massachusetts Institute of Technology, Feb. 1999.

[15] Kong, Edmund M., Optimal Trajectories and Orbit Design for Separated Spacecraft Interferometry, Master's Thesis, Dept. of Aeronautics and Astronautics, Massachusetts Institute of Technology, Nov. 1998.

[16] Yashko, Gregory, Ion Micro-Propulsion and Cost Modelling for Satellite Clusters, Master's Thesis, Dept. of Aeronautics and Astronautics, Massachusetts Institute of Technology, June 1998.

[17] Hacker, Troy L., Performance of a Space-based GMTI Radar System using Separated Spacecraft Interferometry, Master's Thesis, Dept. of Aeronautics and Astronautics, Massachusetts Institute of Technology, May 2000.

[18] Janson, S.W., Helvajian, H., Hansen, W.W., and Lodmell, J., "Microthrusters for nanosatellites," 2nd International Conference on Integraed Micro Nanotechnology for Space Applications (MNT99), Apr. 11-14 1999, Pasadena, CA.

[19] Janson, S.W., Helvajian, H., Hansen, W.W., and Lodmell, J., "Batch-fabricated CW microthrusters for kilogram-class spacecraft," Paper AIAA-99-2722, AIAA Meeting Papers on Disk Vol. 4, No. 3, Proc. Of 35th AIAA/ASME/SAE/ASEE Joint Propulsion Conference, June 20-24, 1999, Los Angeles, CA.

[20] Tajmar, M., Mitterauer, J., and Wang, J., "Field-emission-electric-propulsion (FEEP) plasma modeling: 3D full particle simulations," Paper AIAA-99-2298, AIAA Meeting Papers on Disk Vol. 4, No. 3, Proc. Of 35th AIAA/ASME/SAE/ASEE Joint Propulsion Conference, June 20-24, 1999, Los Angeles, CA.

[21] Martinez-Sanchez, M. and Pollard, J.E., "Spacecraft electric propulsion – An overview," Journal of Propulsion and Power, Vol. 14, No. 5, Sept-Oct 1998, pp. 688-699.

[22] Ridgeway, S.T., “The scientific support for a space interferometry mission,” SPIE Vol. 1947 Spaceborne Interferometry, 1993, pp. 2-11.

[23] Hecht, E., Optics, Addison-Wesley, 1998.

[24] Golay, M., “Point arrays having compact non-redundant autocorrelations, Journal of Optical Society of America, Vol. 61, pg. 272, 1971.

[25] Cornwell, T.J., “A Novel Principle for Optimization of the Instantaneous Fourier Plane Coverage of Correlation Arrays,” IEEE Trans. On Antennas and Propagation, Vol. 36, No. 8, pp. 1165-1167.

[26] Garrett H. B, and Whittlesey A. C., “ Spacecraft Charging, An Update”, IEEE Transactions on Plasma Science, Vol. 28, No. 6, December 2000, pp 2017-28.

[27] Hastings Daniel, Garrett Henry, “Spacecraft –Environment Interactions”, Cambridge University Press, 1996, pp.44-71.

[28] Langmuir, I., and Blodgett, Currents limited by space charge between concentric spheres, Phys. Rev., 24, 49, 1924

[29] Mott-Smith, H. M., and Langmuir, I., “The theory of collectors in gaseous discharges, Phys. Rev., 28, 727-763, 1926

[30] Chopra, K. P., “Interactions of rapidly moving bodies in terrestrial atmospheres”, Rev. Mod. Phys., 33, 153-189, 1961

[31] Whipple, E. C., “ Potentials of surfaces in space”, Rep. Prog. Phys., Vol. 44, pp. 1197-1250, 1981.

[32] Garrett, H. B., “The charging of spacecraft surfaces,” Rev. Geophys., Vol.19, pp. 577-616, 1981

[33] Jung, B., “The origin of solid particles in interstellar space,” Astron. Nach., 263, 1937, pp. 426.

[34] Spitzer, L., “The dynamics of interstellar medium,” Astrophys. J., 93, 369-79, 1941, and “The temperature of interstellar material,” Astrophys. J., 107 6-33, 1948

[35] Cernuschi, F., “The physics of cosmic grains.” Astrophys. J., 105, 241-54, 1947

[36] Savedoff, M. P., and Spitzer, L., “The temperature of interstellar matter,” Astrophys. J., 111, 593-608, 1950

[37] Johnson, C. Y., and Meadows, E. B., "First investigation of ambient positive-ion composition to 219 km by rocket-borne spectrometer", J. Geophys. Res., 60, 193-203, 1955.

[38] Lehnert, B., " Electrodynamic effects connected with the motion of a satellite of the earth", Tellus, 3, 408-409, 1956

[39] Jastrow, R., and Pearse, C. A., " Atmospheric drag on satellite", J. Geophys. Res., 62, 413-423, 1957

[40] Gringauz, K. I., and Zelikman, M. Kh., "Measurement of the concentration of positive ions along the orbit of an artificial satellite", Usp. Fiz. Nauk, 63, 239-252, 1957

[41] Beard, D. B., and Johnson, F. S., "Ionospheric limitations on attainable satellite potential", J. Geophys. Res., 66, 4113-4122, 1961

[42] Whipple, E. C., "The equilibrium electric potential of a body in the upper atmosphere," NASA x-615-65-296, NASA, 1965

[43] DeForest, S. E., and McIlwain, C. E., " Plasma clouds in the magnetosphere", J. Geophys. Res., vol. 76, pp. 3587-3611, 1971

[44] Shaw, R.R., Nanevicz, J. E., Adamo, R. C., "Observations of electrical discharges caused by differential satellite charging, in Spacecraft Charging by Magnetospheric Plasmas," Prog. Astron. Aeron., 47, 61-76, 1976.

[45] Rosen, A. (ed) , "Spacecraft Charging by Magnetospheric Plasmas," Prog. Astron. Aeron., 47 (Cambridge, Mass.: MIT Press), 1976

[46] McPhreson, D. A., and Schober, W. R., Prog. "Spacecraft charging at high altitudes: The SCATHA satellite program in Spacecraft Charging by Magnetospheric Plasmas," Prog. Astron. Aeron., 47, 15-30, 1976

[47] Adamo, R. C., and Matarreze, J. R., "Transient pulse monitor data from the P78-2 (SCATHA) spacecraft", Journal of Spacecraft and Rockets, 20:432-7, 1983

[48] Koons, H. C., " Summary of environmentally induced electrical discharges on the P78-2 (SCATHA) spacecraft", Journal of Spacecraft and Rockets, 20:425-31, 1983

[49] Koons et al, "Severe spacecraft charging events on SCATHA in September 1982", Journal of Spacecraft and Rockets, 25:239-43, 1988

[50] Koons, H. C., and Gorney, D. J., "Relationship between electrostatic discharges on spacecraft P78-2 and the electron environment", Journal of Spacecraft and Rockets, 28:683-8, 1991

[51] Gussenhoven, M. S., and Mullen, E. G., " Geosynchronous environment for severe spacecraft charging", Journal of Spacecraft and Rockets, 20:26-34, 1983

[52] Mullen et al, "SCATHA survey of high-voltage spacecraft charging in sunlight", Journal of Geophysical Research, 91:1474-90, 1986

[53] Craven, P. D., " Potential modulation of the SCATHA satellite, Journal of Spacecraft and Rockets, 24:150-7, 1987

[54] Garrett H. B., and DeFrost, S. E. "An analytical simulation of the geosynchronous plasma environment", Planetary Space Science, 27:1101-09, 1979.

[55] Purvis et al., " Design guidelines for assessing and controlling spacecraft charging effects", NASA TP-2361, NASA, 1984.

[56] Katz et al., " NASCAP programmer's reference manual", Rep. SSS-84-6638, S-Cubed, La Jolla, CA, 1984.

[57] http://powerweb.grc.nasa.gov/pvsee/software/NASCAP.html

[58] Dobrowolny M., and Melchion, E., "Electrodynamic aspects of the first tethered satellite mission," J. Geophys. Res., vol. 98, pp. 13761-13778, 1993

[59] Samanta Roy, R., and Hastings, D. E., " A brief overview of electrodynamic tethers," the Behavior of Systems in the Space Environment, R. N. Dewitt, D. Dwight, and A. K. Hyder, Eds. Norwell, MA: Kluwer, 1993, pp. 825-836

[60] Enloe at al, "The charging hazards and wake studies (CHAWS) experiment", in Proc. 33rd Aerospace Sciences meeting Exhibit. Reno, NV: AIAA, Jan. 9-12, 1995, AIAA 95-00892.

[61] Enloe, C. L. et al, " High-voltage interactions in plasma wakes: Results from the charging hazards and wake studies (CHAWS) flight experiments," J. Geophys. Res., vol. 102, no. Al, pp. 425-433, Jan. 1, 1997.

[62] Cooke, D. L. et al, " Three dimensional calculation of shutter orbiter charging in polar orbit", Spacecraft Environmental Interactions Technology, 1983: NASA Conf. Publ., CP-2359/AFGL-TR-85-0018, 1985

[63] Cooke, D. L. et al, "POLAR user's manual", GL-TR-89-0307, AF Geophysics Lab., Hanscom AFB, MA, 1989

[64] Mandell, M. J., and Davis, V. A., "User's guide to NASCAP/LEO," SSS-R-8507300-R2, NASA Lewis Res. Center, Cleveland, OH, 1990.

[65] Garrett H. B., Schwank, D. C., and DeFrost, S. E " A statistical analysis of the low energy geo-synchronous plasma environment –I. electrons, Planetary Space Science, 29:1021-44, 1981a.

[66] Garrett H. B., Schwank, D. C., and DeFrost, S. E " A statistical analysis of the low energy geo-synchronous plasma environment –I. protons, Planetary Space Science, 29:1045-60, 1981b.

[67] Mullen, E. G., Gussenhoven, M. S., and Hardy, D. A. SCATHA survey of high-voltage spacecraft charging in sunlight, "Journal of Geophysical Research", 91:1474-90, 1986.

[68] Gombosi, T.I., " Physics of The Space Environment", Cambridge University Press",1998.

[69] Chen, Francis F., "Introduction to Plasma Physics and Controlled Fusion, Second Edition, Volume 1: Plasma Physics", Plenum Press, New York and London, 1974, pp. 8-10

[70] Maxwell Technologies System Division, " Interactive Spacecraft Charging Handbook", Space Environment Effect Program, NASA Marshall Space Flight Center.

[71] Osgood, R.N., "Operational status of the space test program P78-2 spacecraft and payloads," reported in Proceedings of 3rd Spacecraft Charging Technology Conference, Nov. 12-14, 1980, NASA Conference Publication 2182, pp. 365-369.

[72] Gussenhoven, M.S., Cohen, H.A., Hardy, D.A., Burke, W.J., and Chesley, A., "Analysis of ambient and beam particle characteristics during the ejection of an electron beam from a satellite in near-geosynchronous orbit on March 30, 1979," reported in Proc. of 3rd Spacecraft Charging Technology Conference, No. 12-14, 1980, NASA Conference Publication 2182, pp. 642-664.

[73] Cohen, H.A., Adamo, R.C., Aggson, T., Chesley, A.L., Clark, D.M., Damron, S.A., Delorey, D.E., Fennell, J.F., Gussenhoven, M.S., Hanser, F.A., Hall, D., Hardy, D.A., Huber, W.B., Katz, I., Koons, H.C., Lau, S.T., Ledley, B., Mizera, P.F., Mullen, E.G., Nanevicz, J.E., Olsen, R.C., Rubin, A.G., Schnuelle, G.W., Saflekos, N.A., Tautz, M.F., and Whipple, E.C., "P78-2 Satellite and payload responses to electron beam operations on March 30, 1979," reported in Proc. of 3rd Spacecraft Charging Technology Conference, Nov. 12-14, 1980, NASA Conference Publication 2182, pp. 509-559.

[74] Osgood, R.N., "Operational status of the space test program P78-2 spacecraft and payloads," reported in Proc. of 3rd Spacecraft Charging Technology Conference, Nov. 12-14, 1980, NASA conference Publication 2182, pp. 412-432.

[75] Whipple, E.C., and Olsen, R.C., "Importance of differential charging for controlling both natural and induced vehicle potentials on ATS-5 and ATS-6," reported in Proc. of 3rd Spacecraft Charging Technology Conference, Nov. 12-14, 1980, NASA Conference Publication 2182, p. 887.

[76] Deininger, W.D., Aston, G., and Pless, L.C., "Hollow-cathode plasma source for active spacecraft charge control," Review of Scientific Instruments, Vol. 58, No. 6, June 1987, pp. 1053-1062.

[77] Serwey, R. A., Beichner, R.J., "Physics for Scientists and Engineers with Modern Physics", Saunders College Publishing, 2000, pp 714.

[78] Ronald W. Humble, Gary N. Henry, Wiley J. Larson, "Space Propulsion Analysis And Design, revised", Space Technology Series, 1995, pp10.

[79] Rayburn C., Campbell R., Hoskins W., Cassady R., "AIAA 2000-3256, Development of a Micro Pulsed Plasma Thruster for the Dawgstar Nanosatellite.", 36th Joint Propulsion Conference & Exhibit, 16-29 July 2000, Huntsville, Alabama.

[80] Jeffery G. Reichbach, Raymond J. Sedwick, Manuel Martinez-Sanchez, "Micropropulsion System Selection for Precision Flying Satellites",SERC #1-01, January 2001.

[81] King, L. B., Parker G. G., Deshmukh, S., Chong, J., "A study of inter-spacecraft coulomb forces and implications for formation flying," AIAA-2002-3671

[82] Chong, J., "Dynamic behaviour of spacecraft formation flying using coulomb forces," Masters' thesis, Michigan Technological University, 2002

[83] King, L. B., Parker G. G., Deshmukh, S., Chong, J., "Spacecraft Formation-flying using Inter-vehicle Coulomb Forces," Final report for Phase I research sponsored by NIAC, 2002, http://www.niac.usra.edu/studies/

Appendix

Matlab-6.0 code for calculating the inter-vehicle Coulomb force and torque. The input to the code was an Excel file SEEdata.xls with position vectors and potentials of individual finite elements, which were obtained from the SEE code.

Code:

```
clear
format long g;
A = xlsread('SEEdata.xls','SEEdata');
        % A is the matrix which contains all the data from SEE handbook
         % SEEdata.xls is the excel file in which the data from SEE program is copied
size = size(A);
rows = size(1,1);   %  rows is the number of surface elements of spacecraft A

for i = 1:rows
   for j = 1:rows
      if i == j;  % i.e. potential at a point due to that charge itself is 0
         r(i,j) = 0;
      else
      r(i,j) = 1/(sqrt((A(i,3)-A(j,3))^2+(A(i,4)-A(j,4))^2+(A(i,5)-A(j,5))^2));
      end
   end;
end;
invr = inv(r);
for i= 1:rows
   v(i,1) = A(i,9);
end
q = invr*(4*pi*8.8542e-12*(v)); % matrix containing charges of all the elements

TotalT = [0;0;0];   % total torque acting on spacecraft A due to spacecraft B
TotalF = [0;0;0];   % total coulomb force acting on spacecraft A due to spacecraft B
TotalP = [0;0;0];   % total dipole moment of spacecraft A
offset = [-100;0;0]; % position vector of center of co-ordinate system for spacecraft B

for i = 1:rows
     Ai = [A(i,3);A(i,4);A(i,5)]; % position vector of i th element of S/C A
     Pi = q(i,1)*Ai;                % dipole moment of i th element of S/C A
     TotalEi = [0;0;0];             % electric field at i th element of S/C A
     centerE = [0;0;0];             % electric field at center of S/C A
     lamdad = 142;                  % lowest debye length in m
          for j = 1:rows
              Bj = [A(j,3);A(j,4);A(j,5)]+offset; % position vector of j th element of SCB
```

```
            BA = Ai - Bj;                  % vector along which the electric field is acting

            magBA = ( BA(1,1)^2+ BA(2,1)^2+ BA(3,1)^2)^0.5;
            magBj = ( Bj(1,1)^2+ Bj(2,1)^2+ Bj(3,1)^2)^0.5;

          Ei = (q(j,1)*BA*exp(-magBA/lamdad))/(4*pi*8.8542e-12*(magBA^3));
              % electric field at ith element of SCA due to jth element of SCB
          centerEj = (q(j,1)*Bj*exp(-magBj/lamdad))/(4*pi*8.8542e-12*(magBj^3));
              % electric field at center of SCA due to jth element of SCB
          TotalEi = TotalEi + Ei;
          centerE = centerE + centerEj;
      end

   Ti = cross(Pi,TotalEi);    % torque acting on i th element of SCA
   TotalT = TotalT + Ti;

   Fi = q(i,1)*TotalEi;      % force acting on i th element of SCA
   TotalF = TotalF + Fi;

   TotalP = TotalP + Pi;      % diapole moment of i th element of SCA

end

magP = ( TotalP(1,1)^2+ TotalP(2,1)^2+ TotalP(3,1)^2)^0.5;
magcenterE = ( centerE(1,1)^2+ centerE(2,1)^2+ centerE(3,1)^2)^0.5;

% results

offset;

TotalT
magTotalT = ( TotalT(1,1)^2+ TotalT(2,1)^2+ TotalT(3,1)^2)^0.5;

TotalF
magTotalF = ( TotalF(1,1)^2+ TotalF(2,1)^2+ TotalF(3,1)^2)^0.5

TotalP
magTotalP = ( TotalP(1,1)^2+ TotalP(2,1)^2+ TotalP(3,1)^2)^0.5;

centerE
magcenterE = ( centerE(1,1)^2+ centerE(2,1)^2+ centerE(3,1)^2)^0.5;

maxT = magP*magcenterE
```